DTIC FILE COPY

4

AD-A229 275

REPORT DOCUMENTATION PAGE

Form Approved
OMB No. 0704-0188

Public reporting burden for this collection of information is estimated to average 1 hour per response, including the time for reviewing instructions, searching existing data sources, gathering and maintaining the data needed, and completing and reviewing the collection of information. Send comments regarding this burden estimate or any other aspect of this collection of information, including suggestions for reducing this burden, to Washington Headquarters Services, Directorate for information Operations and Reports, 1215 Jefferson Davis Highway, Suite 1204, Arlington, VA 22202-4302, and to the Office of Management and Budget, Paperwork Reduction Project (0704-0188), Washington, DC 20503.

1. AGENCY USE ONLY (Leave blank)	2. REPORT DATE	3. REPORT TYPE AND DATES COVERED
	15 Nov 1990	Interim; 1 Oct 89 - 30 Sept 90

4. TITLE AND SUBTITLE
Physics and Technology of III-V Pseudomorphic Structures

5. FUNDING NUMBERS
PE61153N,
R&T#414s002

6. AUTHOR(S)
C.W. Tu

7. PERFORMING ORGANIZATION NAME(S) AND ADDRESS(ES)
Department of Electrical & Computer Engineering
University of California at San Diego
La Jolla, CA 92093-0407

8. PERFORMING ORGANIZATION REPORT NUMBER
TU-ONR-90

9. SPONSORING/MONITORING AGENCY NAME(S) AND ADDRESS(ES)
Office of Naval Research
Code 1114
800 North Quincy Street
Arlington, VA 22217-5000

10. SPONSORING/MONITORING AGENCY REPORT NUMBER

DTIC
ELECTE
NOV 28 1990
S C B D

11. SUPPLEMENTARY NOTES

12a. DISTRIBUTION/AVAILABILITY STATEMENT
Approved for public release; Distribution Unlimited

12b. DISTRIBUTION CODE

13. ABSTRACT (Maximum 200 words)

A AlGaAs/InGaAs modulation-doped field-effect transistors with a nominally $(InAs)_2(GaAs)_2$ channel grown by migration-enhanced epitaxy exhibit better luminescent and device properties than those with a random alloy $In_{.4}Ga_{.6}As$ channel grown by molecular-beam epitaxy (MBE).

We have proposed and applied a new kinetic model, which includes both group-III alkyl and group-V species in the surface chemical reactions, to the growth of GaAs, GaSb, and InAs by metalorganic MBE or chemical-beam epitaxy (CBE).

We have also set up a gas-source MBE system with elemental group-III and doping sources as well as arsine and phosphine. We used the group-V-limited growth mode to determine in situ the exact values of V/III atomic ratios during growth of GaP, InP, AlP, and GaAs. X-ray studies of an InAlAs/InP superlattice indicates the existence of a P/As-intermixed strained interface.

14. SUBJECT TERMS	15. NUMBER OF PAGES
AlGaAs/InGaAs, InP, GaP, GaAs, InAlAs/InP MODFET, migration-enhanced epitaxy (MEE), MBE, GaSb, MOMBE, CBE, GSMBE, growth kinetics, strain	111
	16. PRICE CODE

17. SECURITY CLASSIFICATION OF REPORT	18. SECURITY CLASSIFICATION OF THIS PAGE	19. SECURITY CLASSIFICATION OF ABSTRACT	20. LIMITATION OF ABSTRACT
UNCLASSIFIED	UNCLASSIFIED	UNCLASSIFIED	

Table of Contents

Accession For
NTIS GRA&I ☑
DTIC TAB ☐
Unannounced ☐
Justification
By
Distribution/
Availability Codes
Dist | Avail and/or Special
A-1

QUALITY INSPECTED 1

90 11 27 036

Thin Solid Films, 196 (1990)
PREPARATION AND CHARACTERIZATION

MOLECULAR BEAM EPITAXIAL GROWTH AND CHARACTERIZATION OF PSEUDOMORPHIC MODULATION-DOPED FIELD EFFECT TRANSISTORS*

J. ZHANG, N. C. TIEN, E. W. LIN, H. H. WIEDER, W. H. KU AND C. W. TU
Department of Electrical and Computer Engineering, Mail Code R-007, University of California, San Diego, La Jolla, CA 92093 (U.S.A.)
D. B. POKER
Solid State Division, Oak Ridge National Laboratory, Oak Ridge, TN 37831 (U.S.A.)
S. N. G. CHU
AT&T Bell Laboratories, Murray Hill, NJ 07974 (U.S.A.)
(Received May 25, 1990; accepted August 8, 1990)

We have investigated the luminescent and device properties of pseudomorphic AlGaAs/InGaAs modulation-doped field effect transistors (MODFETs) with different InAs molar fractions in the InGaAs channel. Molecular beam epitaxy, which simultaneously deposits group III atoms and As_4 molecules on the substrate surface, was used to grow the random alloy $In_xGa_{1-x}As$ channel layer for $x \leqslant 0.4$, and migration-enhanced epitaxy (MEE), which alternatingly deposits group III atoms and As_4 molecules on the surface, was used to grow sequential layers of InAs and GaAs in the channel region with large effective x (up to 0.5). For 1 μm gate length MODFETs with random alloy $In_xGa_{1-x}As$ channels the transconductance g_m and saturation drain current I_{dss} exhibit a maximum at $x = 0.17$ because of the superior electron transport properties of InGaAs compared with GaAs. g_m and I_{dss} decrease drastically for x higher than 0.32 as a result of misfit dislocation generation. The photoluminescence peaks of $In_xGa_{1-x}As$ channels of these MODFET samples show a similar trend, strong intensity for the $In_{0.17}Ga_{0.83}As$ channel and very weak intensity for the $In_{0.4}Ga_{0.6}As$ channel. However, MODFETs with a nominally $(InAs)_2(GaAs)_2$ channel grown by MEE exhibit higher g_m, I_{dss} and photoluminescence intensity than those with an $In_{0.4}Ga_{0.6}As$ channel.

1. INTRODUCTION

Pseudomorphic AlGaAs/$In_xGa_{1-x}As$ modulation-doped field effect transistors (MODFETs) have attracted considerable attention recently for high speed integrated circuit and microwave applications[1,2] because $In_xGa_{1-x}As$ has a smaller electron effective mass, larger electron velocity and smaller energy band gap than GaAs. The lattice mismatch between $In_xGa_{1-x}As$ and GaAs must be chosen within

* Presented at the 17th International Conference on Metallurgical Coatings and 8th International Conference on Thin Films, San Diego, CA, U.S.A., April 2–6, 1990.

0040-6090/90/$3.50 © Elsevier Sequoia/Printed in The Netherlands

a critical limit (which depends on x and on the thickness of the $In_xGa_{1-x}As$ layer) so that no misfit defects are generated[3–5]. Typically, the $In_xGa_{1-x}As$ channel thicknesses of 100–200 Å and InAs molar fractions $x \leqslant 0.25$ are used in order to maintain a coherent interfacial strain and a pseudomorphic deformation of the crystal lattice in the active channel.

In this paper we describe our investigation of higher InAs molar fractions in the MODFET channel. Large indium concentration in the $In_xGa_{1-x}As$ ternary alloy might provide better charge carrier transport properties and stronger electron confinement. We report here growth, characterization and device performance of $Al_{0.28}Ga_{0.72}As/In_xGa_{1-x}As/Al_{0.28}Ga_{0.72}As$ MODFETs with x up to 0.5. Both molecular beam epitaxy (MBE) of random alloy $In_xGa_{1-x}As$ and migration-enhanced epitaxy (MEE) of alternating deposition of InAs and GaAs are compared. The MEE technique results in better luminescent and device properties for high indium concentration in the active layer.

2. EXPERIMENTAL PROCEDURES

The MODFET structure, shown in Fig. 1, was grown on a semi-insulating GaAs(100) substrate in a Varian MBE system. The growth sequence was as follows: (1) 2000 Å GaAs buffer and 20 periods of $Al_{0.28}Ga_{0.72}As$(200 Å)/GaAs(15 Å) multiple quantum well (MQW); (2) a delta-doped region in the $Al_{0.28}Ga_{0.72}As$ layer with a silicon sheet concentration of $2 \times 10^{12}\,cm^{-2}$, followed by a 20 Å $Al_{0.28}Ga_{0.72}As$ spacer and a 30 Å GaAs layer to provide a smooth surface; (3) a 150 Å InGaAs channel, the thickness of which is kept constant throughout the experiment; (4) a top delta-doped region in an $Al_{0.28}Ga_{0.72}As$ layer with a silicon sheet doping concentration of $6 \times 10^{12}\,cm^{-2}$ spaced 30 Å from the InGaAs channel; (5) a 300 Å silicon-doped $Al_{0.28}Ga_{0.72}As$ layer with a doping concentration of $10^{17}\,cm^{-3}$; (6) a 400 Å GaAs contact layer with a doping concentration of

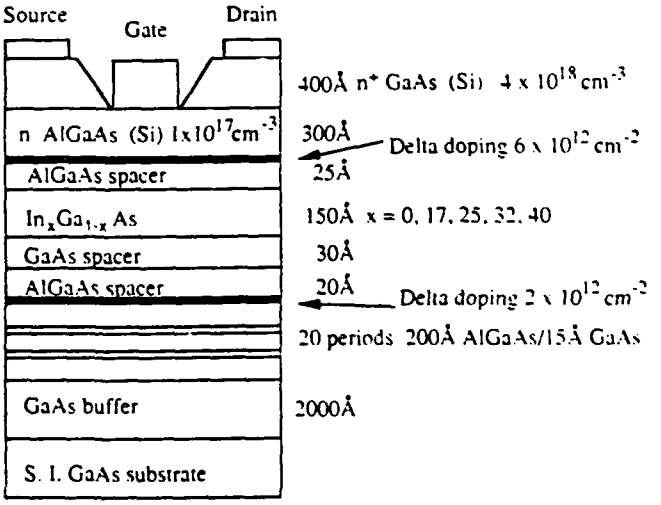

Fig. 1. Schematic diagram of our MODFET structure.

$4 \times 10^{18}\,cm^{-3}$. The growth rate and alloy composition were calibrated by the intensity oscillations of reflection high energy electron diffraction.

The MQW buffer is intended to smooth out surface irregularities, to reduce impurity out-diffusion from the substrate and to provide better carrier confinement. The top AlGaAs layer is lightly doped to $10^{17}\,cm^{-3}$ to reduce the possibility of parallel conduction in the AlGaAs layer and to increase the breakdown voltage compared with conventional, heavily doped AlGaAs electron-supplying layers. The delta-doping technique has been shown to increase the two-dimensional electron concentration in the channel[6]. In order to increase the sheet electron density of the channel even more, we introduced two delta-doped regions on each side of the channel. Hall measurement gives a sheet carrier concentration of about $4 \times 10^{12}\,cm^{-2}$.

We used MBE to grow a sequence of layers to be used for MODFETs with $In_xGa_{1-x}As$ channels and x ranging from 0 to 0.4. For the channel layer with high InAs molar fraction we also used MEE, which provides the possibility of growing this very lattice-mismatched system monolayer by monolayer[7–9]. In MEE the arsenic and group III flux were supplied alternately by shuttering the appropriate molecular beams. In the absence of an arsenic overpressure, the migration length of group III atoms is enhanced. Therefore, the growth temperature can be lowered. The reason for using a low growth temperature of 400 °C is to prevent indium re-evaporation and intermixing between indium and gallium atoms near interfaces[10]. The sequential MEE timing of $(InAs)_2(GaAs)_2$ is shown in Fig. 2. The subscripts refer to the number of monolayers intended. Because the substrate surface is a nearly exact (100) surface, one-monolayer-high interface fluctuation in MBE or MEE $(InAs)_1(GaAs)_1$ is believed to result in a random alloy. On the contrary, there exists a large lattice mismatch (7.2%) between InAs and GaAs. Therefore, we limit the InAs and GaAs layers to be only two monolayers thick in MEE growth of active layers, to compare with MBE-grown random alloys. After the 20 Å GaAs spacer layer was grown to cap the channel layer, the substrate temperature was increased to 580 °C to grow the AlGaAs spacer layer and the subsequent layers.

Figure 3 shows a cross-section transmission electron micrograph of the MODFET structure with a nominally $(InAs)_2(GaAs)_2$ channel. The channel layer exhibits non-uniform composition and undulating interfaces, probably because of

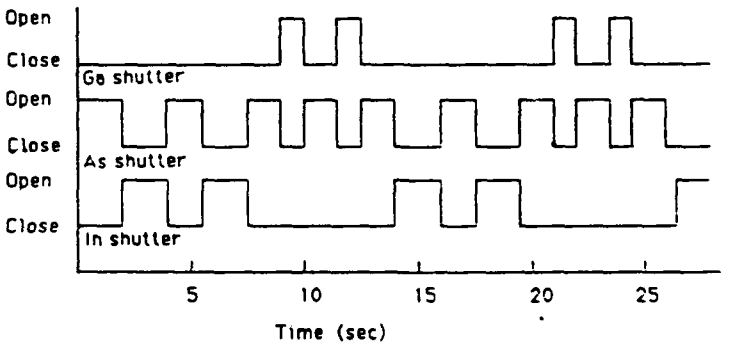

Fig. 2. Sequential MEE growth timing of molecular beams.

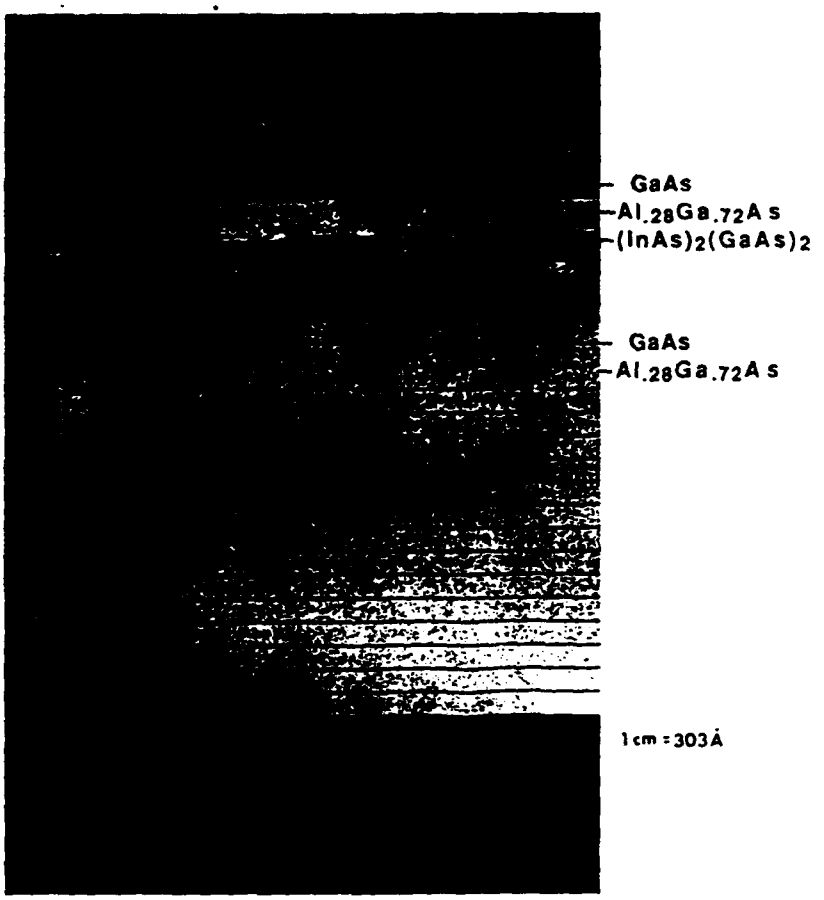

Fig. 3. Cross-section transmission electron micrograph of the MODFET sample with a nominally $(InAs)_2(GaAs)_2$ channel (Magnification, 330000 ×.)

considerable strain from the large lattice mismatch between InAs and GaAs. However, the interfaces are free of misfit-generated dislocations. There is some outdiffusion of indium from the top region of the channel layer, as evidenced by less contrast in the top interface. We have tried to use Rutherford backscattering to estimate the indium concentration. The results are inconclusive owing to the non-uniform film thickness. Because the growth temperature of the nominally $(InAs)_2(GaAs)_2$ channel is low, we believe the average indium composition to be close to 50%. The indium concentration in the channel layer, however, still requires an independent determination.

MODFETs were fabricated using recessed gate technology. Mesas were defined by means of photolithography and an H_3PO_4:H_2O_2:H_2O (1:1:25) etch. The source–drain ohmic contact metallurgy consists of 1000 Å Au:Ge eutectic and 150 Å of nickel. The contacts were alloyed at 430 °C for 30 s under forming gas flow.

Following the source–drain ohmic contact formation, an $NH_4OH:H_2O_2$ (pH=7) selective etchant was used for the recessed gate etching. Finally, 3000 Å of aluminium was deposited to form the gate–contact pad.

3. RESULTS AND DISCUSSION

3.1. Photoluminescence

Photoluminescence measurements at about 40 K were performed in order to determine the quality of layers before device processing. Figure 4 shows photoluminescence spectra ~~with~~ of samples with a random alloy $In_xGa_{1-x}As$ and a nominally $(InAs)_2(GaAs)_2$ channel. The peak at 830 nm is from the GaAs epilayer. Another peak at longer wavelength is the channel subband transition peak which depends on the channel layer thickness, composition and strain relaxation. Figures 4(a) and 4(b)

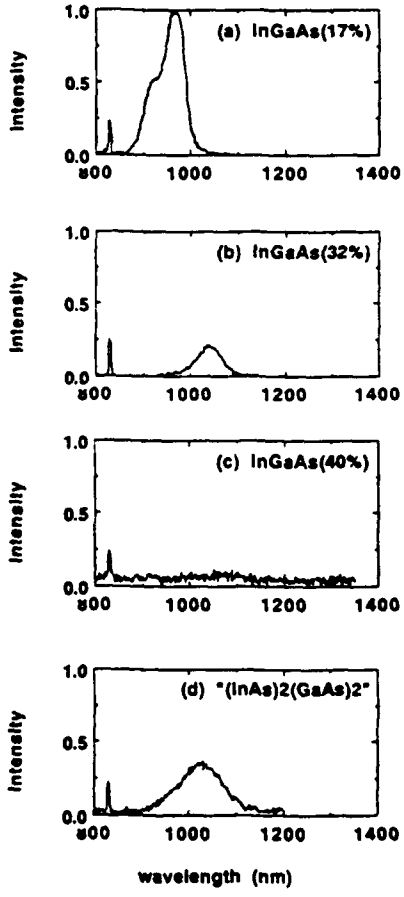

Fig. 4. Photoluminescence spectra at about 40 K. MODFET structure samples using random alloy $In_xGa_{1-x}As$ channel with (a) $x = 0.17$, (b) $x = 0.32$ and (c) $x = 0.4$ (d) MODFET structure samples using a nominally $(InAs)_2(GaAs)_2$ superlattice channel.

are spectra of samples with $In_{0.17}Ga_{0.83}As$ and $In_{0.32}Ga_{0.68}As$ channels respectively. The peak from the $In_{0.32}Ga_{0.68}As$ sample is broader and weaker than the peak from the $In_{0.17}Ga_{0.83}As$ layer. As the indium composition increases to 40% the 150 Å channel layer thickness exceeds the critical layer thickness. The strain relaxation in the channel layer generates misfit dislocations. No subband transition from the channel layer was observed because of poor crystalline quality as shown in Fig. 4(c). However, we do observe a peak at about 1030 nm from the nominally $(InAs)_2(GaAs)_2$ channel (150 Å thick) grown by MEE has a better crystalline quality than random alloy $In_{0.40}Ga_{0.60}As$ channel of the same thickness grown by MBE. Even though this peak is very broad and weak, it suggests that the nominally $(InAs)_2(GaAs)_2$ channel

3.2. I–V characteristics

The device performances for samples with different indium concentrations in the channel are listed in Table I. The MODFET samples with a random alloy $In_{0.17}Ga_{0.83}As$ channel exhibited a transconductance of 340 mS mm^{-1} and a

TABLE I

TRANSCONDUCTANCE g_m, DRAIN SATURATION CURRENT I_{ds_s} MEASURED AT A GATE VOLTAGE V_g OF -1.0 V, AND UNITY POWER GAIN FREQUENCY f_{max} FOR MODFET WITH DIFFERENT In CONCENTRATIONS IN THE InGaAs CHANNEL LAYER.

In concentration (%)	g_m mS mm^{-1})	I_{ds_s} (mA mm^{-1})	f_{max} (GHz)
0	276	430	43
17	342	450	58
25	294	340	30
32	90	125	
40	40	50	
"$(InAs)_2(GaAs)_2$"	130	200	

saturation current of 450 mA mm^{-1} for a device with a 1 μm gate length, 50 μm source-to-drain spacing. The maximum frequency of oscillation was extrapolated to be 58 GHz. The *I–V* characteristics of the device are shown in Fig. 5(a),which also exhibits the low output conductance and excellent pinch-off. The breakdown voltage of this device is about 11–13 V. Figure 6 shows the transconductance and saturation drain current *vs.* indium composition of the channel layer. The lines between the data points are meant only to guide the eye. It is evident that the pseudomorphic InGaAs channel MODFET has better device performance than lattice-matched GaAs channel MODFET. On the other hand contrary, as the indium composition in the channel increases, the lattice mismatch exceeds the pseudomorphic growth range which results in significant degradation in device performance. In Fig. 5(b) we show the *I–V* characteristics of the sample with the $In_{0.40}Ga_{0.60}As$ channel for comparison. For the samples with $In_{0.32}Ga_{0.68}As$ and $In_{0.40}Ga_{0.60}As$ channels we could not make *s* parameter measurements.

Of particular interest is the sample with a nominally $(InAs)_2(GaAs)_2$ superlattice channel, which displays reasonable transistor characteristics, *i.e.* a low output conductance, transconductance of 130 mS mm^{-1} and saturation current of

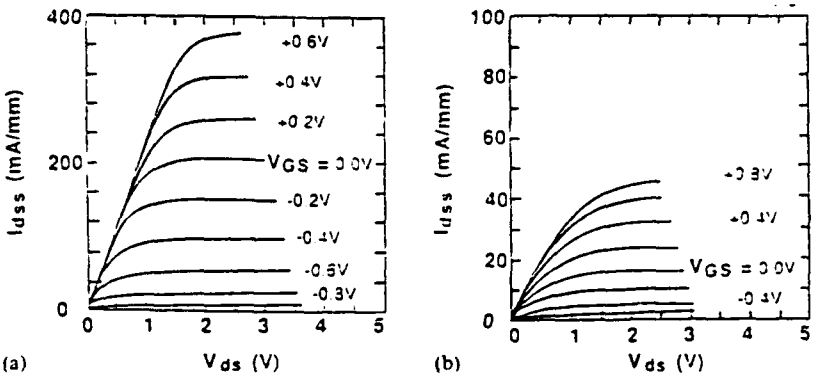

Fig. 5. Drain current–voltage output characteristics for a MODFET with a random alloy $In_xGa_{1-x}As$ channel: (a) $x = 0.17$ and (b) $x = 0.40$.

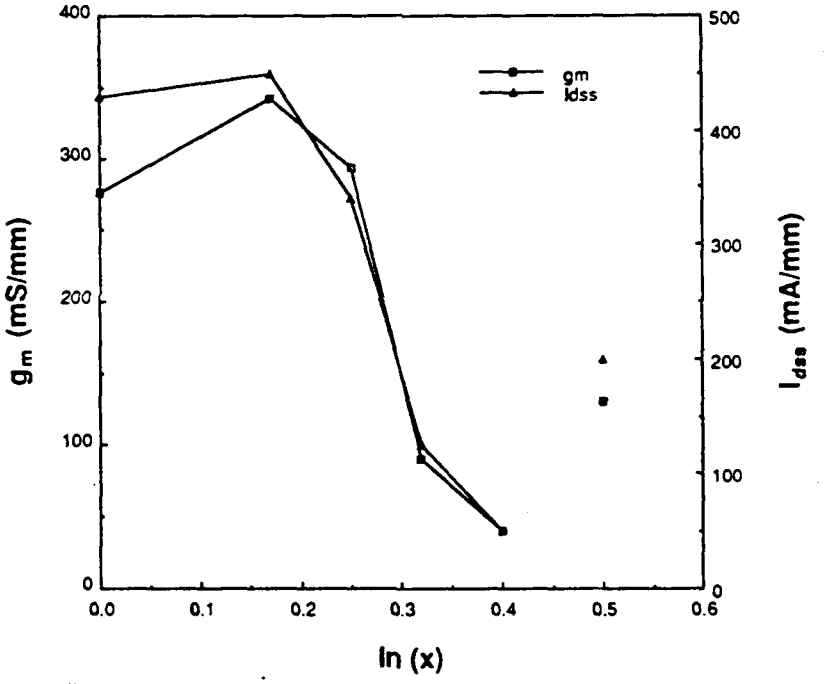

Fig. 6. Transconductance and saturation current vs. InAs molar fraction in the channel.

200 mA mm^{-1}. The drain I–V curves shown in Fig. 7 are to be compared with Fig. 5(b). Although these results are not as good as those obtained from the $In_{0.17}Ga_{0.83}As$ sample, they are much better than those obtained from the $In_{0.40}Ga_{0.60}As$ sample.

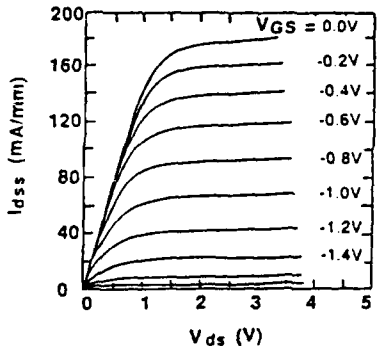

Fig. 7. Current–voltage output characteristics for a MODFET with an $(InAs)_2(GaAs)_2$ superlattice channel, corresponding to an InAs molar fraction of 50%, with transconductance of 120 mS mm^{-1} and saturation current of 200 mA mm^{-1} at $V_g = 1.0$ V.

4. CONCLUSIONS

We have investigated the luminescent and device properties of pseudomorphic AlGaAs/InGaAs MODFETs with indifferent InAs molar fractions in the InGaAs channel. We used MBE to grow the random alloy $In_xGa_{1-x}As$ channels for x up to 0.4, and we used MEE to grow a nominally $(InAs)_2(GaAs)_2$ channel for an effective x of near 0.5. For 1 μm gate length MODFETs with random alloy $In_xGa_{1-x}As$ channels the transconductance g_m and saturation drain current I_{dss} exhibit a maximum at $x = 0.17$, and decrease drastically for x higher than 0.32 owing to misfit dislocation generation. The photoluminescence peaks of $In_xGa_{1-x}As$ channels of these MODFET samples display a similar trend: strong intensity for the $In_{0.1}Ga_{0.83}As$ channel and very weak intensity for the $In_{0.4}Ga_{0.6}As$ channel. However, MODFETs with a nominally $(InAs)_2(GaAs)_2$ channel grown by MEE exhibit higher g_m, I_{dss} and photoluminescence intensity than those with a random alloy $In_{0.4}Ga_{0.6}As$ channel grown by MBE. Cross-section transmission electron micrographs indicate some outdiffusion of indium from the top interface of the nominally $(InAs)_2(GaAs)_2$ superlattice channel. Because the MEE-grown layer was grown at low temperature, we believe that the indium concentration is still close to 0.5. In addition, in cross-section transmission electron microscopy few dislocations are observed at the MEE channel–buffer interface. An independent determination of the effective indium concentration is still required.

ACKNOWLEDGMENTS

This work is partially supported by the Air Force Wright Research and Development Center under Contract F33615-88-C-1861 and by the Office of Naval Research under Grant N00014-89-J-1147. The work of one of the authors (D.B.P.) was supported by the Division of Materials Sciences, U.S. Department of Energy, under Contract De-AC05-84OR21400 with Martin Marietta Energy Systems, Inc.

We wish to thank Professor S. S. Lau, Mr. Wei Xia and Mr. C. Corzzolino for stimulating discussions.

REFERENCES

1 J. J. Rosenberg, M. Benlamri, P. D. Kirchnen, J. M. Woodall and G. D. Pettit, *IEEE Electron Device Lett.*, *6* (1985) 491.
2 H. Morkoç and Unlu, *Semicond. Semimet.*, *24* (1987) 135.
3 J. N. Matthews and A. E. Blakeslee, *J. Cryst. Growth*, *27* (1974) 118.
4 R. People and J. C. Bean, *Appl. Phys. Lett.*, *47* (1985) 322.
5 I. J. Fritz, P. L. Gourly and L. R. Dowson, *Appl. Phys. Lett.*, *51* (1987) 1004.
6 E. F. Schubert, J. E. Cunningham, W. T. Tsang and G. L. Timp, *Appl. Phys. Lett.*, *51* (1987) 1170.
7 Y. Horikoshi, M. Kawashima and H. Yamaguchi, *Jpn. J. Appl. Phys.*, *27* (1988) 169.
8 F. D. Schowengerdt, F. J. Grunthaner and J. K. Liu, *MRS Symposia Proceedings*, Vol. 144, Materials Research Society, Pittsburgh, PA, 1989, p. 201.
9 B. W. Liang, K. Ha, J. Zhang, T. P. Chin and C. W. Tu, *Proc. Soc. Photo-Opt. Instrum. Eng.*, *1285*, 1990, p. 116. ~~in press~~.
10 C. Guille, F. Houzay, J. M. Moison and F. Barthe, *Surf. Sci.*, *189–190* (1987) 1041.

Growth of InAs on GaAs (001) by Migration-Enhanced Epitaxy

B. W. Liang, K. Ha*, J. Zhang, T. P. Chin and C. W. Tu
Department of Electrical and Computer Engineering, R-007
University of California at San Diego
La Jolla, CA 92093-0407

Abstract

Growth of InAs epitaxial layers on GaAs (001) by migration-enhanced epitaxy (MEE) and molecular beam epitaxy (MBE) has been studied. Reflection high-energy-electron diffraction (RHEED) patterns were studied, and persistent RHEED intensity oscillations were observed during MEE growth of InAs. The dependence of RHEED oscillation on MEE growth parameters is discussed. InAs layers grown by MEE at low substrate temperature exhibit comparable quality as MBE layers grown at higher substrate temperature.

1. Introduction

Migration-enhanced epitaxy (MEE) technique has been successfully employed to grow GaAs and AlGaAs epilayers [1-3]. In this technique, group III and V elements are alternatingly deposited onto a substrate. Due to the longer migration length of group-III atoms in the absence of arsenic overpressure, high-quality GaAs and AlGaAs have been achieved at relatively lower substrate temperature. For strained layer epitaxy, MEE experimental results also revealed some improvement in epilayer quality [3,4].

InAs epitaxial films are attractive for their promise of applications in infrared detectors. InAs strained epilayers and InAs/GaAs multiple quantum wells have been grown by molecular-beam epitaxy (MBE) [5-8]. Since InAs substrates are expensive and of relatively poor quality GaAs is preferred as substrate material. The lattice mismatch between the two materials (7.2%) makes epitaxial grov .i difficult. Strained-layer superlattices, such as InGaAs/GaAs, inserteu between InAs and GaAs substrate have been proven important for high-quality epilayers [7]. In this paper, we report on the growth of InAs epitaxial layers on GaAs (001) substrates under various conditions. Reflection high-energy-electron diffraction (RHEED) patterns were studied and persistent RHEED oscillations were observed during MEE growth of InAs. The samples were characterized with Hall effect measurement and X-ray rocking curve analysis. We present details of the experimental procedures in the next section, then compare properties of InAs grown by MEE and MBE.

2. Experimental Procedures

Growth was performed in a modified prototype Perkin-Elmer 425A MBE system. The growth chamber was pumped by a cryopump and an ion pump. Either arsenic or indium furnace was opened or closed alternatingly by a single

motor-controlled rotary shutter. The on-off frequency of the shutter was controlled with a DC power supply. GaAs (001) wafers were used as the substrates. They were etched and cleaned in the usual manner and then mounted with In on molybdenum blocks. The substrate was thermally cleaned at 610°C in vacuum under an overpressure of arsenic. Then, a 1000 Å GaAs buffer layer was grown at 580°C. The substrate temperature was then decreased to 550°C and a 500-Å-thick composition-graded $In_xGa_{1-x}As$ (x from 0 to 0.5) layer, followed by a 5-period InAs (50 Å)/GaAs (25 Å) superlattice at 510°C, was grown via MBE. Then, the substrate temperature was decreased to different InAs growth temperatures, while the arsenic-cell shutter was closed. Typical In beam equivalent pressure at the substrate is estimated to be $2x10^{-6}$ torr. The As_4 beam-equivalent pressure is $4x10^{-6}$ torr for MEE and $2x10^{-5}$ torr for MBE.

3. Results and Discussions

During MEE of InAs at 400°C, the RHEED pattern was a typical As-stablized (2x4) surface reconstruction along the [110] azimuth when the As_4 effusion cell was opened but the In effusion cell was closed. When the In effusion cell was opened but the As_4 effusion cell was closed, the pattern changed instantaneously to an In-stablized (4x2) surface reconstruction along the same azimuth. Figure 1 shows typical RHEED intensity oscillations during

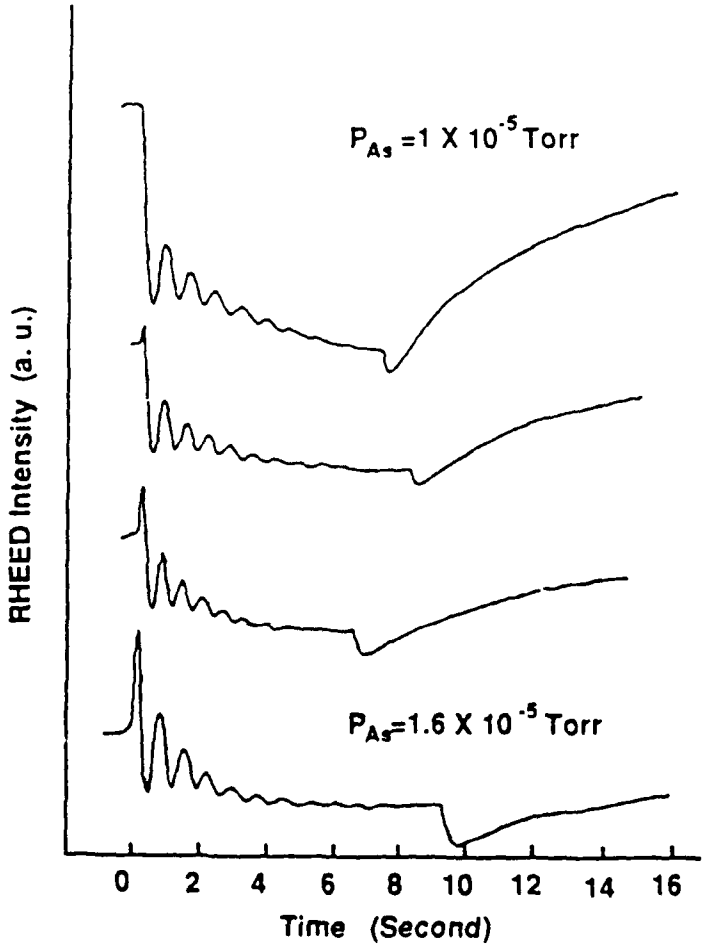

Fig. 1. RHEED intensity oscillations during MBE of InAs at 500°C for different arsenic overpressures.

MBE of InAs for different arsenic overpressures. With increasing As_4 overpressure the RHEED intensity increases first at commencement of growth. Before the In cell was opened, excess arsenic molecules accumulated on the substrate surface, and when In was deposited on the substrate surface, these excess arsenic molecules were removed through reaction with In, resulting in smoother growth front and higher RHEED intensity. The key factors for MEE are therefore relative group-III and group-V beam fluxes and deposition duration for both In and As_4.

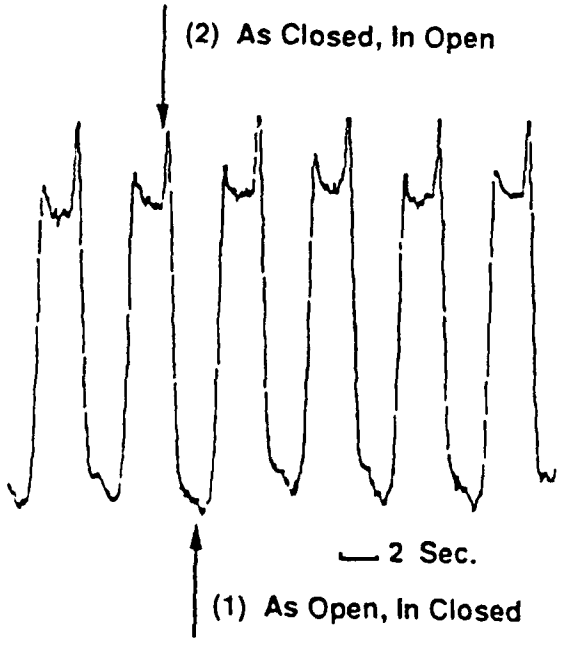

Fig. 2. RHEED intensity modulation during MEE at arsenic overpressure (~ 3 x 10^{-6} torr) higher than optimal.

Figure 2 shows persistent RHEED intensity oscillation when the shutter on-off frequency was low (a period of 5 seconds) and P_{In}=1.8x10^{-6} torr, P_{As}=3.2x10^{-6} torr. This As_4 overpressure was higher than optimal. In region (1), when the arsenic effusion cell was opened, RHEED intensity increased, as in Figure 1. Then, it decreased a little due to some more arsenic accumulating on the surface at such low temperature (400°C). When In was opened and arsenic was closed in region (2), RHEED intensity increased initially since the surface was a little As-rich, and then decreased, similar to the onset of MBE growth.

Figure 3 shows the effect of As_4 pressure on RHEED oscillations during MEE of InAs at a shuttering period of 1.47 second. While In and As_4 fluxes were deposited alternately, the As_4 pressure was reduced from ~ 8 x 10^{-6} torr to ~ 2 x 10^{-6} torr in ~ 90 seconds.With decreasing As_4 pressure the RHEED intensity increased first. This means that in the beginning, As_4 had an over pressure. When As_4 pressure decreased to a certain level, the RHEED intensity reached a maximum and the RHEED intensity oscillation curve looked the smoothest. This means that the As_4 pressure at this level was just right. After that, the oscillation intensity damped quickly because of shortage of As_4 resulting in a damaged surface. A persistent RHEED oscillation was obtained for several hours under the optimized growth condition, as shown in Figure 4.

The quality of InAs epilayers on GaAs grown by MEE and MBE has been characterized with X-ray rocking curve analysis and Hall effect measurement. Figure 5 shows electron concentration as a function of growth temperature for

unintentionally doped epilayers of about 0.6 μm thick grown by MEE and MBE, respectively. Under normal MBE growth conditions, InAs was grown under As_4 overpressure. Because of lower growth temperature compared with that of GaAs and much smaller atomic size ratio of arsenic over indium compared with

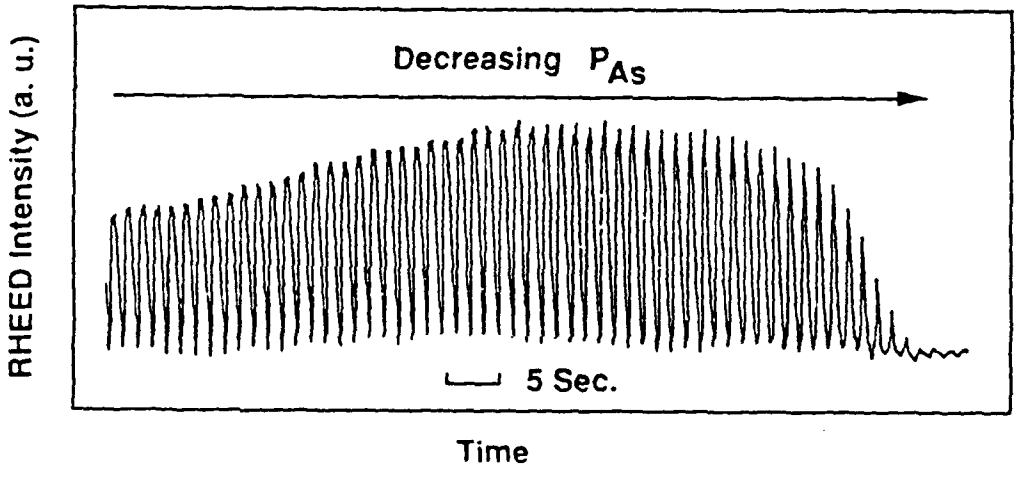

Fig. 3. The effect of arsenic pressure (8×10^{-6} to 3×10^{-6} torr in ~ 90 seconds) on RHEED intensity oscillation during MEE.

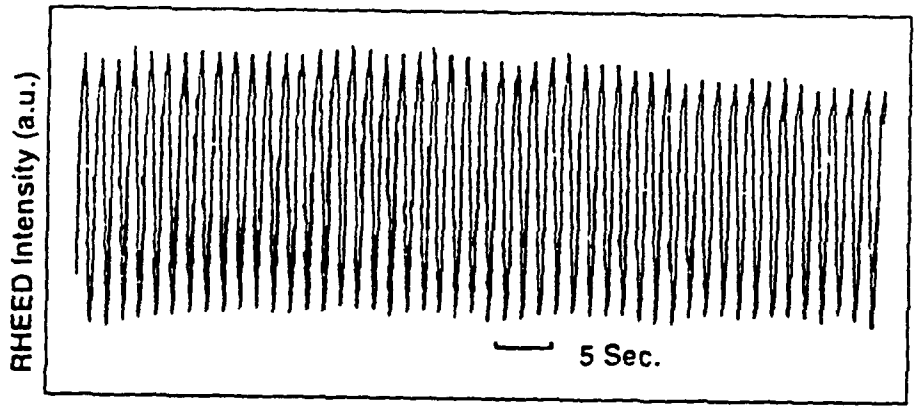

Fig. 4. Persistent RHEED oscillations during MEE of InAs. Growth rate ≈ 0.37 μm/hr, $P_{As} \approx 4 \times 10^{-6}$ torr, Ts = 300°C.

that of arsenic over gallium, one can expect some extra arsenic atoms incorporated into the epilayer. These arsenic atoms will occupy indium sites to produce antisite point defects. This kind of defect probably acts as donors in InAs. Thus, the lower the growth temperature, the higher the arsenic-rich related point defect concentration and the higher the electron concentration. However, because optimal arsenic pressure was much lower in MEE than in MBE (5 times less), it is reasonable to expect that there will be lower arsenic-rich related point defect concentration in MEE than in MBE, as shown in figure 5.

X-ray rocking curve analysis revealed 0.18 degree full widths at half maximum (FWHM) for a 1.4 μm-thick InAs epilayer grown by MEE at about 300 °C but 0.20 and 0.5 degree FWHM for 3.0 μm and 0.74 μm InAs epilayer, respectively, grown by MBE at the same temperature and growth rate

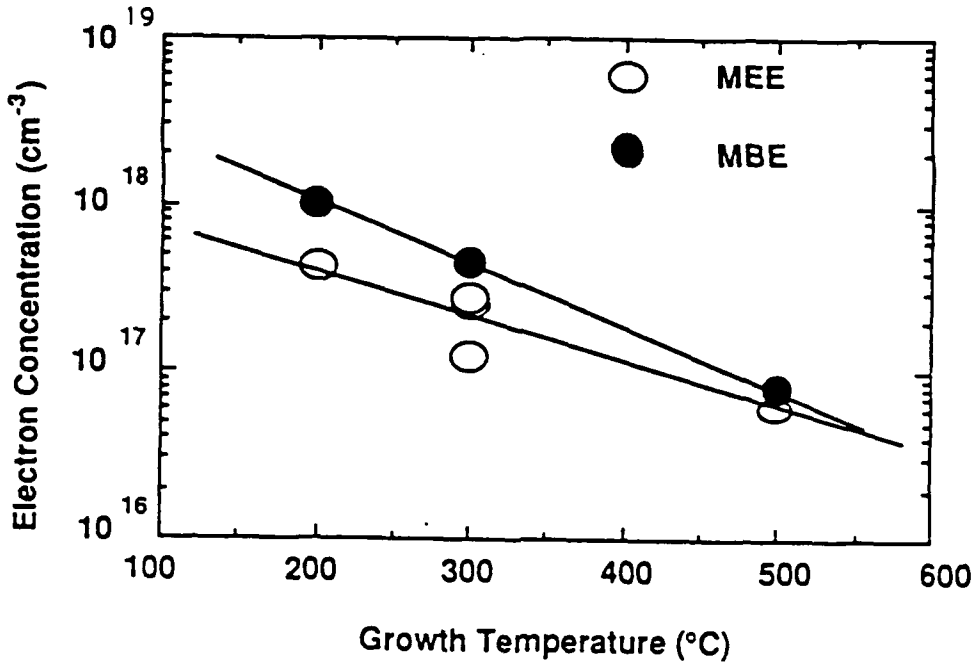

Fig. 5. Electron concentrations in unintentionally doped InAs epilayers as a function of growth temperature for MEE and MBE (~0.6 μm thickness).

of 0.7 μm/hr. It is obvious that the quality of epilayers grown by MEE is better than that grown by MBE at low temperature.

4. Conclusions

Growth of InAs epilayers on GaAs (001) by MEE and MBE has been studied with RHEED. The effect of arsenic pressure on MEE RHEED intensity behavior was studied, and optimized persistent RHEED oscillations was obtained. Hall effect measurement and x-ray rocking curve analysis revealed that at low growth temperature, the quality of InAs epilayer grown by MEE is better than that grown by MBE at the same temperature.

Acknowledgements

This work is partially supported by the Air Force Wright Research and Development Center under contract No. F33615-88-C-1861 and the Office of Naval Research under grant No. N00014-89-J-1147.

References

*Summer student from California Institute of Technology, Pasadena, California.

1. Y. Horikoshi, M. Kawashima, and H. Yamaguchi, *Appl. Phys. Lett.*, **50**, 1686 (1987).
2. M. Asai, F. Sato, H. Imamoto, and M. Shimura, *J. Appl. Phys.*, **64**, 432 (1988).

3. R. Katsumi, H. Ohno, H. Ishii, K. Matsuzaki, Y. Akatsu, and H. Hasegagwa, *J. Vac. Sci. Technol.*, **B6,** 593 (1988).
4. J.M. Gerard and J. Y. Marzin, *Appl. Phys. Lett.*, **53**, 568 (1988).
5. H. Munekata, L.L. Chang, S.C. Wononick and Y.H. Kao, *J. Cryst. Growth*, **81**, 237 (1987).
6. S. Kalem, *J. Appl. Phys.*, **66**, 3097 (1989).
7. J.R. Soderstrom, D.H. Chow and T.C. McGill, *MRS Symposium Proceedings*, **145**, 409 (1989).
8. F.J. Grunthaner, M.Y. Yen, R. Fernandez, T.C. Lee, A. Madhukar, and B.F. Lewis, *Appl. Phys. Lett.*, **46**, 983 (1985).

Growth and characterization of GaAs grown by metalorganic molecular-beam epitaxy using trimethylgallium and arsenic

C. W. Tu, B. W. Liang,[a] T. P. Chin, and J. Zhang
Department of Electrical and Computer Engineering, University of California at San Diego, La Jolla, California 92093-0407

(Received 13 September 1989; accepted 9 December 1989)

We report a study of growth kinetics of metalorganic molecular-beam epitaxy (MOMBE) of GaAs by reflection high-energy electron diffraction (RHEED) intensity oscillation and characterization of these MOMBE-grown GaAs layers by Hall effect measurement and x-ray rocking curve analysis. The growth rate depends not only on the substrate temperature but also on the arsenic pressure. The high p-type doping by carbon, in the high 10^{19}-cm^{-3} range, results in strain and a smaller lattice constant in the epitaxial layer. Rapid thermal annealing, however, can improve the crystalline quality of the layer without degrading the electrical properties.

I. INTRODUCTION

The use of gaseous organometallic sources in a molecular-beam epitaxy (MBE) system—metalorganic MBE (MOMBE) or chemical beam epitaxy (CBE)—has received increasing attention because it combines advantages of metalorganic vapor-phase epitaxy (MOVPE) and MBE.[1] Some of these advantages are high-throughput potential[2,3] and selective-area epitaxy.[4,5] To reduce carbon incorporation, triethylgallium (TEGa) is used. Trimethylgallium (TMGa), however, can be added to the TEGa source to produce a range of p-type doping up to mid 10^{20} cm^{-3} (Ref. 6). Such high carbon doping is useful, e.g., for the base of a heterojunction bipolar transistor (HBT), due to much lower diffusivity of carbon as compared to that of the commonly used Be in MBE.[7]

Monitoring of reflection high-energy electron diffraction (RHEED) intensity oscillations during growth has been used extensively to study growth kinetics of CBE of GaAs using TEGa and arsine,[8,9] but not so much for growth of GaAs using TMGa.[10] Since TMGa is also used in CBE or MOMBE of GaAs for carbon doping, it is therefore important to study in more detail the growth kinetics of GaAs using TMGa. In CBE cracked arsine produces various forms of arsenic hydrides, hydrogen and arsenic molecules, the growth process, therefore, will be more complicated. Also because of the safety issue, in some instances, MOMBE using TMGa and solid arsenic may be preferred.

In this paper we report on the growth kinetics of MOMBE of GaAs using TMGa and solid As_4. We use RHEED intensity oscillations to determine the dependence of growth rates on the substrate temperature and arsenic pressure. Furthermore, we measure the high carbon doping concentration by Hall effect measurement and characterize the samples by x-ray rocking curve analysis and rapid thermal annealing.

II. EXPERIMENTAL PROCEDURE

The growth was performed in a modified prototype Perkin–Elmer 425A MBE system. The growth chamber was pumped by a cryopump and an ion pump. TMGa molecules were directly injected into the growth chamber from a cylinder through a leak valve and an on–off valve upstream. Initially the cracking pattern in the quadruple mass spectrum indicated the presence of extraneous hydrocarbons in the TMGa flux. However, after an initial period of flushing the TMGa flux, the cracking pattern became that of pure TMGa. The RHEED intensity was monitored by a photodiode through an optical fiber. GaAs substrates were etched and cleaned in the usual manner and then mounted on molybdenum blocks. The substrate was thermally cleaned in vacuum under an overpressure of arsenic. The substrate temperature was calibrated by a thermal couple inserted into a Mo block and also independently by a pyrometer. Nevertheless, the uncertainty absolute temperature could still be ~20 °C. Typical fluxes as measured by the ionization gauge behind the substrate holder when the holder is out of the way were 6×10^{-7} and 5×10^{-6} Torr for TMGa and As_4, respectively.

Due to the arrangement of the valves in the TMGa line in our initial setup, for a TMGa flux giving rise to a growth rate of about 1.5 monolayers (ML) per second, we observed an oscillation with slow growth rate due to the residual gas molecules in the tube, even though the TMGa valve was closed. We therefore limited the TMGa flux to obtain a growth rate of about 0.5 ML per second.

III. GROWTH KINETICS

To study the growth kinetics of MOMBE we recorded RHEED oscillations for a variety of growth parameters. The three RHEED oscillation patterns, as shown in Fig. 1, indicate qualitatively the dependence of growth rate as a function of the substrate temperature and arsenic pressure. In the course of the experiment the arsenic cell temperatures were varied without moving the sample out of the way to measure the flux-gauge reading. Therefore, only the arsenic cell temperatures are indicated. The flux-gauge readings were in the 10^{-6}-Torr range, as checked later. Curve (b) was obtained for a growth temperature of about 610 °C and an arsenic cell temperature of 218 °C. Curve (a) was for the same arsenic flux but lower substrate temperature, about 530 °C. Curve (c) was for the same substrate temperature as curve (b), but at a higher arsenic pressure (the cell temperature being 235 °C). Qualitatively the oscillation patterns are similar to

 0734-211X/90/020293-04$01.00 © 1990 American Vacuum Society

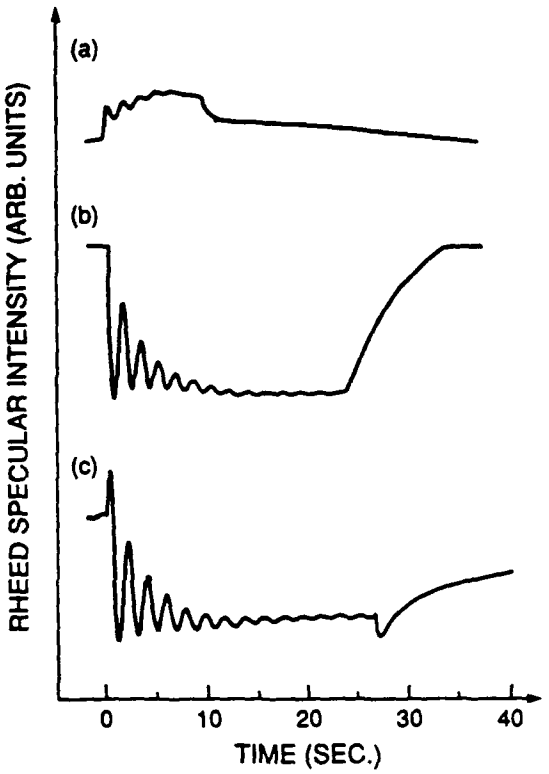

FIG. 1. RHEED oscillation behavior for (a) $T_s \sim 530$ °C and $T(As_4) = 218$ °C, (b) $T_s \sim 610$ °C and $T(As_4) = 218$ °C, and (c) $T_s \sim 610$ °C and $T(As_4) = 235$ °C.

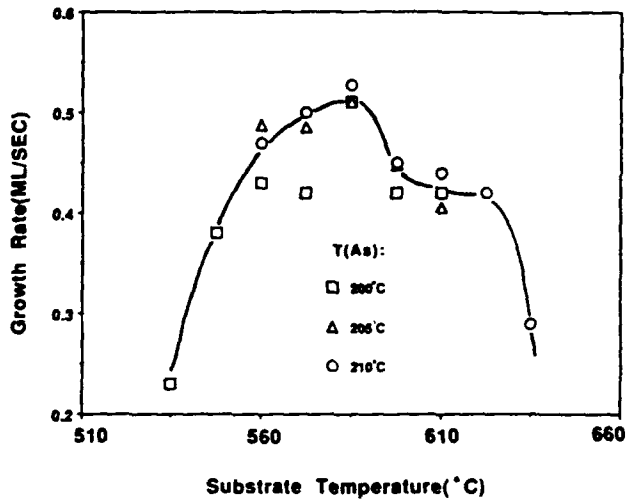

FIG. 2. The growth rate in monolayers per second (ML/s) as a function of the substrate temperature T_s in °C. The data, compiled for three different arsenic pressures, are normalized at the highest growth rate to account for a slight variation of growth rate with arsenic pressure.

those of conventional MBE. The initial decrease or increase of the RHEED intensity after the TMGa valve was opened depends on the surface reconstruction for a particular substrate temperature T_s and arsenic pressure. The recovery time constant is faster for lower arsenic pressure than for higher arsenic pressure, as expected, due to the longer Ga migration length at lower arsenic flux. The growth rate with higher arsenic flux is also lower than that with lower arsenic flux due to the site-blocking mechanism at high arsenic overpressure.[10,11] In general, it is more difficult to observe RHEED oscillations at a low substrate temperature due to incomplete pyrolytic decomposition of the TMGa molecules.

We find that the behavior of the RHEED intensity oscillation for TMGa growth has similarities and differences as compared to that of CBE growth using TEGa and arsine, reported by Chiu *et al.*[10] The growth rate, as determined from gallium-induced oscillations, depends on the growth temperature, but in a more complicated fashion than the TEGa case, as shown in Fig. 2. Instead of a single maximum in the growth rate as a function of growth temperature in the case of TEGa, we observed two local maxima. Our preliminary modeling, not taking into account the effect of arsenic species, indicates that in the low-temperature regime the growth rate is mainly determined by the decomposition of TMGa molecules into various derivatives, whereas in the intermediate temperature regime the growth rate is mainly determined by the decomposition of dimethylgallium (DMGa). At the high-temperature regime, the decrease in growth rate is due to the desorption of adsorbed surface gallium atoms. The combined effects result in the two broad local maxima. This result is in contrast to the case of CBE growth of GaAs using TMGa and arsine where Chiu observed a nearly constant growth rate even at high temperature.[10] The discrepancy could be due to the presence of hydrogen or different arsenic pressures (higher in his case). The detail of our modeling will be reported later.

As mentioned earlier, the growth rate also depends on the arsenic flux. At higher arsenic flux the growth rate decreases due to the site-blocking mechanism where arsenic molecules on the surface can prevent adsorption of the large TMGa molecules and thus decrease the growth rate. This result is similar to that in CBE of GaAs using TEGa and arsine.[10,12] However, unlike Refs. 10 and 12, where only the high arsenic overpressure regime was studied, we could observe the arsenic-induced oscillations at low arsenic pressure regime, where the growth is controlled by the availability of arsenic, rather than gallium species. The details of the arsenic-induced oscillations were reported elsewhere.[11] Under appropriate conditions, when the arsenic flux is absent, the RHEED data indicates the possibility of atomic-layer epitaxy (ALE). This is in sharp contrast to CBE of GaAs using TEGa, but was independently observed by Chiu in the case of CBE using TMGa.[10] Figure 3 shows three RHEED oscillation patterns with four distinct regions for different arsenic overpressures but the same growth temperature of 580 °C. Region 1 is the starting condition where only arsenic was present. Then at $t = 0$ TMGa molecules were introduced, and growth of GaAs commenced. This is region 2. Region 3 is the period when the shutter of the arsenic cell was closed but the TMGa valve remained open. Region 4 is similar to region 1, where the TMGa valve was closed and the shutter of the arsenic cell was opened.

In the top curve (a), the arsenic pressure was sufficiently high that when the shutter was closed, the background arsenic pressure was still high. (In this MBE system the ar-

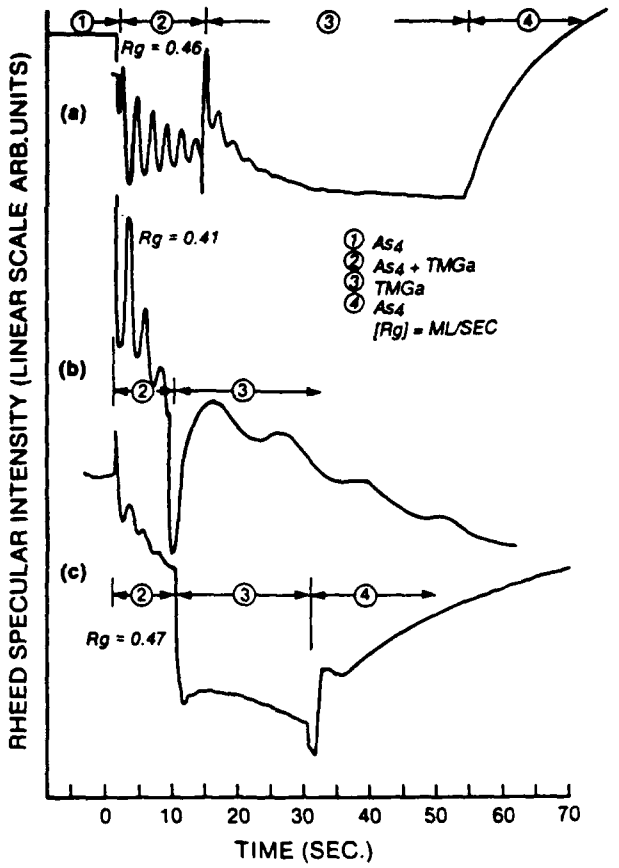

FIG. 3. The RHEED intensity behavior for high, intermediate, and low arsenic overpressures, (a), (b), and (c), respectively. Region 1 was the quiescent state with only arsenic overpressure. Even for the case (c), the growth was controlled by the group III flux in region 2. Arsenic shutter is closed in region 3, while the TMGa flux continued to impinge on the surface. Region 4 is the recovery state where the TMGa valve was closed and the arsenic shutter was opened.

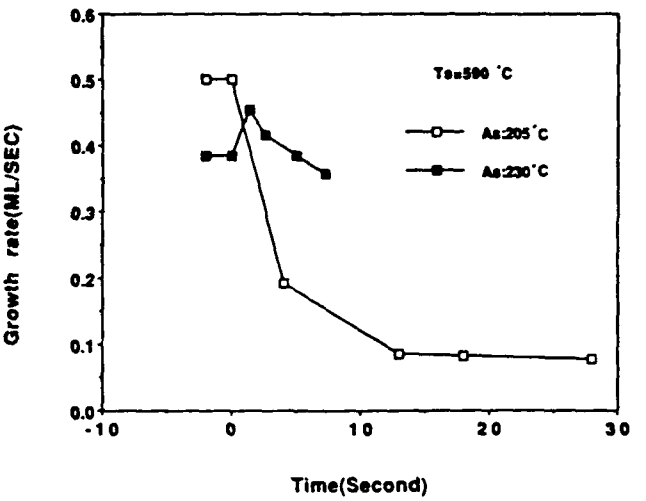

FIG. 4. Growth rate as a function of time for curves (a) and (b) in Fig. 3. The arsenic shutter was closed at $t = 0$ s. For curve (b) the growth was controlled by the background arsenic pressure. In curve (a) the initial increase in growth rate reflects the more complicated situation in MOMBE of GaAs, as compared to MBE.

senic pressure decreases only about a factor of 3 in the first few seconds after the shutter is closed.) Therefore, with enough As_4 in the background, in region 3 the growth was still controlled by the TMGa flux. When the growth was interrupted, the RHEED intensity recovered (region 4). When the arsenic cell temperature was decreased, the middle curve (b) showed the slow oscillation in region 3. In this case the arsenic pressure was sufficiently low that the growth was controlled by the background available arsenic flux. Figure 4 plots the growth rates as a function of time for curves (a) and (b). The initial increase in the growth rate for the case (a) is another indication that there is a maximum growth rate at a particular arsenic pressure for a given substrate temperature.[11]

When the arsenic flux was decreased still further, indicating to a nearly stoichiometric condition, in region 3 we observed only half an oscillation although we had deposited equivalent to several monolayers of TMGa. When the TMGa valve was closed and the shutter to the arsenic cell was opened, we saw a dip and then a recovery, corresponding to roughly one monolayer of growth. This behavior is different from CBE of GaAs using TEGa and arsine, where in region 4 arsenic-induced oscillation was observed for several periods. This difference in the behavior between TMGa and TEGa has also been independently observed by Chiu[10] in the CBE case. The likely explanation is the existence of a metastable methylgallium overlayer which prevents additional adsorption of gallium species. Therefore, the process is self-limiting, forming the basis for atomic-layer epitaxy (ALE), where the TMGa and arsenic are supplied to the substrate alternatingly. We should note that the observed RHEED intensity behavior is just an indication, not a direct proof, of ALE. We shall explore this possibility of ALE in the MOMBE configuration further.

IV. MATERIALS PROPERTIES AND RTA

Similar to a number of reports,[6] we obtained very high p-type doping by carbon, in the high 10^{19}-cm^{-3} range for a growth rate of about 0.5 ML per second. The measurements were performed on a double ac Hall setup.[13] Sample results are 6.8×10^{19} and 9.4×10^{19} cm^{-3} with room temperature Hall mobilities of 92 and 78 cm^2/V s, respectively. It is expected that the doping concentration would be higher for higher growth rate.

X-ray rocking curve measurement, taken with a four-crystal diffractometer, indicates the presence of strain due to heavy carbon doping, showing a small peak with a smaller lattice constant. This is as expected due to the smaller size of the carbon atoms, compared to those of Ga and As. However, this is in contrast to the result reported by Yamada *et al.*[14] and Houng *et al.*,[15] who showed no change in lattice constants in heavily carbon-doped GaAs. Figure 5 shows three x-ray rocking curves for (a) as-grown sample, (b) the same sample after furnace annealing at 400 °C for 30 min, and (c) another piece after rapid thermal annealing (RTA) at 900 °C for 10 s. RTA was performed in a homemade setup under a flow of forming gas. The samples were placed under

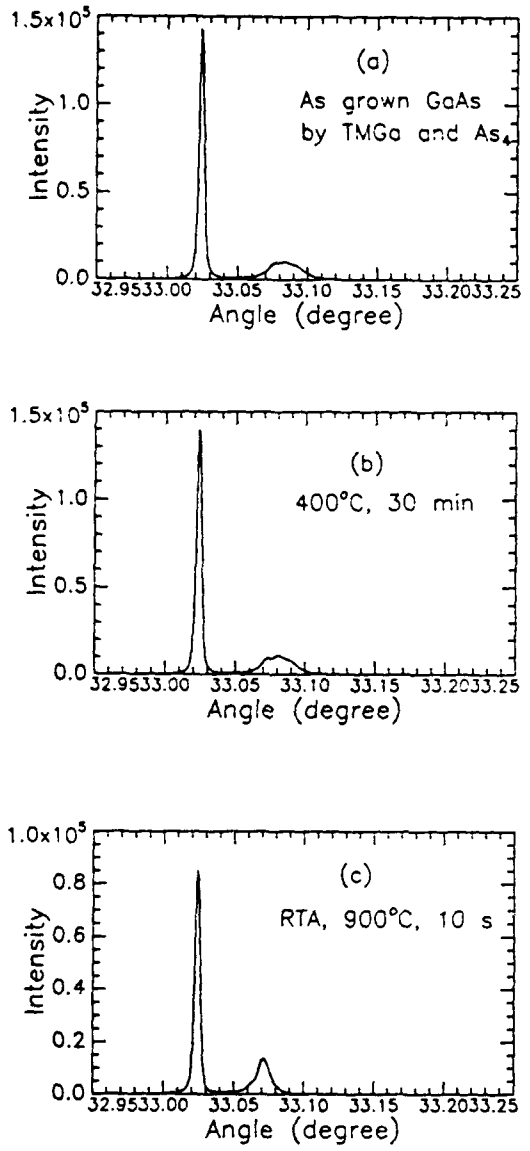

FIG. 5. X-ray rocking curves of heavily carbon-doped GaAs for (a) as-grown sample, (b) the same sample after furnance annealing, and (c) another piece after RTA. The abscissa is rocking curve angles in degrees, and the ordinate Y is the x-ray intensity in an arbitrary unit. The sharp peak is due to the substrate, and the smaller and broader peak is due to the epitaxial layer.

a piece of GaAs wafer and were first soaked at 550 °C for 10 s. Then the temperature was raised to 900 °C in 5 to 8 s and stayed for 10 s. Subsequently the power supply was turned off for rapid cool down.

It is clear that furnace annealing has no appreciable effect on the x-ray data but RTA improves the structural quality of the layer. The full width at maximum of the unannealed sample is ~90 arc s, whereas that of the sample after RTA is ~45 arc s. After RTA there is also a slight shift of the lattice constant towards that of GaAs. Hall measurement for a sample after RTA shows a small decrease in the carrier concentration, from 7.6×10^{19} to 6.8×10^{19} cm^{-3} with no change in the hole mobility (from 83 to 79 cm^2/V s). The decrease in the free carrier concentration could be due to precipitate formation or site switching of the carbon atoms. Further study on the effect of RTA is required to elucidate this point. Nevertheless, RTA is a beneficial method for improving the crystalline structure without degrading electrical properties of the film.

V. SUMMARY

We observe that MOMBE growth of GaAs is much more complicated than conventional MBE due to the surface chemistry of organometallic molecues. MOMBE of GaAs using TMGa and As_4 is different from CBE using TEGa or TMGa and arsine. We also observe an indication of ALE for MOMBE growth using TMGa for low arsenic overpressure. GaAs films grown with TMGa have high carrier concentration; however, the high carbon doping degrades the structural quality. Nevertheless, we demonstrate that RTA can improve structural quality without degrading electrical properties.

ACKNOWLEDGMENTS

This work is partially supported by the Air Force Wright Aeronautical Laboratory under Contract No. F33615-88-C-1861 and by the Office of Naval Research under Grant No. N00014-89-J-1259. We wish to thank Professor H. H. Wieder and Dr. Art Clawson, Dr. Heng Chiu, and Dr. Alex Robertson, Jr. for fruitful discussions. We also want to thank Mr. Wei Xia and Professor S. S. Lau for the help in using the RTA setup and Professor Wieder for the Hall measurement setup. We wish to acknowledge AT&T Bell Laboratories for loaning the MBE system to UCSD.

[a] On leave from the Shanghai Institute of Metallurgy, Academia Sinica, Shanghai, China.

[1] For a review, see W. T. Tsang, J. Cryst. Growth **81**, 261 (1987).
[2] L. Fraas, G. R. Girard, V. Sundaram, C. Master, C. Nelson, and R. A. Stall, Mater. Res. Soc. Symp. Proc. **145**, 253 (1989).
[3] Y-M. Houng, Y-C. Pao, and P. McLeod, Ref. 2, p. 63.
[4] V. M. Donnelly, C. W. Tu, J. C. Beggy, V. R. McCrary, M. G. Lamont, T. D. Harris, F. A. Baiocchi, and R. C. Farrow, Appl. Phys. Lett. **52**, 1065 (1988).
[5] H. Sugiura, R. Iga, T. Yamada, and M. Yamaguchi, Appl. Phys. Lett. **54**, 335 (1989).
[6] M. Weyers, N. Putz, H. Heniecke, M. Heyen, H. Luth, and P. Balk, J. Electron. Mater. **15**, 57 (1986).
[7] R. J. Malik, R. N. Nottenberg, E. F. Schubert, J. F. Walker, and R. W. Ryan, Appl. Phys. Lett. **53**, 2661 (1988).
[8] W. T. Tsang, T. H. Chiu, J. E. Cunningham, and A. Robertson, Jr., Appl. Phys. Lett. **50**, 1376 (1987).
[9] T. H. Chiu, W. T. Tsang, J. E. Cunningham, and A. Robertson, Jr., J. Appl. Phys. **62**, 2302 (1987).
[10] T. H. Chiu, Mater. Res. Soc. Symp. Proc. **145**, 47 (1989).
[11] B. W. Liang, T. P. Chin, and C. W. Tu, Appl. Phys. (in press).
[12] T. H. Chiu, J. E. Cunningham, and A. Robertson, Jr., J. Cryst. Growth **95**, 136 (1989).
[13] P. Chu, S. Niki, J. W. Roach, and H. H. Wieder, Rev. Sci. Instrum. **58**, 1764 (1987).
[14] T. Yamada, E. Tokumitsu, K. Saito, T. Akatsuka, M. Miyauchi, M. Konagai, and K. Takahashi, J. Cryst. Growth **95**, 145 (1989).
[15] Y.-M. Houng, J. N. Miller, B-J. Lee, and T. S. Low, J. Vac. Sci. Technol. B **8**, 355 (1990).

Reflection high-energy electron-diffraction study of metalorganic molecular-beam epitaxy of GaAs using trimethylgallium and arsenic

B. W. Liang,[a] T. P. Chin, and C. W. Tu
Department of Electrical and Computer Engineering, University of California at San Diego, La Jolla, California 92093-0407

(Received 2 October 1989; accepted for publication 22 January 1990)

The growth behavior of metalorganic molecular-beam epitaxial (MOMBE) growth of GaAs using trimethylgallium and solid arsenic is studied by the intensity oscillation behavior of reflection high-energy electron-diffraction (RHEED). The growth process is more complicated than conventional MBE using elemental sources. In MOMBE the growth rate depends not only on the substrate temperature but also on the arsenic pressure. In addition, the RHEED behavior indicates a possibility of atomic layer epitaxy using trimethylgallium.

The use of gaseous sources for group III elements in growing III-V compound semiconductors in a molecular-beam epitaxy (MBE) system has gained increasing interest not only for the fundamental studies of growth kinetics[1-3] but also for device applications due to its potential for high throughput[4,5] and selective-area epitaxy.[6,7] To reduce carbon incorporation, triethylgallium (TEGa) is used. Trimethylgallium (TMGa), however, can be added to the TEGa source to produce a range of *p*-type doping[8] up to 10^{21} cm^{-3}. Such high carbon doping is useful, e.g., for the base of a heterojunction bipolar transistor (HBT), due to the much lower diffusivity of carbon[9] as compared to that of the commonly used Be in MBE.

The intensity oscillation of the reflection high-energy electron-diffraction (RHEED) has been used extensively to study the growth kinetics of CBE growth of GaAs using TEGa,[10,11] but not so much for the growth of GaAs using TMGa.[12] Since TMGa is also used in CBE or MOMBE of GaAs for carbon doping,[8,13] it s therefore important to study in more detail the growth kinetics of GaAs using TMGa. Because of the safety issue and the simplicity of operation, we study the MOMBE growth of GaAs using TMGa and solid arsenic.

The experiment is performed in a modified PHI 425A MBE system. The TMGa molecules are directly injected into the growth chamber without hydrogen carrier gas through a leak valve and an on-off valve upstream. The RHEED intensity is monitored by a photodiode through an optical fiber. To optimize the growth conditions we record RHEED oscillations for a variety of growth parameters. Figure 1 shows the growth rates as a function of the arsenic beam-equivalent pressure for different growth temperatures. The growth kinetics of MOMBE is complicated as compared to conventional MBE. The growth rate decreases at high arsenic overpressure, similar to the observation on CBE using TEGa.[12] The explanation is most likely the kinematical site-blocking model, where the arsenic dimers or tetramers adsorbed on the surface prevent adsorption of the large TMGa molecules.[12] Therefore, the higher the arsenic overpressure is, the lower the TMGa coverage on the surface, resulting in lower growth rates. Unlike the reported monotonic decrease of growth rates with arsenic pressure in CBE using TEGa,[14] we studied the growth behavior also in the regime of lower arsenic pressure. We found that the growth rates decreased with lower arsenic pressure. We note that in this regime studied, the surface still exhibited an arsenic-stabilized (2×4) surface reconstruction pattern. This observation indicates that in a surface reaction forming GaAs arsenic species are involved in a rate-limiting step. This situation is different from solid-source MBE where the rate-limiting step in an arsenic-stabilized regime involves only gallium surface concentration. We also note that the peak growth rate moved to higher arsenic pressure as the substrate temperature was increased. This is due to the increasing desorption of adsorbed arsenic species with increasing substrate temperature. Therefore, high arsenic flux is required to maintain the same V/III ratio at a higher substrate temperature.

Figure 2 shows the growth rate as a function of the substrate temperature for different arsenic overpressures. At low substrate temperature surface pyrolysis is inefficient and the growth rate is low. The growth rate increases with increasing temperature on the low side, but starts to decrease after about 600 °C probably due to desorption of adsorbed TMGa molecules or the derivatives. The data for different arsenic pressures are incomplete in some cases due to the difficulty in observing RHEED oscillations in those cases. We note that the growth rate exhibits a peak at a substrate temperature at about 585 °C. This behavior is also observed by Yamada *et al.* (using solid arsenic)[13] and Isu, Hata, and Watanabe (using arsine).[14] At present we are modeling the growth mechanisms of MOMBE of GaAs[15] and InAs,[16] taking into account the role of arsenic, and the results will be presented elsewhere.

Finally we shall address the issue of atomic layer epitaxy (ALE). ALE has been actively pursued by a number of groups working on MOCVD.[17] In the MOMBE case we can use the powerful *in situ* real-time RHEED intensity oscillation technique to pinpoint the precise condition for ALE. Figure 3 shows three RHEED oscillation patterns with four distinct regions for different arsenic overpressures but the same growth temperature of 580 °C. Region 1 is the starting condition where only arsenic is present. Then at $t = 0$ the

[a] On leave from the Institute of Metallurgy, Academia Sinica, Shanghai, China.

 0021-8979/90/094393-03$03.00 © 1990 American Institute of Physics

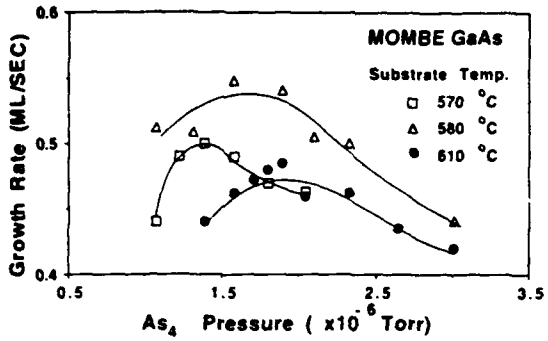

FIG. 1. Growth rates in ML (monolayers)/s as a function of arsenic beam-equivalent pressure (BEP) for three different growth temperatures. The lines are drawn to guide the eyes.

TMGa molecules are introduced, and the growth of GaAs commences. This is region 2. In region 3 the shutter of the arsenic cell is closed but the TMGa valve remains open. Region 4 is similar to region 1, where the TMGa valve is closed and the shutter of the arsenic cell is opened.

In the top curve (a) the arsenic pressure is sufficiently high so that when the shutter is closed, the background arsenic pressure is still high. In this MBE system the arsenic pressure decreases only about a factor of 3 in the first few seconds after the shutter is closed. Therefore, in region 3 the growth is still controlled by the TMGa flux. When the growth is interrupted, the RHEED intensity recovers. When the arsenic cell temperature is decreased, the middle curve (b) shows the slow oscillation in region 3. In this case the arsenic pressure is sufficiently low so that the growth is controlled by the background available arsenic flux. When the arsenic flux is decreased still further, corresponding to a nearly stoichiometric condition, we observe in region 3 only half an oscillation although we have deposited equivalent to several monolayers of TMGa. When the TMGa valve is closed and the shutter to the arsenic cell is opened, we see a dip and then a recovery. This behavior is different from CBE of GaAs using TEGa and arsine, where in region 4 arsenic-induced oscillation is observed for several periods. This difference in the behavior between TMGa and TEGa has also been independently observed by Chiu.[14] The likely explanation is the existence of a metastable methylgallium overlayer which prevents additional adsorption of gallium species. Therefore, the process is self-limiting, forming the basis for atomic layer epitaxy (ALE), where the TMGa and arsenic are supplied to the substrate alternatingly.

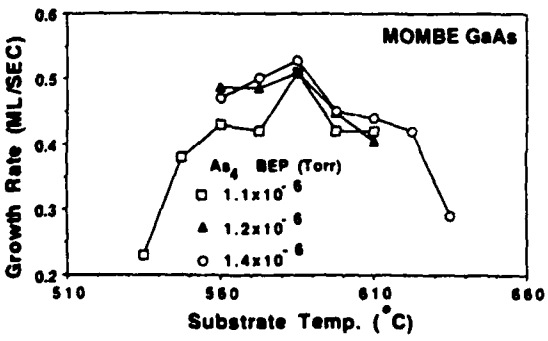

FIG. 2. Growth rates in ML/s as a function of substrate temperatures T_s in °C for three different arsenic overpressures. The lines are drawn to guide the eyes.

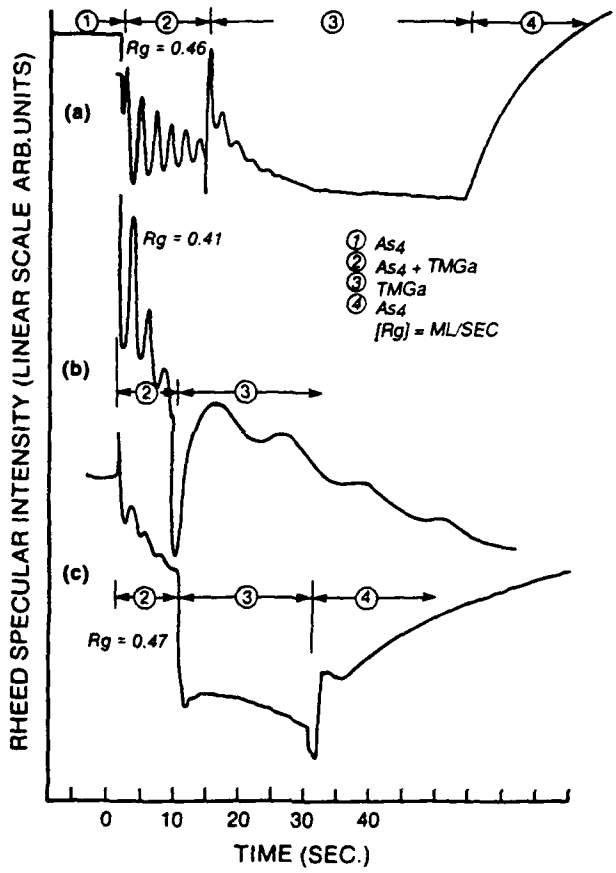

FIG. 3. RHEED intensity behavior for high, intermediate, and low arsenic overpressures, (a), (b), and (c), respectively. Region 1 is the quiescent state with only arsenic overpressure. In region 2 both arsenic shutter and TMGa valve are open. The arsenic shutter is closed in region 3. Region 4 is the recovery state where the TMGa valve is closed and the arsenic shutter is opened.

In summary, we observe that the MOMBE growth of GaAs is much more complicated than conventional MBE due to the surface chemistry of the organometallic molecules and arsenic. The RHEED oscillation behaviors as a function of arsenic pressure and substrate temperature exhibit similarity and difference between TMGa and TEGa. The RHEED behavior at low arsenic overpressure indicates the presence of a metastable methylgallium species on the surface, resulting in ALE of GaAs. Electrical and structural characterization are reported separately.[18]

This work is partially supported by the Air Force Wright Aeronautical Laboratory under Contract No. F33615-88-C-1861 and by the Office of Naval Research under Grant No. N00014-89-J-1147. We wish to thank Professor Harry Wieder and Dr. Art Clawson, Dr. T. H. Chiu, and Dr. Alex Robertson, Jr. for fruitful discussions. We also wish to acknowledge AT&T Bell Laboratories for loaning the MBE system to UCSD.

[1]E. Venhoff, W. Pletschen, P. Balk, and H. Luth, J. Cryst. Growth **55**, 30 (1981).
[2]W. T. Tsang, Appl. Phys. Lett. **45**, 1234 (1984).
[3]S.Horiguchi, K. Kimura, K. Kamon, M. Mashita, M. Shimazu, M. Mihara, and M. Ishii, Jpn. J. Appl. Phys. **25**, L979 (1986).
[4]L. Fraas, G. R. Girard, V. Sundarain, C. Master, C. Nelson, and R. A. Stall, MRS Symp. Proc. **145**, 253 (1989).
[5]Y.-M. Houng, Y.-C. Pao, and P. McLeod, MRS Symp. Proc. **145**, 63 (1989).
[6]V. M. Donnelly, C. W. Tu, J. C. Beggy, V. R. McCrary, M. G. Lamont, T. D. Harris, F. A. Baiocchi, and R. C. Farrow, Appl. Phys. Lett. **52**, 1065 (1988).
[7]H. Sugiura, R. Iga, T. Yamada, and M. Yamaguchi, Appl. Phys. Lett. **54**, 335 (1989).
[8]M. Weyers, N. Putz, H. Heniecke, M. Heyen, H. Luth, and P. Balk, J. Electron Mater. **15**, 57 (1986).
[9]R. J. Malik, R. N. Nottenberg, E. F. Schubert, J. F. Walker, and R. W. Ryan, Appl. Phys. Lett. **53**, 2661 (1988).
[10]W. T. Tsang, T.H. Chiu, J. E. Cunningham, and A. Robertson, Jr., Appl. Phys. Lett. **50**, 1376 (1987).
[11]T. H. Chiu, W. T. Tsang, J. E. Cunningham, and A. Robertson, Jr., J. Appl. Phys. **62**, 2302 (1987).
[12]T. H. Chiu, MRS Symp. Proc. **145**, 47 (1989).
[13]T. Yamada, E. Tokumitsu, K. Saito, T. Akatsuka, M. Miyauchi, M. Konagai, and K. Takahashi, J. Cryst. Growth **95**, 145 (1989).
[14]T. Isu, M. Hata, and A. Watanabe, Second International Conference on Chemical Beam Epitaxy and Related Growth Techniques, Paper TP9, Houston, Texas, December 11–13, 1989, J. Cryst. Growth (in press).
[15]B. W. Liang, L. Y. Wang, and C. W. Tu (unpublished).
[16]C. W. Tu, B. W. Liang, and T. P. Chin, J. Cryst. Growth (in press).
[17]For a review, see C. H. L. Goodman and M. V. Pessa, J. Appl. Phys. **60**, R65 (1986).
[18]C. W. Tu, B. W. Liang, T. P. Chin, and J. Zhang, J.Vac. Sci. Technol B **8** (in press).

Journal of Crystal Growth 105 (1990) 195–198
North-Holland

THE EFFECTS OF ARSENIC OVERPRESSURE IN METALORGANIC MOLECULAR BEAM EPITAXY OF GaAs AND InAs

C.W. TU, B.W. LIANG * and T.P. CHIN

Department of Electrical and Computer Engineering, University of California at San Diego, La Jolla, California 92093-0407, USA

GaAs and InAs grown by metalorganic molecular beam epitaxy (MOMBE) using trimethyl compounds and arsenic are compared. Not only the substrate temperature but also the arsenic overpressure play a very important role in affecting the growth rates. A simple growth kinetics model for MOMBE of InAs can explain quantitatively the growth behavior for various substrate temperatures and arsenic pressure.

1. Introduction

Metalorganic molecular beam epitaxy (MOMBE) or chemical beam epitaxy (CBE) has received increasing attention because of its potential as a high-throughput (multiple wafers per growth run) technique and because of its ease of composition grading through the use of electronic mass flow controllers [1], similar to metalorganic chemical vapor deposition (MOCVD). Preliminary results of such a multiple-wafer reactor, based on MOMBE (also called vacuum chemical epitaxy), has been reported recently [2]. In this reactor, a single gas line is fanned out into multiple injection points in the growth chamber so that a large-area uniform beam can be generated. Because of the long mean free path of the molecules in a typical MOMBE operating pressure ($< 10^{-4}$ Torr), gas phase reactions are not important as in MOCVD. MOMBE growth occurs through surface pyrolysis of organometallic molecules on the heated substrate surface, and the growth behavior for various growth parameters will be determined by detailed surface chemical reactions [3].

Initial growth data indicated that the growth rate, measured by the cleave-and-stain method, behaved in a manner similar to that of MBE; i.e., the growth rate is independent of substrate temperature and arsenic pressure over a large range of values [4]. However, once the reflection high-energy electron diffraction (RHEED) intensity oscillation technique was used to monitor growth rates under a variety of CBE growth conditions of GaAs, the growth rate was found to depend sensitively on the substrate temperature due to the nature of surface chemical reactions [5]. Recently the growth rate of CBE of GaAs was found to decrease at high arsenic overpressure, and this was attributed to the site-blocking effect [6]. Too much arsenic on the surface would prevent adsorption of alkylgallium molecules and result in lower growth rate. These data, however, did not cover the range of low arsenic overpressure. Furthermore, the only quantitative kinetics model that can fit the growth rate data from CBE of GaAs does not take into account the effect of arsenic [3].

In this paper we show that not only the substrate temperature, but also the arsenic species play a very important role in affecting the growth behavior of MOMBE of GaAs and InAs. For the case of InAs we have developed a quantitatively predictive growth kinetics model that includes the effect of arsenic [7]. In fact, it is difficult to say which species would determine the growth rate in MOMBE. The control of substrate temperature and arsenic overpressure is thus very stringent in achieving layer thickness and composition uniformity in a multiple-wafer MOMBE system.

* On leave from the Shanghai Institute of Metallurgy, Academia Sinica, People's Rep. of China.

0022-0248/90/$03.50 © 1990 – Elsevier Science Publishers B.V. (North-Holland)

2. Experimental procedures

The experiments were performed in a modified prototype Perkin-Elmer 425A MBE system. The organometallic molecules, trimethylgallium (TMGa) and trimethylindium (TMIn), were injected directly into the growth chamber without carrier gas through an ultrahigh vacuum leak valve. Reflection high-energy electron diffraction (RHEED) intensity oscillations were used to measure the growth rates, and mass spectroscopy was used to monitor background gas-phase species and, more importantly, how they were affected by the substrate temperature and arsenic pressure. The substrate temperature was calibrated by a thermal couple inserted into a Mo block and also independently by a pyrometer. InAs was grown directly onto the GaAs(001) substrate. The detail of the setup is described elsewhere [8].

3. Results and discussion

Figs. 1 and 2 show the growth rates of GaAs and InAs, respectively, as a function of substrate temperature for three different arsenic overpressures. The lines through data points for GaAs are drawn to guide the eye [9], but those for InAs are calculations from our kinetics model [7], which will be discussed later. The initial increase in growth rate at low substrate temperature range is due to increased pyrolysis of the organometallic

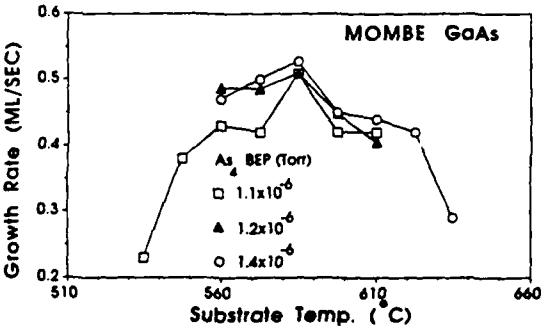

Fig. 1. Growth rate of MOMBE of GaAs using TMGa and As_4, measured by RHEED intensity oscillations, as a function of substrate temperature for different arsenic overpressures. The lines are drawn to guide the eye.

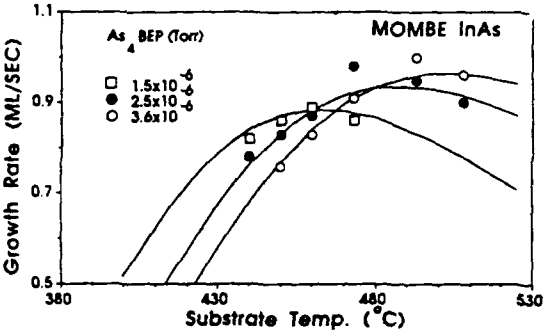

Fig. 2. Growth rate of MOMBE of InAs, using TMIn and As_4, as a function of substrate temperature for different arsenic overpressures. The lines are calculations based on our kinetics model [7].

molecules, while the decrease in growth rate at high substrate temperature range is due to desorption of organometallic molecules adsorbed on the surface. To get an idea of what the principal molecular species were on the surface during growth, we also monitored gas-phase species by mass spectroscopy as a function of substrate temperature and arsenic overpressure. Since the incident or desorbing beam was not modulated, the molecules detected had made a number of collisions with the walls. However, they still were affected by the growth parameters. Dimethylindium (DMIn) signal was found to increase more rapidly at a temperature that corresponds to the onset of decreasing growth rate with increasing substrate temperature. We therefore postulate that DMIn surface population controls the growth [7]. For the case of GaAs, mass spectroscopy was not performed, but it is reasonable to assume that cleavage of one methyl radical from DMGa would be the rate-limiting step. Because monomethylgallium (MMGa) and monomethylindium (MMIn) are expected to chemisorb strongly (so that desorption is unlikely) and have much lower activation barriers to liberate Ga or In on the surface, the cleavage of the last methyl group from MMGa and MMIn occurs much faster than the previous cleavage steps [10]. Therefore, the rate-limiting step is most likely the decomposition of dimethyl molecules. This situation is similar to that of CBE of GaAs using TEGa and arsine [3].

Figs. 3 and 4 show the growth rates of GaAs and InAs, respectively, as a function of arsenic pressure for different substrate temperatures. We see that the growth rate depends sensitively on the arsenic overpressure. The curves through data points for GaAs were drawn to guide the eye, but those for InAs are again calculations predicted by our growth kinetics model [7]. The decrease of growth rate at high arsenic overpressure can be interpreted to be due to the site-blocking effect [10]. However, for InAs grown at 490 °C the growth rate increases with increasing arsenic overpressure. To understand this phenomenon, we need a detailed reaction kinetics model. What differentiates our model from others is that we also take into account the effect of arsenic by requiring the presence of arsenic in the decomposition of DMIn. That is, the growth rate is proportional to the product of surface DMIn and arsenic concentrations, not just on surface DMIn concentration alone. In addition, the presence of arsenic also enhances desorption of trimethylindium species on the surface to take into account the site-blocking effect.

In our model we assume that no In atoms desorb from the growing surface in the temperature range studied because the In signal is negligible in our mass spectrometer until the substrate temperature is above 540°C. Another assumption is that the arsenic sticking coefficient, and hence the arsenic surface concentration, is independent

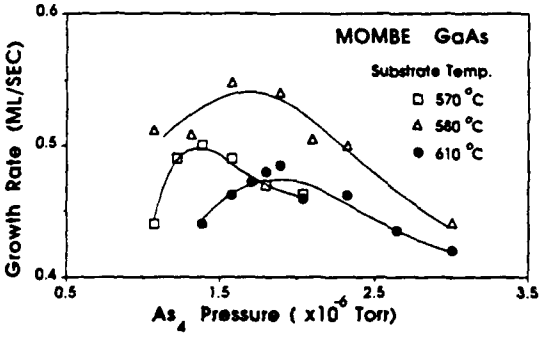

Fig 3. Growth rate of MOMBE of GaAs as a function of arsenic overpressure at different substrate temperatures. The lines are drawn to guide the eye.

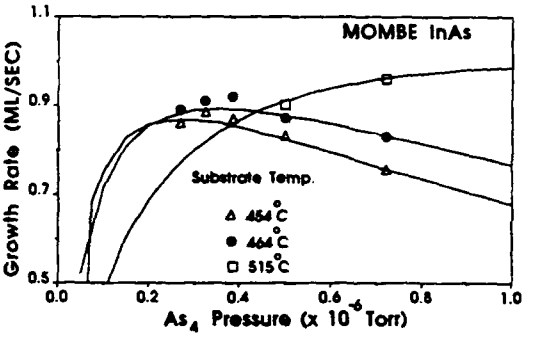

Fig. 4. Growth rate of MOMBE of InAs as a function of arsenic surface coverage at different substrate temperatures. The lines are calculations based on our kinetics model [7], which fits the arsenic overpressure to arsenic surface coverage.

of substrate temperature for a given arsenic and TMIn flux. Although there is no experimental verification of this assumption for growing InAs, Chow and Fernandez have shown that the sticking coefficient of As_4 is constant on a GaAs(001) surface up to 540 °C. Details of the model for InAs are described elsewhere [7].

In principle, MOMBE of GaAs using TMGa or TEGa and arsenic can be derived from a similar kinetics model as for InAs, but the situation is more complicated for the case of TMGa. The growth rate versus substrate temperature indicates another reaction pathway, resulting in "anomalous" growth behavior [11]. In addition, because GaAs is grown at relatively higher substrate temperature, we may have to take into account the fact that the surface arsenic sticking coefficient and therefore coverage start to decrease at a substrate temperature greater than 540 °C. Our initial fitting of MOMBE of GaAs with TEGa looks promising, however. Experimentally we find some similarities but also some differences between MOMBE of GaAs and InAs. We have observed a possibility of atomic layer epitaxy (ALE) using TMGa and arsenic [9], similar to Chiu's data [10], but not for TMIn. Carbon doped GaAs is p-type at high concentrations ($< 10^{20}$ cm^{-3} for growth rate of 0.5 monolayers per second [12]), but carbon doped InAs is n-type, in the mid 10^{18} cm^{-3} range for the substrate temperature range studied.

4. Summary

MOMBE is shown to be a complicated process due to surface reactions. As expected, the growth rate depends sensitively on substrate temperatures. However, arsenic overpressure is shown to influence the growth rate very much as well. The kinetics model proposed by the authors fits the InAs data very well. The model for GaAs is expected to be more complicated due to the possibility of temperature-dependent arsenic coverage and a second reaction pathway.

Acknowledgments

This work is partially supported by the Air Force Wright Research and Development Center under contract No. F33615-88-C-1861 and the Office of Naval Research under grant No. N00014-89-J-1147. We also thank Dr. A. Clawson for the trimethylindium cylinder, L.Y. Wang for help in data fitting, and the reviewer for critical comments.

References

[1] W.T. Tsang, J. Crystal Growth 81 (1987) 261.
[2] L. Fraas, G.R. Girard, V. Sundaram, C. Master, C. Nelson and R.A. Stall, in: III–V Heterostructures for Electronic/Photonic Devices, Mater. Res. Soc. Symp. Proc. 145, Eds. C.W. Tu, V.D. Mattera and A.C. Gossard (Mater. Res. Soc., Pittsburgh, PA, 1989) p. 253.
[3] A. Robertson, Jr., T.H. Chiu, W.T. Tsang and J.E. Cunningham, J. Appl. Phys. 64 (1988) 877.
[4] W.T. Tsang, Appl. Phys. Letters 45 (1984) 1234.
[5] W.T. Tsang, T.H. Chiu, J.E. Cunningham and A. Robertson, Jr., Appl. Phys. Letters 50 (1987) 1376.
[6] T.H. Chiu, J.E. Cunningham, and A. Robertson, Jr., J. Crystal Growth 95 (1989) 136.
[7] B.W. Liang and C.W. Tu, unpublished.
[8] B.W. Liang, T.P. Chin, L. Wang and C.W. Tu, J. Crystal Growth 105 (1990) 240.
[9] B.W. Liang, T.P. Chin and C.W. Tu, J. Appl. Phys. (Rapid Commun.) (May 1, 1990).
[10] T.H. Chiu, in: III–V Heterostructures for Electronic/Photonic Devices, Mater. Res. Soc. Symp. Proc. 145, Eds. C.W. Tu, V.D. Mattera and A.C. Gossard (Mater. Res. Soc., Pittsburgh, PA, 1989) p. 47.
[11] T. Isu, M. Hata and A. Watanabe, J. Crystal Growth 105 (1990) 209.
[12] C.W. Tu, B.W. Liang, T.P. Chin and J. Zhang, J. Vacuum Sci. Technol. B8 (1990) 293.

Journal of Crystal Growth 105 (1990) 240–243
North-Holland

A STUDY OF METALORGANIC MOLECULAR BEAM EPITAXY GROWTH OF InAs BY MASS SPECTROMETRY AND REFLECTION HIGH-ENERGY ELECTRON DIFFRACTION

B.W. LIANG *, T.P. CHIN, L.Y. WANG and C.W. TU

Department of Electrical and Computer Engineering, Mail Code R-007, University of California at San Diego, La Jolla, California 92093-0407, USA

Mass spectrometry and reflection high-energy electron diffraction intensity oscillations have been used to study metalorganic molecular beam epitaxy growth of InAs using trimethylindium and arsenic. We find that the growth rate increases and then decreases with increasing arsenic beam flux, as well as with increasing substrate temperature and that the decrease of growth rate at higher temperature seems to correspond to the increase of dimethylindium (DMIn) signal in mass spectroscopy.

1. Introduction

The use of organometallic sources in molecular-beam epitaxy (MBE) systems has attracted wide attention in recent years [1–3] due to its potential for high throughput [4] and selective-area epitaxy [5,6]. The dependence of growth rates of GaAs on substrate temperature in metalorganic MBE (MOMBE), where solid arsenic is used, or chemical-beam epitaxy (CBE), where arsine is used, has been reported [7,8]. Surface chemical reactions are very important in determining the growth behavior. Growth rates were measured with reflection high-energy electron diffraction (RHEED) intensity oscillations, but chemical identification of the dominant surface species in limiting the growth rate were not known but conjectured for a reaction model [7]. We studied InAs growth because trimethylindium (TMIn) is a common indium source in both metalorganic chemical vapor deposition (MOCVD) and MOMBE. Little is known about its surface reactions. We find that the growth rate of InAs depends not only on substrate temperature but also on arsenic overpressure. Mass spectroscopy (MS) data also confirm, indirectly, our postulate that decomposition of dimethylindium (DMIn) is the rate-limiting step.

2. Experimental procedure

The growth was performed in a modified prototype Perkin-Elmer 425A MBE system, as shown in fig. 1. The growth chamber was pumped by a cryopump and an ion pump. TMIn was directly injected into the growth chamber through a leak valve without hydrogen carrier gas. The RHEED intensity oscillation was monitored by a photodiode through an optical fiber. A Dycor quadrupole mass analyzer (QMA) was put in the central port

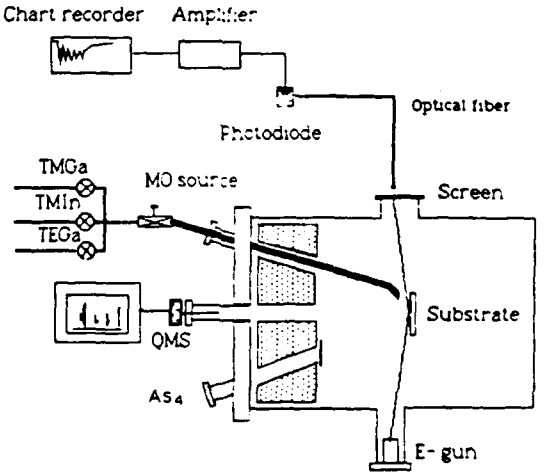

Fig. 1. A schematic diagram of our MOMBE system including mass spectroscopy and reflection high-energy electron diffraction.

* On leave from the Shanghai Institute of Metallurgy, Academia Sinica, Shanghai, People's Rep. of China.

0022-0248/90/$03.50 © 1990 – Elsevier Science Publishers B.V. (North-Holland)

of the source flange. GaAs substrates were cleaned and etched in the usual manner. InAs was grown directly on a GaAs (001) substrate. Substrate temperature was calibrated with a thermal couple and pyrometer. Growth temperature was in the range of 440 to 520°C.

3. Results and discussion

Fig. 2 shows the growth rate as a function of substrate temperature for two different arsenic overpressures. The growth rate increases with increasing substrate temperature due to more efficient pyrolysis of TMIn on the surface, but then the growth rate decreases at higher substrate temperature due to desorption of some TMIn-derived species from the surface. We use mass spectroscopy (MS) to provide some clues as to how various mass components behave with growth parameters. Because the incident or desorbing beam was not modulated, MS signals were from the ambient as molecules made a number of collisions with the walls before being detected. However, the signals were still affected by substrate temperatures and arsenic overpressures. Fig. 3 shows a typical mass spectrum during MOMBE growth of InAs. Peaks with mass numbers 90, 105 and 120 amu are identified to be $As(CH_3)^+$, $As(CH_3)_2^+$ and $As(CH_3)_3^+$, respectively. Peaks

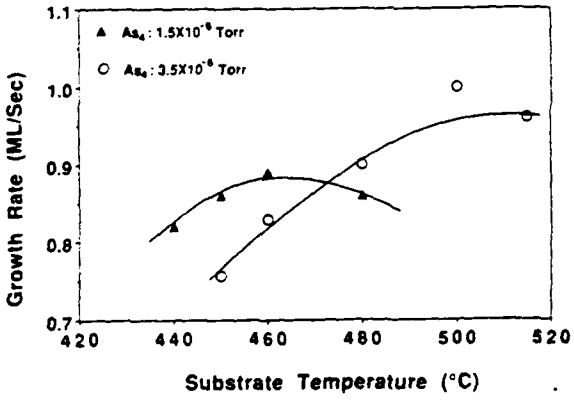

Fig. 2. MOMBE growth rate of InAs versus substrate temperature at two different arsenic overpressures. The curves are fitted by kinetics model [9].

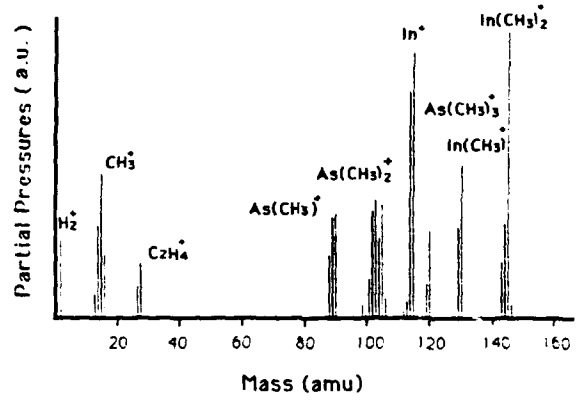

Fig. 3. A typical mass spectrum recorded during MOMBE growth of InAs using TMIn and arsenic.

with 115, 130 and 145 amu are In^+, $In(CH_3)^+$ (monomethylindium or MMIn) and $In(CH_3)_2^+$ (dimethylindium or DMIn), respectively. Peaks with 2, 15 and 28 amu are H_2^+, CH_3^+ and $C_2H_4^+$, respectively.

MS signals were recorded at different substrate temperatures and arsenic overpressures. Figs. 4a, 4b, and 4c show the dependence of MS signal of In, MMIn and DMIn on the substrate temperature without arsenic present and at different arsenic overpressures, respectively. The partial pressures of In, MMIn and DMIn increase with increasing substrate temperature. DMIn partial pressure increases more rapidly and becomes higher than that of In at some critical substrate temperature. This critical temperature increases with increasing arsenic coverage on the surface. In^+ can come from cracking TMIn, DMIn, or MMIn or from In itself; MMIn can come from TMIn, DMIn or MMIn itself; and DMIn can come from TMIn and DMIn. Since the ratio of partial pressures of DMIn and MMIn is constant over the substrate temperature studied, we conclude that the MMIn and DMIn signals mainly come from DMIn. Since the ratio of partial pressures of DMIn and In increases at the critical temperature and in conventional solid-source MBE the growth rate does not decrease until the substrate temperature is above 530°C, we conclude that the In^+ signal in MOMBE growth does not come from indium desorption but mainly from TMIn.

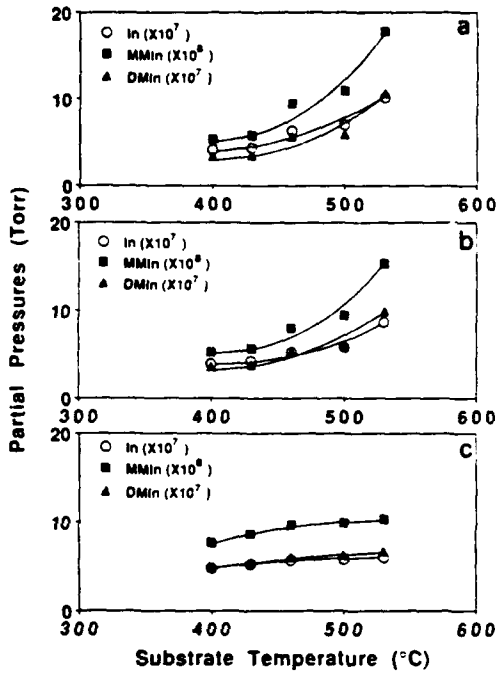

Fig. 4. Partial pressures of In, MMIn and DMIn versus substrate temperature at different arsenic overpressures: (a) 3.5×10^{-6} Torr; (b) 1.5×10^{-6} Torr; (c) As_4 shutter closed.

Fig. 4b suggests that the decrease in MOMBE growth rate above 470°C, shown in fig. 1 is a result from DMIn desorption. Although TMIn desorption increases with increasing substrate temperature, the growth rate still keeps on increasing. This is not contradictory since the higher the substrate temperature is, the more TMIn molecules desorb instead of reflect from the surface. At the same time, TMIn molecules pyrolyze more efficiently. The observation that the cross-over temperature for the DMIn partial pressure over the In partial pressure increases with arsenic overpressure suggests that DMIn is the surface species that controls the growth rate and that arsenic assists in decompsition of DMIn. It is resonable to postulate that the decomposition of DMIn would be the rate-limiting step because MMIn, with two methyl groups cleaved, is expected to be more reactive and decompose fast to form InAs with arsenic.

We therefore set up a kinetic model for MOMBE growth of InAs using TMIn and arsenic. Unlike previous model for CBE, our model also includes the roles of arsenic in the surface reactions. The details of the model are descrided elsewhere [9]. A schematic depiction of the two key steps involving arsenic species in MOMBE of InAs is shown in fig. 5. In fig 5a, TMIn molecules physisorb on the substrate surface, but the presence of arsenic can block adsorption sites for TMIn or enhance desorption of TMIn from the surface. Fig. 5b shows cleavage of one methyl group from TMIn to form DMIn. Fig. 5c shows the critical step of involving arsenic and DMIn to form InAs. The growth rate therefore equals the

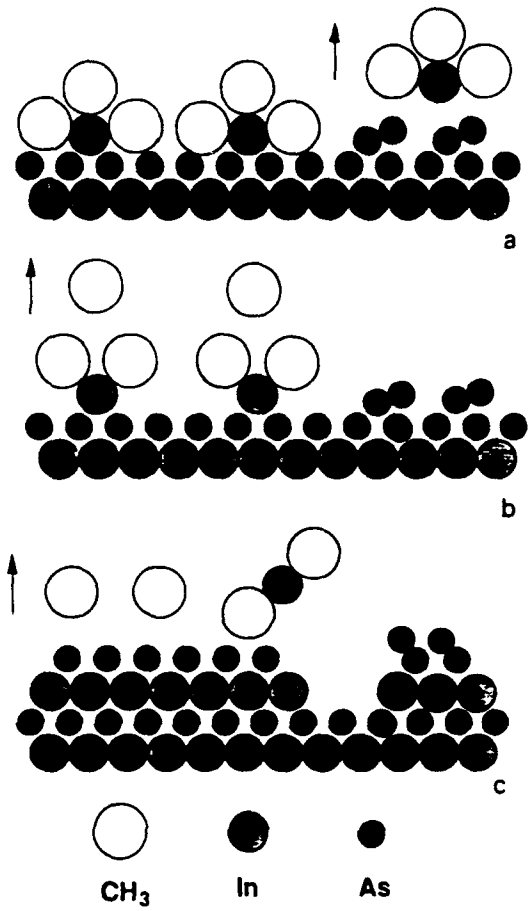

Fig. 5. A schematic depiction of MOMBE growth process of InAs using TMIn and arsenic: (a) shows the site-blocking mechanism; (b) shows cleavage of one methyl group from TMIn to form DMIn. We also drew arsenic on the surface to show its importance in combining with DMIn to form InAs in (c).

product of reaction constant and surface populations of DMIn and arsenic. By this model, we can calculate the growth rates versus substrate temperature and arsenic pressure. The calculated curves fit the experimental results very well as shown in fig. 2. According to the model, arsenic plays two different, but important, roles in the surface reactions. On the one hand, arsenic reacts with DMIn and creates InAs. Details of intermediate steps are not important for numerical simulation. Therefore, the higher is the arsenic overpressure, the higher the growth rate, and the higher the DMIn-In cross-over temperature in fig. 4. On the other hand, too much arsenic on the surface will enhance desorption of TMIn, and decrease the growth rate. These two roles that arsenic plays in MOMBE growth of InAs make the relation between growth rates and substrate temperature as well as arsenic overpressure more complicated than that of conventional MBE.

4. Conclusions

We have studied MOMBE growth of InAs with MS and RHEED and find that the growth rates of InAs depend on both substrate temperature and arsenic overpressure. The decrease of growth rate at higher temperature may be caused by the desorption of DMIn on the surface. Arsenic plays very important roles in the surface reactions, making the growth behavior of InAs by MOMBE more complicated than that of conventional MBE.

Acknowledgements

This work is partially supported by the Air Force Wright Research and Development Center under contract No. F33615-88-C-1861 and the Office of Naval Research under grant No. N00014-89-J-1147. We wish to thank critical comments of Dr. Tom Foxon.

References

[1] E. Veuhoff, W. Pletschen, P. Balk, and H. Lüth, J. Crystal Growth 55 (1981) 30.
[2] W.T. Tsang, Appl. Phys. Letters 45 (1984) 1234.
[3] S. Horiguchi, K. Kamon, M. Mashita, M. Shimazu, M. Mihara and M. Ishii, Japan. J. Appl. Phys. 25 (1986) L979.
[4] L. Fraas, G.R. Girard, V. Sundarain, C. Master, C. Nelson and R.A. Stall, in: III-V Heterostructures for Electronic/Photonic Devices, Mater. Res. Soc. Symp. Proc. 145, Eds. C.W. Tu, V.D. Mattera and A.C. Gossard (Mater. Res. Soc., Pittsburgh, PA, 1989) p. 253.
[5] Y.M. Houng, Y.C. Pao and P. McLeod, in: III-V Heterostructures for Electronic/Photonic Devices, Mater. Res. Soc. Symp. Proc. 145, Eds. C.W. Tu, V.D. Mattera and A.C. Gossard (Mater. Res. Soc., Pittsburgh, PA, 1989) p. 63.
[6] V.M. Donnelly, C.W. Tu, J.C. Beggy, V.R. McCrary, M.G. Lamont, T.D. Harris, F.A. Baiocchi and R.C. Farrow, Appl. Phys. Letters 52 (1988) 1065.
[7] A. Robertson, Jr., T.H. Chiu, W.T. Tsang and J.E. Cunningham, J. Appl. Phys. 64 (1987) 877.
[8] N. Kobayashi, J.L. Benchimol, F. Alexandre and Y. Gao, Appl. Phys. Letters 51 (1987) 1907.
[9] B.W. Liang and C.W. Tu, unpublished.

Surface kinetics of chemical beam epitaxy of GaAs

B. W. Liang[a] and C. W. Tu
Department of Electrical and Computer Engineering, Mail Code R-007, University of California at San Diego, La Jolla, California 92093-0407

(Received 14 February 1990; accepted for publication 4 June 1990)

A new kinetic model for chemical beam epitaxy of GaAs using triethylgallium and arsine is proposed. Both group III and group V species are equally important in the surface reactions. This model can fit experimental data very well. Various aspects of the growth rate as a function of substrate temperature, triethylgallium and arsine flow rates are examined.

Metalorganic molecular beam epitaxy (MOMBE) or chemical beam epitaxy (CBE) as a thin-film growth technique has become an active field. Because the mean free paths of source molecules are very long compared to the source-to-substrate distance, one can expect that gas phase reactions are unimportant, unlike metalorganic chemical vapor deposition (MOCVD). However, surface reactions play an important role in determining the MOMBE or CBE growth process. Growth behaviors and growth kinetics mechanisms of GaAs and InAs, grown by CBE or MOMBE, have been studied by several authors.[1-8] The first kinetic model proposed by Robertson *et al.* considered only triethylgallium (TEGa) decomposition paths.[6] The role of arsenic species was presumed secondary. Subsequently, group V species, unlike in conventional MBE, were found to have strong effect on the growth rate. This model therefore cannot explain the effects of arsenic species. In this letter we propose a new kinetic model, taking into account the effect of arsenic species for the first time, for CBE of GaAs using TEGa and arsine (AsH_3). The model can fit the experimental data of Chiu[5] very well, and we gain some more insights into the effect of arsine and TEGa flow rates on the CBE growth process.

The model assumes that diethylgallium (DEGa) decomposition—in the presence of arsenic—is the rate-limiting step for growing GaAs. We expect that monoethylgallium, with two ethyl groups cleaved off, would be very reactive and chemisorb strongly to the surface. Cleavage of the last ethyl group and subsequent incorporation of GaAs would occur very fast due to small activation barrier. This situation is similar to Robertson's model where DEGa decompositon is the rate-limiting step.[6] What differentiates our model is that this DEGa decomposition step includes an arsenic species. Experimentally, the growth rate decreases with increasing arsine flow rate, and this is attributed to the site-blocking effect.[5] In our preliminary study, the site-blocking mechanism does not agree with experimental data. Furthermore, the site-blocking model is more applicable when the TEGa and arsenic fluxes are supplied alternate, as in atomic layer epitaxy (ALE).[9] We therefore propose enhanced desorption of TEGa by excess arsenic on the surface in the continuous CBE or MOMBE process. The proposed chemical reactions on the substrate surface are as follows:

$$\text{(1) } \mathrm{TEGa}(g) \xrightarrow{FS_0} \mathrm{TEGa(ad)},$$

$$\text{(2) } \mathrm{TEGa(ad)} \xrightarrow{k_3} \mathrm{DEGa(ad)},$$

$$\text{(3) } \mathrm{TEGa(ad)} + \mathrm{As_2(ad)} \xrightarrow{k'} \mathrm{TEGa}(g) + \tfrac{1}{2}\mathrm{As_4}(g),$$

$$\text{(4) } \mathrm{DEGa(ad)} \xrightarrow{k_2} \mathrm{DEGa}(g),$$

$$\text{(5) } \mathrm{DEGa(ad)} + \mathrm{As_2(ad)} \xrightarrow{k} \mathrm{GaAs} + \text{other products}.$$

In reaction (1), F is the TEGa beam flux and S_0 is the adsorption probability. k's are various reaction rate coefficients. Similar to Robertson's model, we postulate the cleavage of the second ethyl radical to be the rate-limiting step. In our model, the growth rate (R_g) depends not only on the DEGa surface concentration X_2, but also on the arsenic surface concentration C_{As}.

$$R_g = kX_2 C_{As}. \tag{1}$$

In the steady-state condition, concentrations of adsorbed TEGa(X_3) and DEGa(X_2) are independent of time. Solving for X_2 and X_3 and assuming Arrhenius behavior for the reactions, $k_i = A_i \exp(-E_i/RT)$, we obtain

$$R_g = \frac{FS_0}{[1 + (A_1/C_{As})e^{-\Delta E_1/RT}](1 + A_2 C_{As} e^{-\Delta E_2/RT})}, \tag{2}$$

where $A_1 = A_{-2}/A$, $A_2 = A'/A_3$, $\Delta E_1 = E_{-2} - E$, and $\Delta E_2 = E' - E_3$. There are six unknown parameters (A_1, A_2, ΔE_1, ΔE_2, FS_0, and C_{As}). Note that in this model, we have further assumed that (1) there is no Ga desorption because the growth temperature is below that of Ga desorption, and (2) the temperature dependence of S_0 and C_A is small in the range studied. Chow and Fernandez have measured As_2 and As_4 sticking probabilities on GaAs (001) in conventional MBE to be independent of substrate temperature up to 540 °C.[10] As arsenic species on the surface are depleted during growth, they are replenished by the incoming flux.

We use Eq. (2) to fit experimental data from Ref. 5. First, we fit the growth rate versus substrate temperature at 0.64 sccm of TEGa flow rate and 2.2 sccm of AsH_3 flow rate. We obtain the fitting parameters as follows:

[a] On leave from the Shanghai Institute of Metallurgy, Academia Sinica, Shanghai, China.

 0003-6951/90/330689-03$02.00 © 1990 American Institute of Physics

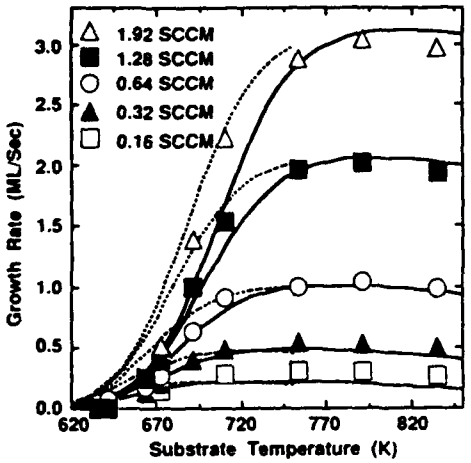

FIG. 1. Growth rate vs substrate temperature for different TEGa and arsine flow rates. Symbols are experimental data from Ref. 5 for arsine flow rate of 2.2 sccm and various TEGa Flow rates (0.16–1.92 sccm). Curves are calculation results from our model. Solid lines are for 2.2 sccm arsine flow rate and dashed lines for 1.0 sccm of arsine flow rate.

$A_1 = 1.6\times10^4$ ML, $\Delta E_1 = 22$ kcal/mol, $A_2 = 1.0\times10^{-14}$ ML^{-1}, $\Delta E_2 = -46$ kcal/mol, $FS_0 = 1.09$ ML/cm^2 s, and $C_{As} = 0.25$ ML. (A discussion on the reasonableness of these numbers is presented later in this letter.) Then, we fix the values of A_1, A_2, ΔE_1, and ΔE_2, and adjust FS_0 and C_{As} to other growth-rate curves, as shown in Fig. 1. Here we note that the model fits the low-temperature region better than the model without taking into account the effect of arsenic.[6] Figure 2 shows arsenic surface concentration C_{As}, obtained from the fittings, as a function of TEGa flow rate. In the range of lower TEGa flow rate, C_{As} increases linearly with TEGa flow rate. In the range of higher TEGa flow, C_{As} tends toward saturation. This is reasonable because higher TEGa flow rate, resulting in higher growth rate, requires higher arsenic surface concentration. However, when the TEGa flow rate is too high, C_{As} will be limited by the available arsenic species.

From the relation between FS_0 and TEGa flow, we can obtain S_0, as shown by the solid line with solid squares in

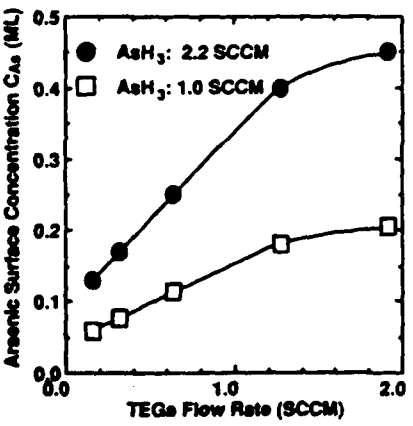

FIG. 2. Arsenic surface concentration (C_{As}) in units of monolayers (ML), obtained from curve fittings, vs TEGa flow rate at two different arsine flow rates.

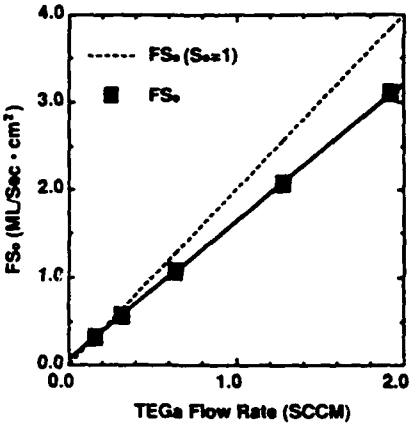

FIG. 3. FS_0 of TEGa vs TEGa flow rate. The dashed line is a calculation with $S_0 = 1$ for comparison. The data indicates $S_0 = 0.8$.

Fig. 3. The dashed line is a calculation, with $S_0 = 1$, for comparison. It appears that in our model the adsorption probability of TEGa is constant, $S_0 \sim 0.8$, independent of TEGa flow rate. In the model of Robertson *et al.* S_0 is assumed to be unity.[6] Using these parameters we calculate the growth rate as a function of C_{As}, as shown in Fig. 4 for various substrate temperatures used in Ref. 5. Because we do not know the As_2 flux on the substrate surface, it is not possible to quantify C_{As}, from the fittings as a function of AsH_3 flow rate. However, qualitatively these curves agree well with data in Ref. 5.

At lower substrate temperature, Eq. (2) can be simplified into $R_g = FS_0 A_2^{-1} C_{As}^{-1} \exp(-|\Delta E_2|/RT)$. The growth rate increases with increasing substrate temperature, as shown in Fig. 1, because higher substrate temperature results in more TEGa decomposition into DEGa. At higher substrate temperature, Eq. (2) can be simplified into $R_g = FS_0 A_1^{-1} C_{As} \exp(\Delta E_1/RT)$. The growth rate decreases with increasing substrate temperature, but very slowly because ΔE_1 is small. In Fig. 4, at lower substrate temperature, the growth rate at lower AsH_3 flow rate is higher than that at higher AsH_3 flow rate because too

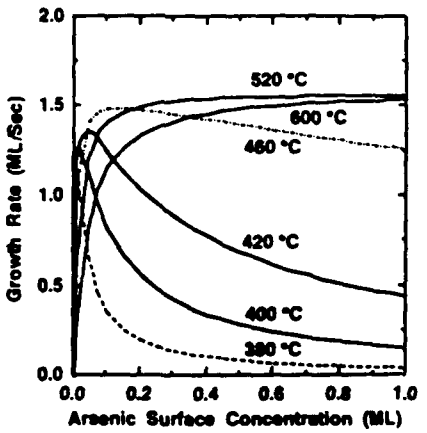

FIG. 4. Calculations of growth rate vs arsenic surface concentration at different substrate temperatures. The TEGa flow rate is 0.96 sccm. These curves qualitatively agree with data in Ref. 5.

much arsenic on the surface will enhance desorption of TEGa. However, at high substrate temperature the growth rate increases with increasing AsH_3 flow rate because surface reactions become fast. At high AsH_3 flow rate, the growth rate is independent of AsH_3 flow. In this region of high temperature and large AsH_3 flow, the CBE process is similar to solid-source MBE.

We now discuss the parameters obtained from the model. Consider first $\Delta E_1 = E_{-2} - E$, where E_{-2} is the activation energy of DEGa desorption and E is the activation energy for reaction (5). Since DEGa and As_2 are reactive, E is probably small. Therefore, $\Delta E_1 \simeq E_{-2}$, which means $E_{-2} \simeq 22$ kcal/mol. According to Robertson *et al.*,[6] if the activation energies for cleaving the first and second ethyl groups are comparable (~ 13 kcal/mol), then the desorption energy of DEG would be ~ 26 kcal/mol.[6] This value compares well with our result. Now consider $\Delta E_2 = E' - E_3$, where E' is the activation energy of arsenic-enhanced desorption, and E_3 is the activation energy for TEGa decomposing into DEGa. The upper limit on ΔE_2 given by Robertson *et al.* is -49 kcal/mol.[6] Our best fitting result is -46 kcal/mol. Since the binding energy for physiosorbed large molecules as TEGa should be in the range of 1–10 kcal/mol,[6] E_3 is in the range of 47–56 kcal/mol. This value, close to the gas phase value of 46 kcal/mol,[11] seems to be somewhat larger than expected, for surface species. This discrepancy may be a result of inaccurate substrate temperature measurement because fitting data depends sensitively on substrate temperature.

In summary, we have developed a growth kinetic model for CBE of GaAs using TEGa and AsH_3. The model can fit the experimental data very well and explain how TEGa and arsine flow rates influence the growth rate. Although our model may not be complete or unique, it does reveal that arsenic plays an equally important role as TEGa in CBE growth of GaAs.

This work is partially supported by the Air Force Wright Research and Development Center under contract No. F33615-88-C-1861 and the Office of Naval Research under grant No. N00014-89-J-1147. We wish to thank L. Y. Wang and H. Q. Hou for help in fitting the data.

[1] E. Veuhoff, W. Pletschen, P. Balk, and H. Luth, J. Cryst. Growth **55**, 30 (1981).
[2] W. T. Tsang, Appl. Phys. Lett. **45**, 1234 (1984).
[3] S. Horiguchi, K. Kimura, K. Kamon, M. Mashita, M. Shimazu, M. Michara, and M. Ishii, Jpn. J. Appl. Phys. **25**, L979 (1986).
[4] For a review, see W. T. Tsang, J. Cryst. Growth **81**, 261 (1987).
[5] T. H. Chiu, Mater. Res. Soc. Symp. Proc. **145**, 47 (1989).
[6] A. Robertson, Jr., T. H. Chiu, W. T. Tsang, and J. E. Cunningham, J. Appl. Phys. **64**, 877 (1988).
[7] B. W. Liang, T. P. Chin, and C. W. Tu, J. Appl. Phys. **67**, 4393 (1990).
[8] B. W. Liang, L. Y. Wang, and C. W. Tu, State-of-the-Art Program on Compound Semiconductors XII, Montreal, Canada, edited by D. C. D'Avanzo (to be published by the Electrochemical Society, 1990).
[9] D. E. Aspnes, E. Colas, A. A. Studna, R. Bhat, M. A. Koza, and V. G. Keramidas, Phys. Rev. Lett. **61**, 2782 (1988).
[10] R. Chow and R. Fernandez, Mater. Res. Soc. Symp. Proc. **145**, 13 (1989).
[11] M. Tirtowidjojo and R. Pollard, J. Cryst. Growth **77**, 200 (1986).

Proc. State-of-the-art Prog.
on Comp. Semicond. XII (1990)

A KINETIC MODEL FOR METAL-ORGANIC MOLECULAR BEAM EPITAXY OF InAs

B.W. Liang,* L.Y. Wang, and C.W. Tu
Department of Electrical and Computer Engineering
Mail Code R-007, University of California at San Diego
La Jolla, CA 92093-0407

A growth-kinetics model for metal-organic molecular-beam epitaxy (MOMBE) of InAs is proposed and compared with experimental data. The model includes, for the first time, the effect of arsenic overpressure in MOMBE. Increasing arsenic at low arsenic flux increases the growth rate, but increasing arsenic at high arsenic flux decreases the growth rate.

Metal-organic Molecular Beam Epitaxy (MOMBE) or Chemical Beam Epitaxy (CBE) has received increasing attention as a thin-film growth technique since the first publications several years ago.[1,2] Because the mean free paths of source molecules are very long compared to the source-to-substrate distance, one can expect that gas-phase reactions are unimportant, unlike metal-organic chemical vapor deposition (MOCVD). However, surface reactions play an important role in determining the MOMBE growth process. Robertson *et al.* have recently proposed a kinetic model for CBE growth of GaAs with triethylgallium (TEGa) and arsine.[3] In that model, only the decomposition pathways of TEGa are considered. The role of arsenic, although seen in CBE growth-rate studies,[4] is not taken into account in the model. In our previous studies of MOMBE growth of GaAs and InAs using trimethylgallium (TMGa), trimethylindium (TMIn) and arsenic, we also found that arsenic in MOMBE plays a very important role, unlike in conventional solid-source MBE.[5-7]

In this paper, we propose a growth-kinetics model for MOMBE of InAs, taking into account the effect of the presence of arsenic. The model assumes that dimethylindium (DMIn) decomposition in the presence of arsenic is the rate-limiting step for growing InAs. This assumption is reasonable because we expect that monomethylindium, with two methyl groups cleaved off, would be very reactive and chemisorb strongly to the surface. Cleavage of the last methyl group and subsequent incorporation of InAs would occur very fast due to small activation barrier. This situation is similar to Robertson's model where diethylgallium decomposition is the rate-limiting step. In our quadruple mass spectrometer we observed a faster increase of DMIn signal at a temperature where the growth rate started to decrease. What differentiates our model from previous models is that this DMIn decomposition step includes an arsenic species. Experimentally, the growth rate initially increases with arsenic overpressure. At high arsenic overpressure, however, the growth rate decreases, indicating either a site-blocking effect[4] or enhanced desorption. In our preliminary study, the site-blocking model does not agree with experimental data. Furthermore, the site-blocking model is more applicable when the TMIn and arsenic fluxes are supplied alternatingly. We, therefore, propose enhanced desorption of TMIn by excess arsenic in a continuous MOMBE process. The following is the proposed growth reaction sequence in our kinetic model.

(1) $TMIn(g) \xrightarrow{FS_0} TMIn(ad)$

(2) $TMIn(ad) \xrightarrow{k_3} DMIn(ad)$

(3) $TMIn(ad) + As_2(ad) \xrightarrow{k'} TMIn(g) + \frac{1}{2} As_4(g)$

(4) $DMIn(ad) \xrightarrow{k_{-2}} DMIn(g)$

(5) $DMIn(ad) + As_2(ad) \xrightarrow{k} \text{intermediate steps} \xrightarrow{fast} InAs + \text{otherproducts}$

In reaction (1) F is the TMIn beam flux, and S_0 is the adsorption possibility. k's are various reaction rate coefficients. As_2 comes from decomposition of As_4, which has a low activation energy (0.5eV).[8] Since we postulate that reaction (5) is the rate-limiting step, the growth rate (R_g),

$$R_g = kX_2 C_{As} \tag{1}$$

where X_2 is the concentration of adsorbed DMIn on the surface and C_{As} the arsenic surface concentration. Under the steady-state conditions, the concentrations of adsorbed TMIn (X_3) and DMIn (X_2) are independent of time.

$$dX_2/dt = K_3X_3 - K_{-2}X_2 - KX_2C_{As} = 0$$
$$\text{and } dX_3/dt = FS_0 - K_3X_3 - K'X_3 C_{As} = 0 \tag{2}$$

Solving for X_2 and X_3 and assuming an Arrhenius behavior for the reactions, $k_i = A_i \exp(-E_i/RT)$, we obtain

$$R_g = \frac{FS_0}{(1 + \frac{A_1}{C_{As}} e^{-\Delta E_1/RT})(1 + A_2 C_{As} e^{-\Delta E_2/RT})} \tag{3}$$

where $A_1 = A_{-2}/A$; $A_2 = A'/A_3$; $\Delta E_1 = E_{-2} - E$ and $\Delta E_2 = E' - E_3$. There are six unknown parameters: A_1, A_2, ΔE_1, ΔE_2, FS_0, and C_{As}. Note that in this model, we have further assumed that (1) there is no indium desorption; (2) the temperature dependence of S_0 and C_{As} is small in the range studied; and (3) no CH_3 occupies surface site. As arsenic species on the surface are depleted in growing GaAs, they are replenished by the arsenic overpressure. In a separate experiment, we observed desorption only for substrate temperature higher than 540°C. Chow and Fernandez have measured the As_2 and As_4 sticking probabilities on GaAs(001) in conventional MBE to be independent of substrate temperature up to 540°C.[9]

Using equation (3) to fit the growth rate versus substrate temperature at 3.8×10^{-7} Torr arsenic overpressure, we obtained the following parameters: $FS_0 = 1.37$ ML/cm^{2}s, $A_1 = 4.2 \times 10^4$ ML, $\Delta E_1 = 19.5$ kcal/mol, $A_2 = 5 \times 10^{-9}$ ML^{-1}, $\Delta E_2 = -27.8$ kcal/mol and $C_{As} = 0.27$ ML. ML stands for monolayers. Then, fixing these parameters, except C_{As}, we fit other experimental growth rates versus substrate temperatures, for different arsenic overpressures, as shown in Figure 1. Figure 2 shows that the

best C_{As} for each curves turns out to be linearly dependent on the arsenic overpressure P_{As_4} from the flux measurement. Using these parameters, we then calculate the growth rate as a function of arsenic surface concentrations for different growth temperatures. The results are plotted in Figure 3. Various symbols are experimental data, and they agree with calculations remarkably well.

Due to the surface catalytic effect, E_3, the activation energy for cleaving a methyl radical from adsorbed TMIn, should be lower than that in the gas phase. If E' is less than 10 kcal/mol, E_3 is less than 37.8 kcal/mol. This is reasonable compared to 47.2 kcal/mol in the gas phase.[10] Because both DMIn and As_2 are reactive, the activation energy of reaction (5), E, should be small. Suppose it is 10 kcal/mol, then E_{-2} the activation energy for DMIn desorption, is about 30 kcal/mol. This value is similar to the activation energy for DMGa desorption of 25 kcal/mol.[11]

Based on this model, we can now interpret the growth behaviors physically. At high substrate temperature or low arsenic surface concentration, equation (3) can be simplified to $R_g = FS_0\, C_{As}\, A_1^{-1} \exp(\Delta E_1/RT)$. The growth rate increases with increasing arsenic surface concentration or decreases with increasing substrate temperature because higher C_{As} will enhance reaction (5), and thus, increase the growth rate. On the other hand, at higher substrate temperature reaction (4) is accelerated and the surface population of DMIn decreases, so the growth rate decreases. At low substrate temperature or high arsenic surface concentration, equation (3) can be simplified into $Rg = FS_0\, C_{As}^{-1}\, A_2^{-1} \exp(\Delta E_2/RT)$. The growth rate decreases with increasing arsenic surface coverage or increases with increasing substrate temperature. The higher C_{As} will enhance reaction (3), TMIn desorption, and thus, decrease the growth rate. On the other hand, the higher substrate temperature will accelerate reaction (2), decomposition of TMIn, and at the same time accelerate reaction (3), desorption of TMIn. Since the latter is slower than the former, the growth rate still increases with increasing substrate temperature. The growth-rate behavior at high substrate temperature and high arsenic pressure is similar to that in conventional solid-source MBE.

In summary, we have proposed a growth-kinetics model for MOMBE, taking into account the effect of arsenic explicitly for the first time. Our model can explain all the experimental observation of growth rate as a function of substrate temperature and arsenic overpressure. This model should also be applicable to MOMBE of other compounds, which we are currently investigating.

This work is partially supported by the Air Force Wright Research and Development Center under contract No. F33615-88-C-1861 and Office of Naval Research under grant No. N00014-89-J-1147. We wish to thank T.P. Chin for assistance in MOMBE growth and Dr. V.M. Donnelly for valuable discussions.

REFERENCES

* On leave from the Shanghai Institute of Metallurgy, Academia Sinica, Shanghai China.

1. E. Veuhoff, W. Pletschen, P. Balk, and H. Luth, *J. Cryst. Growth* **55**, 30 (1981).
2. W.T. Tsang, *Appl. Phys. Lett.* **45**, 1234 (1984).
3. R. Robertson, Jr., T.H. Chiu, W.T. Tsang, and J.E. Cunningham, *J. Appl. Phys.* **64**, 877 (1988).
4. T.H. Chiu, in *III-V Heterostructures for Electronic/Photonic Devices*, editors C.W. Tu, V.D. Mattera, and A.C. Gossard, *MRS Symp. Proc.* **145**, 47 (1989).
5. B.W. Liang, T.P. Chin, and C.W. Tu, *J. Appl. Phys.* **67**, 4393 (1990).
6. B.W. Liang, T.P. Chin, L.Y. Wang, and C.W. Tu, *J. Cryst. Growth*, in press.
7. C.W. Tu, B.W. Liang, and T.P. Chin, *J. Cryst. Growth*, in press.
8. J.E. Cunningham, *Private Communication* (1989).
9. R. Chow and R. Fernandez, in *III-V Heterostructures for Electronic/Photonic Devices*, editors, C.W. Tu, V.D. Mattera, and A.C. Gossard, *MRS Symp. Proc.* **145**, 13 (1989).
10. M.G. Jacko and S.J.W. Price, *Can. J. Chem.* **42**, 1198 (1964).
11. E. Coltrin and R.J. Kee, in *III-V Heterostructures for Electronic/Photonic Devices*, editors, C.W. Tu, V.D. Mattera, and A.C. Gossard, *MRS Symp. Proc.* **145**, 119 (1989).

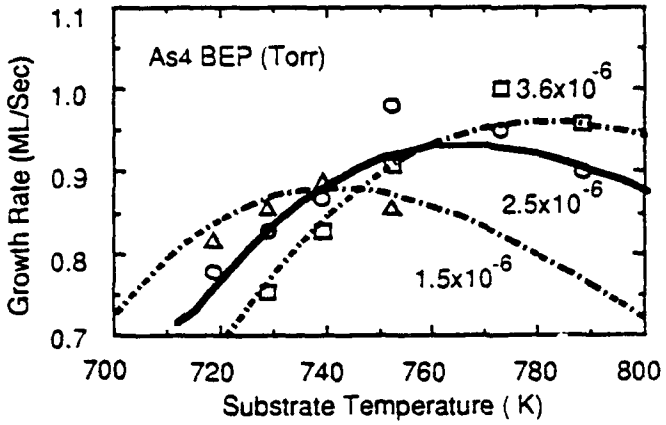

Figure 1 MOMBE growth rate of InAs versus substrate temperature at different arsenic surface concentrations.

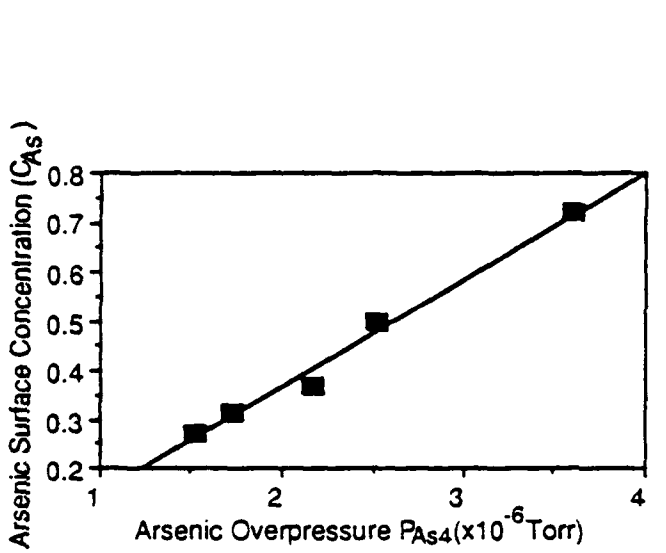

Figure 2 The relation between arsenic surface concentration (C_{As}) and arsenic overpressure (P_{As_4}).

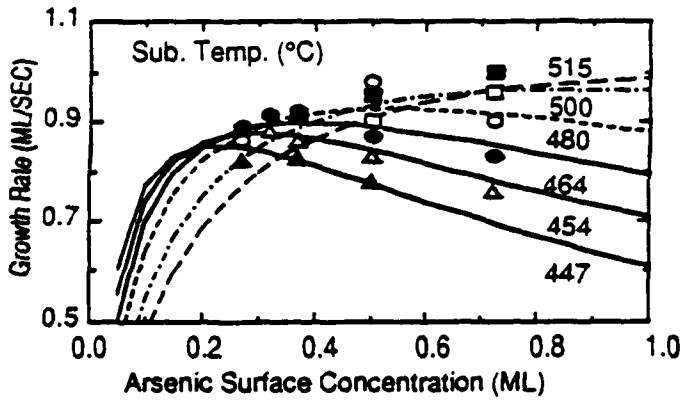

Figure 3 MOMBE growth rate of InAs versus arsenic surface concentration for different substrate temperatures.

METALORGANIC MOLECULAR-BEAM EPITAXY: GROWTH KINETICS AND SELECTIVE-AREA EPITAXY

C.W. TU and B.W. LIANG*,

Department of Electrical and Computer Engineering, University of California at San Diego, La Jolla, California 92093, U.S.A.,

V.M. DONNELLY

AT&T Bell Laboratories, Murray Hill, New Jersey 07974, U.S.A.

Metalorganic molecular-beam epitaxy (MOMBE) or chemical-beam epitaxy (CBE) is interesting because its growth kinetics is different and relatively unexplored compared to that of solid-source MBE and metalorganic chemical vapor deposition (MOCVD) and because its capability of selective-area epitaxy has potential novel applications, quantitatively, in optoelectronics. We propose a new kinetic model for MOMBE of GaAs and InAs. The model can explain the important effects of arsenic overpressure on growth rate for the first time. Group-III and group-V species are equally important in the surface chemical reactions during MOMBE. Excimer-laser-enhanced MOMBE of GaAs was also observed at low substrate temperature with nearly unity efficiency. The effect is due to transient heating during the pulsed laser irradiation.

1. INTRODUCTION

Metalorganic molecular-beam epitaxy (MOMBE)[1] or chemical-beam epitaxy (CBE)[2] has gained increasing interest not only for fundamental studies of growth kinetics[3–5] but also for optoelectronic device applications due to its potential for high throughput[6] and selective-area epitaxy.[7,8]

This paper summarizes our recent results on growth kinetics[4,5,9,10] and laser-enhanced MOMBE of III-V compounds.[7] The kinetic model for MOMBE or CBE that is proposed so far considers only group-III alkyl decomposition pathways[3] and, therefore, cannot explain effects of group-V species. We propose a new kinetic model that includes both group-III alkyls and arsenic in the surface chemical reactions, for the first time.[4,5] The model can fit the growth-rate data for GaAs and InAs very well and leads to new insights into the MOMBE process.

Another interesting aspect of MOMBE is selective-area epitaxy. We have observed excimer-laser-enhanced MOMBE growth of GaAs using triethylgallium (TEGa) and arsenic[4] at substrate temperatures below 450°C, where pyrolytic growth is very slow. From the strong dependence of the enhanced growth rate on laser fluence and X-ray photoelectron spectroscopy of laser-induced decomposition of TEGa molecules,[11] we conclude that at high laser fluences the growth enhancement process appears to be pyrolytic in nature, not photolytic. The enhanced growth is due to rapid transient heating by the laser pulses.

Atomic layer epitaxy (ALE) can be achieved with trimethylgallium (TMGa) more easily than triethylgallium (TEGa).[9,10,14] In addition, using TMGa can result in ultrahigh p-type carrier concentration from high 10^{19} cm^{-3} to high 10^{20} cm^{-3} range.[9] Such high p-type doping with low diffusivity of carbon may be useful in a variety of device applications. These results have been presented elsewhere.[9,10]

2. EXPERIMENTAL PROCEDURES

The growth was performed in a modified prototype Perkin-Elmer 425A MBE system, as shown in Figure 1. The growth chamber was pumped by a cryopump and an ion pump. TMGa, TEGa, and trimethylindium (TMIn) molecules were directly injected into the growth chamber without hydrogen carrier gas through a leak valve and an

*On leave from the Shanghai Institute of Metallurgy, Shanghai, China.

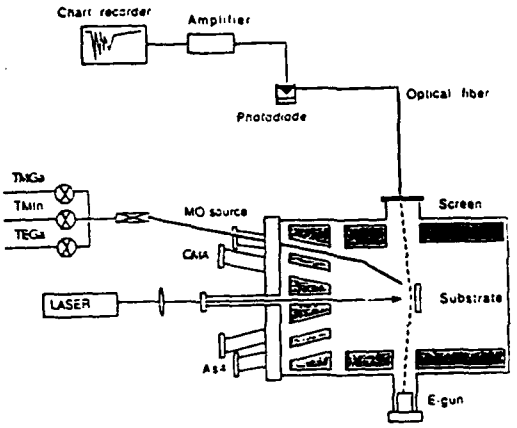

FIGURE 1
A schematic diagram of the MOMBE system.

on-off valve upstream. The reflection-high-energy-electron diffraction (RHEED) intensity was monitored by a photodiode through an optical fiber. GaAs substrates were etched and cleaned in the usual manner and then mounted on molybdenum (Mo) blocks. The substrate was thermally cleaned in vacuum under an overpressure of arsenic. The substrate temperature was calibrated by a thermal couple inserted into a Mo block and also independently by a pyrometer. Nevertheless, the uncertainty in absolute temperature could still be ~20°C. Fluxes were measured by the ionization gauge behind the substrate holder with the holder out of the way.

ArF excimer laser (Lumonics Hyper EX460) was used for the selective-area-epitaxy experiment. The laser delivered 100-300 mJ, 15 ns pulses at 193 nm. The 0.5×2 cm^2 beam was collimated with a 3-m-focal-length, fused silica lens and directed at the substrate at normal incidence. No mask or additional focusing elements were employed in these studies. The absolute intensity of the laser beam was measured as a function of *(x,y)* position in the plane of the substrate by reflecting the beam off a mirror and positioning a pinhole and detector at the appropriate distance. This laser-MOMBE system was also used in a separate study of laser-modified MBE growth reported elsewhere.[12] The RHEED-intensity-oscillation measurement was not set up yet during the laser-assisted MOMBE experiment.

3. GROWTH KINETICS

3.1 CBE of GaAs

Because the mean free paths of source molecules are very long compared to the source-to-substrate distance, one can expect that gas-phase reactions are unimportant, unlike metal-organic chemical vapor deposition (MOCVD). However, surface reactions play an important role in determining the MOMBE or CBE growth process. Growth behaviors and growth kinetics mechanisms of GaAs and InAs, grown by CBE or MOMBE, have been studied by several authors.[1-5,13,14] The first kinetic model proposed by Robertson *et al.* considered only triethylgallium (TEGa) decomposition paths.[3] The role of arsenic species was presumed secondary. Subsequently, group-V species, unlike in conventional MBE, were found to have a strong effect on the growth rate.[14,15] This model therefore cannot explain the effects of arsenic species. We propose a new kinetic model, taking into account the effect of arsenic species for the first time, for CBE of GaAs using TEGa and arsine (AsH_3).[4] The model can fit the experimental data of Chiu *et al.* very well,[14] and we gain some more insights into the effect of arsine and TEGa flow rates on the CBE growth process.

The model assumes that diethylgallium (DEGa) decomposition--in the presence of arsenic--is the rate-limiting step for growing GaAs. We expect that monoethylgallium, with two ethyl groups cleaved off, would be very reactive and chemisorb strongly to the surface. Cleavage of the last ethyl group and subsequent incorporation of GaAs would occur very fast due to small activation barrier. This situation is similar to Robertson's model where DEGa decomposition is the rate-limiting step.[3] What differentiates our model is that this DEGa decomposition step includes an arsenic species. Experimentally, the growth rate decreases with increasing arsine flow rate, and this is attributed to the site-blocking effect.[14] In our preliminary study, the site-blocking mechanism does not agree with experimental data. Furthermore, the site-blocking model is more applicable when the TEGa and arsenic fluxes are supplied alternatingly, as in atomic-layer epitaxy (ALE).[16] We therefore propose enhanced desorption of TEGa by excess arsenic on the surface in the continuous CBE or MOMBE process. The proposed chemical reactions on the substrate surface are as follows,

(1) $TEGa(g) \xrightarrow{FS_0} TEGa(ad)$

(2) $TEGa(ad) \xrightarrow{k_1} DEGa(ad)$

(3) $TEGa(ad) + As_2(ad) \xrightarrow{k} TEGa(g) + \frac{1}{2}As_4(g)$

(4) $DEGa(ad) \xrightarrow{k_{-2}} DEGa(g)$

(5) $DEGa(ad) + As_2(ad) \xrightarrow{k} GaAs + \text{other products}$

In reaction (1), F is the TEGa beam flux, and S_0 is the adsorption probability. k's are various reaction rate coefficients. Similar to Robertson's model, we postulate the cleavage of the second ethyl radical to be the rate-limiting step. In our model, the growth rate (R_g) depends not only on the DEGa surface concentration X_2, but also on the arsenic surface concentration C_{As}.

$$R_g = kX_2 C_{As}. \quad (1)$$

In the steady-state condition, concentrations of adsorbed TEGa (X_3) and DEGa (X_2) are independent of time. Solving for X_2 and X_3 and assuming Arrhenius behavior for the reactions, $k_i = A_i \exp(-E_i/RT)$, we obtain

$$R_g = \frac{FS_0}{(1 + \frac{A_1}{C_{As}} e^{-\Delta E_1/RT})(1 + A_2 C_{As} e^{-\Delta E_2/RT})} \quad (2)$$

where $A_1 = A_{-2}/A$; $A_2 = A'/A_3$; $\Delta E_1 = E_{-2} - E$ and $\Delta E_2 = E' - E_3$. There are six unknown parameters (A_1, A_2, ΔE_1, ΔE_2, FS_0, and C_{As}). Note that in this model, we have further assumed that (1) there is no Ga desorption because the growth temperature is below that of Ga desorption; and (2) the temperature dependence of S_0 and C_{As} is small in the range studied. Chow and Fernandez have measured As_2 and As_4 sticking probabilities on GaAs (001) in conventional MBE to be independent of substrate temperature up to 540°C.[17] As arsenic species on the surface are depleted during growth, they are replenished by the incoming flux.

We use equation (2) to fit experimental data from reference [14]. First, we fit the growth rate versus substrate temperature at 0.64 sccm of TEGa flow rate and 2.2 sccm of AsH_3 flow rate. We obtain the fitting parameters as follows: $A_1 = 1.6 \times 10^4$ ML, $\Delta E_1 = 22$ kcal/mol, $A_2 = 1.0 \times 10^{-14} ML^{-1}$, $\Delta E_2 = -46$ kcal/mol, $FS_0 = 1.09$ ML/cm^{2}s, and $C_{As} = 0.25$ ML. ML stands for monolayers. (A discussion on the reasonableness of these numbers is presented later in this paper.) Then, we fix the values of A_1, A_2, ΔE_1, and ΔE_2, and adjust FS_0 and C_{As} to other growth-rate curves, as shown in Figure 2.

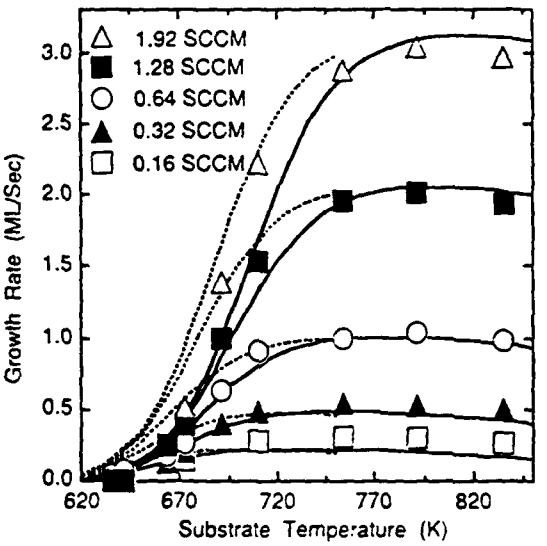

FIGURE 2
Growth rate versus substrate temperature for different TEGa and arsine flow rates. Symbols are experimental data from Ref. [14] for arsine flow rate of 2.2 sccm and various TEGa flow rates (0.16 sccm to 1.92 sccm). Curves are calculation results from our model. Solid lines are for 2.2 sccm arsine flow rate and dashed lines for 1.0 sccm of arsine flow rate.

Here we note that the model fits the low temperature region better than the model without taking into account the effect of arsenic.[6] Figure 3 shows arsenic surface concentration C_{As}, as a function of TEGa flow rate. In the range of lower TEGa flow rate, C_{As} increases linearly with TEGa flow rate. In the range of higher TEGa flow, C_{As} tends toward saturation. This is reasonable because higher TEGa flow rate, resulting in higher growth rate, requires higher arsenic surface concentration. However, when the TEGa flow rate is too high, C_{As} will be limited by the available species.

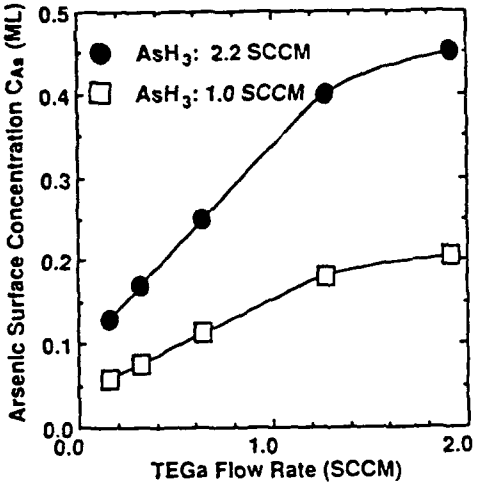

FIGURE 3
Arsenic surface concentration (C_{As}) in units of monolayers (ML) versus TEGa flow rate at two different arsine flow rates.

From the relation between FS_0 and TEGa flow, we can obtain S_0, as shown by the solid line with solid circles in Figure 4. The dashed line is a calculation, with $S_0 = 1$, for comparison. In our model it appears that the adsc ption probability of TEGa is constant, $S_0 \sim 0.8$,

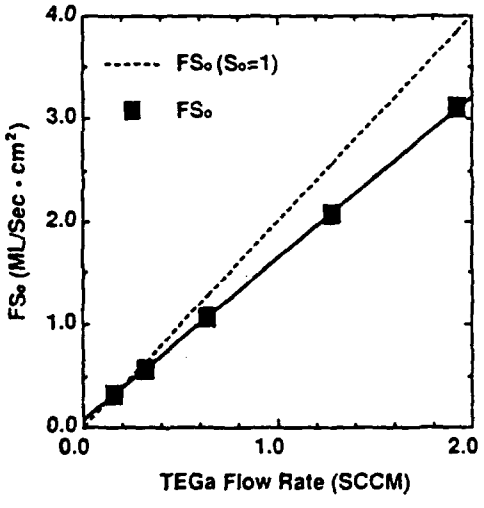

FIGURE 4
FS_0 of TEGa versus TEGa flow rate. The dashed line is a calculation with $S_0 = 1$ for comparison. The data indicates $S_0 = 0.8$.

independent of TEGa flow rate, whereas Robertson *et al.* assume that S_0 is unity.[3]

Using these parameters we calculate the growth rate as a function of C_{As}, as shown in Figure 5 for various substrate temperatures used in Ref. 14. Because we do not know the As_2 flux on the substrate surface, it is not possible to quantify C_{As}, from the fittings, as a function of AsH_3 flow rate. However, qualitatively these curves agree well with data in Ref. 14.

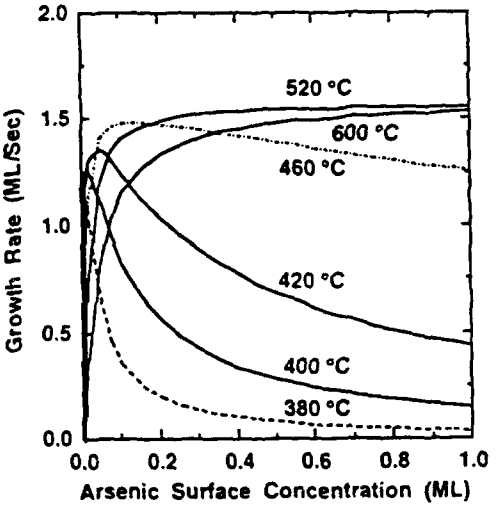

FIGURE 5
Calculations of growth rate versus arsenic surface concentration at different substrate temperatures. The TEGa flow rate is 0.96 sccm. These curves qualitatively agree with data in Ref. [14].

Figure 6 shows a three-dimensional plot of calculated growth rates as a function of substrate temperature and surface arsenic concentration.

At lower substrate temperature, equation (2) can be simplified into $R_g = FS_0 A_2^{-1} C_{As}^{-1} \exp(-|\Delta E_2|/RT)$. The growth rate increases with increasing substrate temperature, as shown in Figures 2 and 6, because higher substrate temperature results in more TEGa decomposition into DEGa. At higher substrate temperature, equation (2) can be simplified into $R_g = FS_0 C_{As} A_1^{-1} \exp(\Delta E_1/RT)$. The growth rate decreases with increasing substrate temperature, but very slowly because ΔE_1 is small. In Figures 5 and 6, at lower

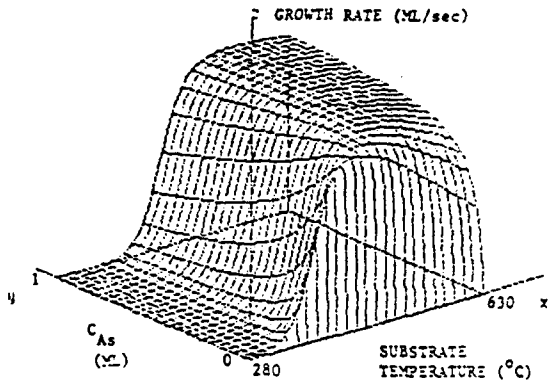

FIGURE 6
Calculated growth rate versus substrate temperature and surface arsenic concentration.

substrate temperature, the growth rate at lower AsH_3 flow rate is higher than that at higher AsH_3 flow rate because too much arsenic on the surface will enhance desorption of TEGa. However, at high substrate temperature the growth rate increases with increasing AsH_3 flow rate because surface reactions become fast. At high AsH_3 flow rate, the growth rate is independent of AsH_3 flow. In this region of high temperature and large AsH_3 flow, the CBE process is similar to solid-source MBE.

We now discuss the parameters obtained from the model. Consider first $\Delta E_1 = E_{-2} - E$, where E_{-2} is the activation energy of DEGa desorption and E is the activation energy for reaction (5). Since DEGa and As_2 are reactive, E is probably small. Therefore, $\Delta E_1 = E_{-2}$, which means E_{-2} = 22 kcal/mol. According to Robertson *et al.*,[3] if the activation energies for cleaving the first and second ethyl groups are comparable (~13 kcal/mol), then the desorption energy of DEG would be ~ 26 kcal/mol.[3] This value compares well with our result. Now consider $\Delta E_2 = E' - E_3$, where E' is the activation energy of arsenic-enhanced desorption, and E_3 is the activation energy for TEGa decomposing into DEGa. The upper limit on ΔE_2 given by Robertson *et al.* is -49 kcal/mol.[3] Our best fitting result is -46 kcal/mol. Since the binding energy for physisorbed large molecules such as TEGa should be in the range of 1-10 kcal/mol,[3] E_3 is in the range of 47 to 56 kcal/mol. This value, close to the gas-phase value of 46 kcal/mol,[18] seems to be somewhat larger than expected, for surface species. This discrepancy may be a result of inaccurate substrate temperature measurement because fitting data depends sensitively on substrate temperature.

In summary, we have developed a growth kinetic model for CBE of GaAs using TEGa and AsH_3. The model can fit the experimental data very well and explain how TEGa and arsine flow rates influence the growth rate. Although our model may not be complete or unique, it does reveal that arsenic plays an equally important role as TEGa in CBE growth of GaAs.

3.2 MOMBE OF InAs

We have applied the same kinetic model to MOMBE of InAs grown with TMIn and As_4.[5] Using equation (3) to fit the growth rate versus substrate temperature at 3.8×10^{-7} Torr arsenic overpressure, we obtained the following parameters: $FS_0 = 1.37$ ML/cm^{2}s, $A_1 = 4.2 \times 10^4$ ML, $\Delta E_1 = 19.5$ kcal/mol, $A_2 = 5 \times 10^{-9}$ ML^{-1}, $\Delta E_2 = -27.8$ kcal/mol and $C_{As} = 0.27$ ML. Then, fixing these parameters, except C_{As}, we fit other experimental growth rates versus substrate temperatures, for different arsenic overpressures, as shown in Figure 7.

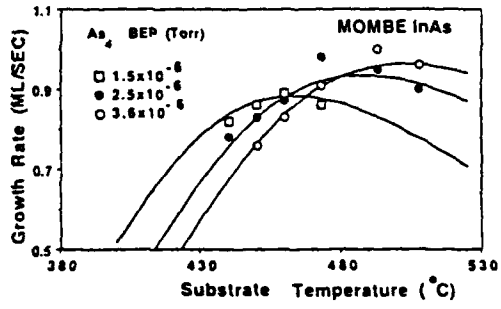

FIGURE 7
MOMBE growth rate of InAs versus substrate temperature at different arsenic surface concentrations.

Figure 8 shows that the best C_{As} for each curves turns out to be linearly dependent on the arsenic overpressure P_{As_4} from the flux measurement.

Using these parameters, we then calculate the growth rate as a function of arsenic surface concentrations for different growth temperatures. The results are plotted in

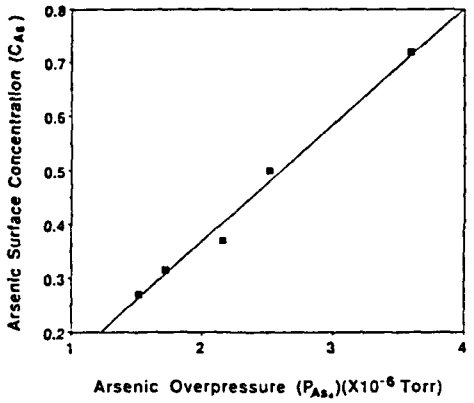

FIGURE 8
The relation between arsenic surface concentration (C_{As}) and arsenic overpressure (P_{As_4}).

Figure 9. Various symbols are experimental data, and they agree with calculations remarkably well. Figure 10 shows a three-dimensional plot of growth rates as a function of substrate temperature and surface arsenic concentration.

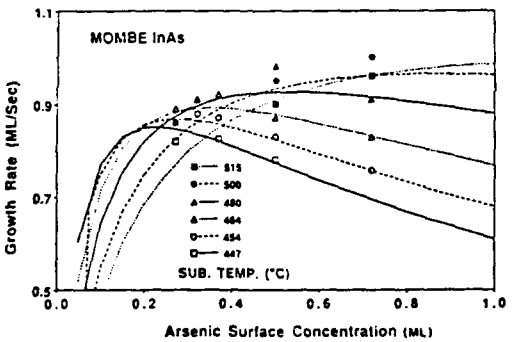

FIGURE 9
MOMBE growth rate of InAs versus arsenic surface concentration for different substrate temperatures.

Due to the surface catalytic effect, E_3, the activation energy for cleaving a methyl radical from adsorbed TMIn, should be lower than that in the gas phase. Because both DMIn and As_2 are reactive, the activation energy of reaction (5), E, should be small, less than 10 kcal/mol. Then E_3 is less than 37.8 kcal/mol, as

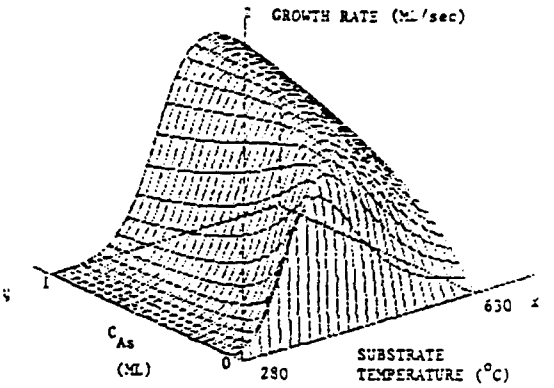

FIGURE 10
Calculated growth rate of InAs versus substrate temperature and surface arsenic concentration.

expected. E_{-2}, the activation energy for DMIn desorption is then less than 30 kcal/mol. This value is similar to the activation energy for TMGa desorption of 25 kcal/mol.[19]

The physical interpretation is similar to that discussed for CBE of GaAs. The growth-rate behavior at high substrate temperature and high arsenic pressure is similar to that in conventional solid-source MBE.

4. LASER-ASSISTED SELECTIVE-AREA EPITAXY OF GaAs

Selective-area growth is attractive because it could make possible the deposition of patterned layers, which could then be covered with layers of a different pattern or composition. Laser-assisted MOCVD and MOMBE have been reported recently. Specifically, Aoyagi *et al.* reported laser-assisted atomic layer epitaxy[20] and MOMBE[21] using argon ion laser. However, we chose ArF excimer laser because the large beam area (~1 cm^2) and short wavelength (193 nm) make possible the growth of chip-size patterns by projection lithography.

Once the surface oxide had desorbed and the growth temperature was established, the laser beam was directed at the substrate, followed immediately by the TEGa beam. Laser-enhanced growth rates were measured with a stylus profiler (Sloan Dektak model II). Excimer laser radiation leads to growth of ~2×10 mm^2 area GaAs films. The growth rate enhancement in the center of the film, in

the region of highest laser intensity, is plotted as a function of average substrate temperature in Figure 11. At 520°C the growth of GaAs resulting from pyrolysis of TEGa occurs with maximum efficiency; hence laser enhancement does not occur. However, below ~450°C pyrolysis becomes inefficient, and laser-enhanced growth dominates. The growth rate at low temperature is 0.15 Å pulse^{-1} or 3.0 Å s^{-1} at 20 Hz laser repetition rate.

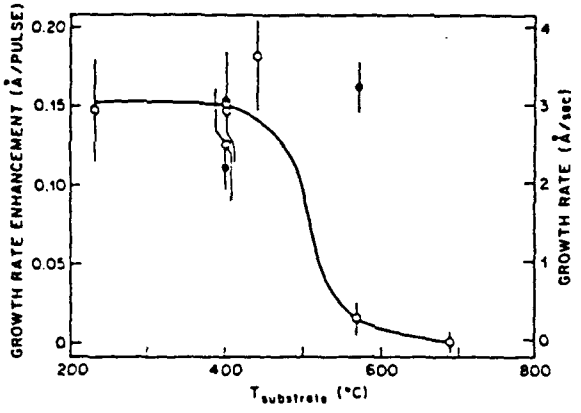

FIGURE 11
Growth rates as a function of steady-state substrate temperature (i.e., neglecting laser heating). (o): Laser-induced growth in Å pulse^{-1} and Å s^{-1}, (•): Total growth rate in Å s^{-1}. TEGa and As_4 beam pressures (uncorrected for ionization guage sensitivity) were 1.5×10^{-6} and 5×10^{-6} Torr, respectively. Laser fluence = 0.01 ± 0.01 J cm^{-2} pulse^{-1}. Repitition rate = 20 Hz.

The laser-enhanced growth rate of 3 Å s^{-1} at low temperature can be compared with the absolute TEGa beam flux. We can compute the TEGa flux from the TEGa pressure measured with the ionization gauge. A sensitivity factor of 5.3 for TEGa (relative to N_2) was compted from empirical methods.[22,23] Taking into account geometric factors, we estimate the flux to be 8.4×10^{14} molecules cm^{-2}s^{-1} under the conditions used to obtain the data in Figure 11. From this flux we compute a maximum growth rate of ~3.8 Å s^{-1} for GaAs. Consequently, at T≤500°C, where pyrolytic deposition is inefficient, TEGa molecules impinging on the surface near the region exposed to the most intense laser radiation react to form GaAs with near unity efficiency.

Of the possible mechanisms responsible for enhanced growth, gas-phase photodissociation can be ruled out, since the duty cycle of the laser is so small (3×10^{-7}) and the gas-phase number density is so low (1×10^{-6} Torr). Consequently, the laser must be dissociating adsorbed TEGa. Furthermore, TEGa must stick on GaAs longer than the time between laser pulses (50 ms), otherwise desorption would cause the laser-enhanced growth rate to fall well below the TEGa impingement rate, contrary to observations.

Laser-induced decomposition of adsorbed TEGa could occur by a photolytic (photodissociate TEGa), electronic (create electron-hole pairs in GaAs which aid in TEGa decomposition), or pyrolylitic process (thermally decompose TEGa because of transient heating of GaAs by the pulsed laser). We can gain more insight into these processes by determining the dependence of growth rate on laser fluence (J cm^{-2} pulse^{-1}). This was accomplished by measuring the film thickness along the short dimension of the beam with the stylus profiler and then comparing thickness with laser intensities determined from the beam profile measurements. A stylus profile is shown in Fig. 12, along with the laser intensity. Thickness falls off rapidly as a function of laser fluence, indicating a highly nonlinear process.

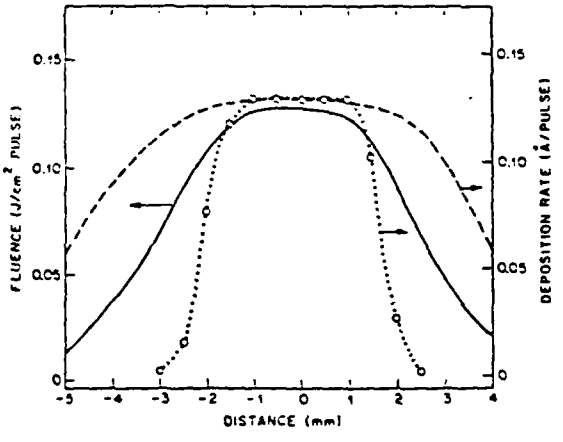

FIGURE 12
Deposition rate and laser intensity as a function of distance from the center of the laser beam across the short dimension. Beam pressures are the same as for Fig. 1. Substrate temperature = 400°C. (o); peak laser fluence = 0.12 J cm^{-2} pulse^{-1}, repetition rate = 20 Hz. Solid curve: laser intensity. Dashed curve: predicted deposition rate based on photochemical model.

We have shown elsewhere that the photochemical mechanism would result in a growth-rate enhancement nearly following the laser fluence profile as shown by dashed line in Fig. 12. Since the observed deposition rate falls off much more rapidly, we can exclude the simple photochemical model to explain laser-enhanced growth.[7] From the lack of laser-enhanced deposition at 0.05 J/cm^2 and below, we estimate the photodissociation absorption cross section to be at least ten times lower than the gas-phase value.[7] Likewise, an electron-hole pair mechanism would not depend so strongly on laser fluence and so does not seem likely.

We ascribe enhanced growth to pyrolysis of $TEGa_{(ads)}$ due to transient heating of the GaAs surface from pulsed laser irradiation. Such a process would be much more strongly dependent on peak laser power than the photolysis mechanism, as observed. Based on a numerical solution to the one-dimensional heat flow equation, we estimate a peak temperature rise T_{peak} of ~ 700°C at a fluence of 0.1 J/cm^2. From an Arrhenius plot of log growth rate versus $1/T_{peak}$ across the laser beam, we obtain an activation energy of 22-15 kcal/mol in the region where the film thickness is falling off rapidly with distance from the center. This is in fair agreement with the activation energy for TEGa pyrolysis of 20 kcal/mol derived from data by Pütz *et al.*[25] and with activation energies of 18 and 21 kcal/mol for the growth rate of GaAs from TEGa.[26] One piece of supporting evidence is the lack of wavelength dependence at high fluence for relative carbon coverage versus number of laser pulses. Carbon coverage was measured by x-ray photoelectron spectroscopy on a TEGa-covered GaAs surface as a function of the number of laser pulses at various laser intensities. At low fluence, the carbon coverage depends on laser wavelength, indicating a photolytic effect. At high fluence, the carbon coverage is independent of laser wavelengths, indicating pyrolytic, not photolytic, effects dominate.

Crystalline quality was studied by RBS for samples deposited at 400 and 570°C. In all cases, X_{min}'s were low (3-5%), indicating good crystal quality. Some dechanneling was observed in some cases near the film-substrate interface, indicating defects. However, the best results were obtained at the highest laser intensity (0.13 J pulse^{-1}) and at a substrate temperature of 400°C, where no interface could be found, and the RBS channeling spectrum was indistinguishable from a single crystal substrate. Low-temperature (2 K)-photoluminescence spectra (Fig. 13) revealed the added benefit of layer-by-layer laser annealing on luminescence intensity. the peak at 835 nm is identified as an acceptor band associated with a carbon impurity. The regions exposed to the highest excimer laser intensity during growth exhibited the most intense luminescence, most likely because of laser annealing of defects in the growing epitaxial film, which otherwise acts as a nonradiative recombination center. However, the overall quality of the material is still rather low since the exciton bands are not observed, the most intense peak is broad and due to carbon imputity, and the overall intensity is relatively small. We attribute this to the relatively poor-quality vacuum system in which these preliminary experiments were carried out, compared to state-of-the-art MBE systems. Similar effects were obvserved in GaAs grown from elemental Ga.

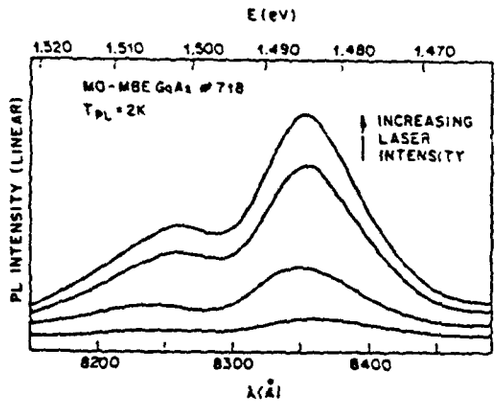

FIGURE 13
Low-temperature photoluminescence spectrum of GaAs deposited at 570°C. TEGa and As_4 beam pressures (uncorrected for ion gauge sensitivity) were 1.3×10^{-5} and 1.7×10^{-5} Torr, respectively. Laser repetition rate = 20 Hz. Laser fluence = 0.095 J cm^{-2} pulse^{-1} for top curve and ≤ 0.01 for bottom curve. The other two curves are for levels of radiation between these two extremes.

In summary, 193 nm ArF excimer laser irradiation enhances the growth of GaAs from triethylgallium and As_4. Below ~ 450°C, growth is controlled by the laser. Film growth is epitaxial, as confirmed by RBS.

Photoluminescence yields are also increased because of laser annealing of the growing film. The mechanism is dominated by laser pyrolysis (as oposed to photolysis) of adsorbed TEGa. Laser-induced growth is very efficient, with ~ 100% of the impinging TEGa being dissociated by the laser to form GaAs. Finally, we have demonstrated the potential for selective area growth, since at low substrate temperature there is no growth in the absence of laser irradiation.

ACKNOWLEDGMENT

The work at UCSD is partially supported by the Air Force Wright Research and Development Center under Contract No. F33615-88-C-1861 and by the Office of Naval Research under Grant No. N00014-89-J-1147. We wish to thank T.P. Chin, L.Y. Wang, and H.Q. Hou for assistance in MOMBE data taking and analysis and V.R. McCrary and J.C. Beggy for assistance during laser-assisted MOMBE.

REFERENCES

1. E. Veuhoff, W. Pletschen, P. Balk and H. Luth, J. Cryst. Growth 55 (1981) 30.
2. W.T. Tsang, Appl. Phys. Letters 45 (1984) 1234.
3. R. Robertson, Jr., T.H. Chiu, W.T. Tsang and J.E. Cunningham, J. Appl. Phys. 64 (1988) 877.
4. B.W. Liang and C.W. Tu, Appl. Phys. Letters, August 13, 1990.
5. B.W. Liang, L.Y. Wang and C.W. Tu, Proc. XII State-of- the-art Prog. on Comp. Semicond., in press.
6. L. Fraas, G.R. Girard, V. Sundaram, C. Master, C. Nelson and R.A. Stall, Mater. Res. Soc. Symp. Proc. 145 (1989) 253.
7. V.M. Donnelly, C.W. Tu, J.C. Beggy, V.R. McGrary, M.G. Lamont, T.D. Harris, F.A. Baiocchi and R.C. Farrow, *Appl. Phys. Letters 52 (1988) 1065.*
8. H. Sugiura, R. Iga, T. Yamada and M. Yamaguchi, Appl. Phys. Letters 54 (1989) 335.
9. C.W. Tu, B.W. Liang, T.P. Chin and J. Zhang, J. Vac. Sci. Technol. B 8 (1990) 293.
10. B.W. Liang, T.P. Chin and C.W. Tu, J. Appl. Phys. 67 (1990) 4393.
11. J.A. McCaulley, V.R. McCrary and V.M. Donnelly, J. Phys. Chem. 93 (1988) 1148.
12. C.W. Tu, V.M. Donnelly, J.C. Beggy, F.A. Baiocchi, V.R. McCrary, T.D. Harris and M.G. Lamont, Appl. Phys. Letters 52 (1988) 966.
13. S. Horiguchi, K. Kimura, K. Kamon, M. Mashita, M. Shimazu, M. Michara and M. Ishii, Jpn. J. Appl. Phys. 25 (1986) L979.
14. T.H. Chiu, Mater. Res. Soc. 145 (1989) 47.
15. C.W. Tu, B.W. Liang and T.P. Chin, J. Cryst. Growth, in press.
16. D.E. Aspnes, E. Colas, A.A. Studna, R. Bhat, M.A. Koza and V.G. Keramidas, Phys. Rev. Letters 61 (1988) 2782.
17. R. Chow and R. Fernandez, Mater. Res. Soc. Symp. Proc. 145 (1989) 13.
18. M. Tirtowidjojo and R. Pollard, J. Cryst. Growth 77 (1986) 200.
19. E. Coltrin and R.J. Kee, *Mater. Res. Soc. Symp.* Proc. 145 (1989) 119.
20. Y. Aoyagi, A. Doi, T. Meguro, S. Iwai, K. Nagata and S. Nonoyama, Chemtronics 4 (1989) 117.
21. K. Nagata, Y. Iimura, Y. Aoyagi and S. Namba, J. Cryst. Growth 95 (1989) 142.
22. D.K. Sharma and A.N. Pandey, J. Acta Ciencia Indica 1 (1974) 35.
23. K.J. Miller and J.A. Savchik, J. Am. Chem. Soc. 101 (1979) 7206.
24. V.R. McCrary and V.M. Donnelly, J. Cryst. Growth 84 (1987) 253.
25. N. Pütz, E. Veuhoff, H. Heinecke, M. Heyen, H. Lüth and P. Balk, J. Vac. Sci. Technol. B 3 (1985) 671.
26. P. Balk, M. Fisher, D. Grundmann, R. Lückerath, M. Lüth and W. Richter, J. Vac. Sci. B 4 (1987) 1453.

To be published in J. Crystal Growth
(1991)

THE ROLES OF GROUP-V SPECIES IN METALORGANIC MOLECULAR-BEAM EPITAXY AND CHEMICAL-BEAM EPITAXY OF III-V COMPOUNDS

B.W. LIANG and C.W. TU

Department of Electrical and Computer Engineering, University of California at San Diego, La Jolla, California 92093-0407, U.S.A.

Our kinetic model for metal-organic molecular-beam epitaxy (MOMBE) and chemical-beam epitaxy (CBE) of GaAs has been extended to GaSb. This model can fit experimental data for growth with triethylgallium (TEGa) and antimony. The roles of group-V species in MOMBE of III-V compounds are summarized. Group-V species are as important as group-III species in determining the growth rates in MOMBE and CBE.

1. Introduction

More and more people are interested in metalorganic molecular-beam epitaxy (MOMBE) or chemical-beam epitaxy (CBE) [1,2] because of its special properties, such as different growth kinetics from conventional MBE [3-5], atomic layer epitaxy (ALE) [7,10,11], high carbon doping [6,7], and selective-area epitaxy [8,9]. In previous papers [4,5], we have studied the growth kinetics of MOMBE of GaAs and InAs. We found that arsenic plays an important role in MOMBE or CBE. The growth rate is very sensitive to arsenic beam flux. Our kinetic model can fit experimental results very well and provide more insights into the growth process.

In this paper, we extend our model to MOMBE of GaSb with triethylgallium (TEGa) and antimony and summarize the roles of group-V species in MOMBE of III-V compounds.

2. Growth Kinetics

2.1 MOMBE of GaSb

Because the mean-free paths of molecules are very long compared to the source-to-substrate distance, one can expect that gas-phase reactions are unimportant in MOMBE, unlike in metalorganic chemical vapor deposition (MOCVD). Surface reactions dominate the growth process. The first kinetic model proposed by Robertson et al. considered only triethylgallium (TEGa) decomposition paths [3]. The role of arsenic species was presumed secondary. Subsequently, group-V species, unlike in conventional MBE, were found to have a strong effect on the growth rate. This model therefore cannot explain the arsenic dependence of growth rates. Another model proposed by Kaneko et al. [12] for MOMBE of GaSb assumes the growth rate is controlled by the antimony vacancy and provides the relation between growth and antimony surface concentration with $R_g \sim f(T)^*[Sb]^{-n}$, where n is the number of antimony vacancy. According to their model, if [Sb]=0, growth rate of GaSb is infinity. Obviously, it is not right because the growth rate of GaSb must be zero without antimony. We have proposed a new kinetic model [4], taking into account the effect of arsenic species for the first time, for CBE of GaAs using TEGa and arsine (AsH_3). The model can fit the experimental data of Chiu et al.[11] very well.

The model assumes that diethylgallium (DEGa) decomposition, in the presence of arsenic, is the rate-limiting step for growing GaAs. We expect that monoethylgallium (MMGa), with two ethyl radicals cleaved off, would be very

reactive and chemisorb strongly to the surface. Cleavage of the last ethyl radical and subsequent incorporation of GaAs would occur very fast due to small activation barrier. This situation is similar to Robertson's model. What differentiates our model is that this DEGa decomposition step includes an arsenic species. Experimentally, the growth rate decreases with increasing arsine flow rate, and this has been attributed to the site-blocking effect [11]. In our preliminary study, the site-blocking mechanism does not agree with experimental data. We therefore propose enhanced desorption of TEGa by excess arsenic on the surface in the continuous CBE or MOMBE process. Similar to GaAs, for GaSb, the proposed surface chemical reactions are as follows,

(1) $TEGa(g) \xrightarrow{FS_o} TEGa(ad)$

(2) $TEGa(ad) \xrightarrow{k3} DEGa(ad)$

(3) $TEGa(ad) + Sb_2(ad) \xrightarrow{k\text{-}3} TEGa(g) + 1/2\ Sb_4(g)$

(4) $DEGa(ad) \xrightarrow{k\text{-}2} DEGa(g)$

(5) $DEGa(ad) + Sb_2(ad) \xrightarrow{k} GaSb + \text{other products}$

In reaction (1), F is the TEGa beam flux, and S_o is the adsorption probability. *k*'s are various reaction rate coefficients. Similar to Robertson's model, we postulate the cleavage of the second ethyl radical to be the rate-limiting step. In our model, the growth rate (R_g) depends not only on the DEGa surface concentration X_2, but also on the antimony surface concentration C_{Sb}.

$$R_g = k X_2 C_{Sb} \qquad (1)$$

In the steady-state condition, concentrations of adsorbed TEGa (X_3) and DEGa (X_2) are independent of time. Solving for X_2 and X_3 and assuming Arrhenius behavior for the reactions, $ki = k X_2 C_{Sb}$, we obtain

$$R_g = FS_o/[1+A_1 \exp(-\Delta E_1/RT)/C_{Sb}]/[1+A_2 C_{Sb} \exp(-\Delta E_2/RT)] \quad (2)$$

where $A_1 = A_{-2}/A$; $A_2 = A'/A_3$; $\Delta E_1 = E_{-2} - E$ and $\Delta E_2 = E' - E_3$. There are six unknown parameters (A_1, A_2, ΔE_1, ΔE_2, FS_o and C_{Sb}). Note that in this model, we have further assumed that (1) there is no Ga desorption because the growth temperature is below that of Ga desorption; and (2) the temperature dependence of S_o and C_{Sb} is small in the range studied.

We use equation (2) to fit experimental data from Ref.12. First, we fit the growth rate versus substrate temperature at 2.0 sccm of TEGa flow rate and 1.2×10^{-6} torr of antimony beam equivalent pressure since their data points under this condition look relatively complete and have relatively small scatter compared with the other two sets of data. We obtain the fitting parameters as follows: A_1=3000 ML, ΔE_1=21 Kcal/mol, $A_2 = 5 \times 10^{-10}$ ML^{-1}, ΔE_2=-34.8Kcal/mol, FS_o=0.7 ML/cm^2s, and C_{Sb}=0.48 ML. ML stands for monolayers. Then we fix the values of A_1, A_2, ΔE_1, and ΔE_2, and adjust FS_o and C_{Sb} to fit other growth-rate curves, as shown in figure 1. It should be mentioned that because the data points scatter, we ignored the highest point in the set of points for which TEGa flow rate is 1.0 sccm.

Using these parameters we calculate the growth rate as a function of C_{Sb}, as shown in figure 2 for various substrate temperatures used in Ref.12. Qualitatively these curves agree well with the data in Ref. 12.

We now discuss the parameter obtained from the model. Consider first $\Delta E_1 = E_{-2} - E$, where E_{-2} is the activation energy of DEGa desorption and E is the

activation energy for reaction (5). Since DEGa and Sb_2 are reactive, E is probably small. Therefore, $\Delta E_1 \approx E_{-2}$, which means $E_{-2} \approx 21$Kcal/mol. This value is almost the same as our previous result for GaAs [4], and it indicates that the DEGa desorption activation energy is the same on GaSb as on GaAs surface. Now, consider $\Delta E_2 = E' - E_3$, where E' is the activation energy of antimony-enhanced desorption, and E_3 is the activation energy for TEGa decomposing into DEGa. Since the binding energy for physisorbed molecules should be in the range of 1-10 kcal/mol, E_3 is in the range 35.8-45 kcal/mol. This value is reasonable compared with the gas-phase value of 46 kcal/mol.

2.2 The Roles of Group-V Species in MOMBE and CBE

Surveying the growth behaviors of MOMBE of GaAs, InAs and GaSb, as shown in figure 3, 4 and 5, we can come to a conclusion that group-V species play very important roles in MOMBE and CBE. For TEGa, in the low group-V surface concentration range, The group-V affects growth rates very seriously, especially in low substrate temperature range. For TMIn, even though arsenic affects the growth rate too, but not as much as that in TEGa. This may be because of the difference between TEGa and TMIn in chemistry. According to our kinetic model, there are two competing reactions, reaction (2) and (3), during MOMBE or CBE of III-V compounds. For example, in GaSb, one is TEGa decomposing into DEGa, the other is antimony-enhanced TEGa desorption. At low substrate temperature, reaction (2) is slow, thus reaction (3) plays the major role. Growth rate increases with increasing the surface concentration of group-V species first and then decreases very quickly. But at high substrate temperature, both reaction (2) and (5) are very fast. So, reaction (3) does not play important role anymore. The growth rate behaves like conventional MBE.

In summary, group-V species play an important role in MOMBE and CBE, especially in low substrate temperature. On the one hand, group-V species on the surface react with alkyl-group-III radical, such as DEGa and this kind of reaction limits growth rate, so the higher the surface concentration of group-V species, the higher the growth rate; On the other hand, too much group-V species on the surface may enhance desorption of alkyl-group-V molecules, then growth rate decreases with increasing group-V beam flux. So, accurate controlling of both group-V beam flux and substrate temperature is a critical issue in MOMBE and CBE. we have succeeded in extending our kinetics model for MOMBE of GaAs and InAs to GaSb. The model can fit the experimental data very well and explain how TEGa flow rate and antimony surface concentration influence the growth rate.

Acknowledgment

This work was partially supported by the Air Force Wright Research and Development Center and the Office of Naval Research. We wish to thank H.Q.Hou for help in fitting the data.

References

1. E. Veuhoff, W. Pletschen, P. Balk and H. Luth, J. Cryst. Growth 55 (1981) 30.
2. W.T. Tsang, Appl. Phys. Lett. 45 (1984) 1234.
3. R. Robertson, Jr., T.H. Chiu, W.T. Tsang and J.E. Cunningham, J. Appl. Phys. 64 (1988) 877.
4. B.W.Liang and C.W. Tu, Appl. Phys. Lett. 57 (1990) 689.
5. B.W. Liang, L.Y. Wang and C.W. Tu, Proc. XII State-of-the-art Prog. on Comp. Semicon., in press.

6. M. Weyers, N. Putz, H. Heniecke, M. Heyen, H. Luth, and P. Balk, J. Electron. Mater. 15 (1986) 57.
7. C.W.Tu, B.W. Liang, T.P. Chin, and J. Zhang, J. Vac. Sci. Technol., B8 (1990) 293.
8. V.M. Donnelly, C.W.Tu, J.C.Beggy, V.R. McGrary, M.G. Lamont, T.D. Harris, F.A. Baiocchi and R.C. Farrow, Appl. Phys. Lett. 52 (1988) 1065.
9. H. Sugiura, R. Iga, T. Yamada and M. Yamaguchi, Appl. Phys Lett. 54 (1989) 335.
10. B.W. Liang, T.P. Chin and C.W. Tu, J. Appl. Phys. 67 (1990) 4393.
11. T.H. Chiu, Mater. Res. Soc. Proc. 145 (1989) 47.
12. T. Kaneko, H. Asahi, Y. Okuno, T.W. Kang and S. Gonda, J. Cryst. Growth 105 (1990) 69.

Figure Caption

Figure 1. The relation between growth rate of GaSb by MOMBE and substrate temperature.

Figure 2. The dependence of growth rate of GaSb on antimony surface concentration resulting from our model.

Figure 3. Growth rate of InAs using TMIn and As_4 as a function of substrate temperature (from 280 °C to 630 °C) and arsenic surface concentration.

Figure 4. Growth rate of GaAs using TEGa and arsine as a function of substrate temperature (from 280 °C to 630 °C) and arsenic surface concentration.

Figure 5. Growth rate of GaSb using TEGa and Sb_4 as a function of substrate temperature (from 280 °C to 630 °C) and arsenic surface concentration.

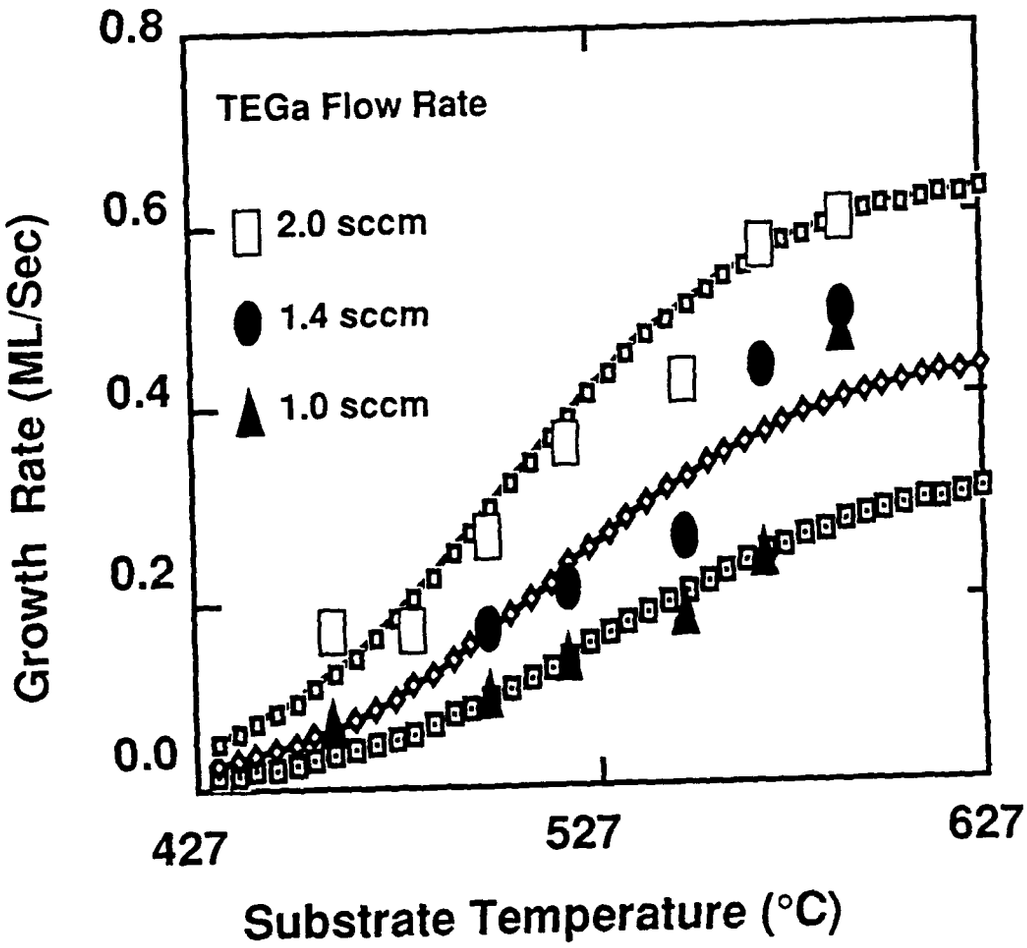
0.8
0.6
0.4
0.2
0.0
TEGa Flow Rate
2.0 sccm
1.4 sccm
1.0 sccm
Growth Rate (ML/Sec)
427
527
627
Substrate Temperature (°C)

Figure 1

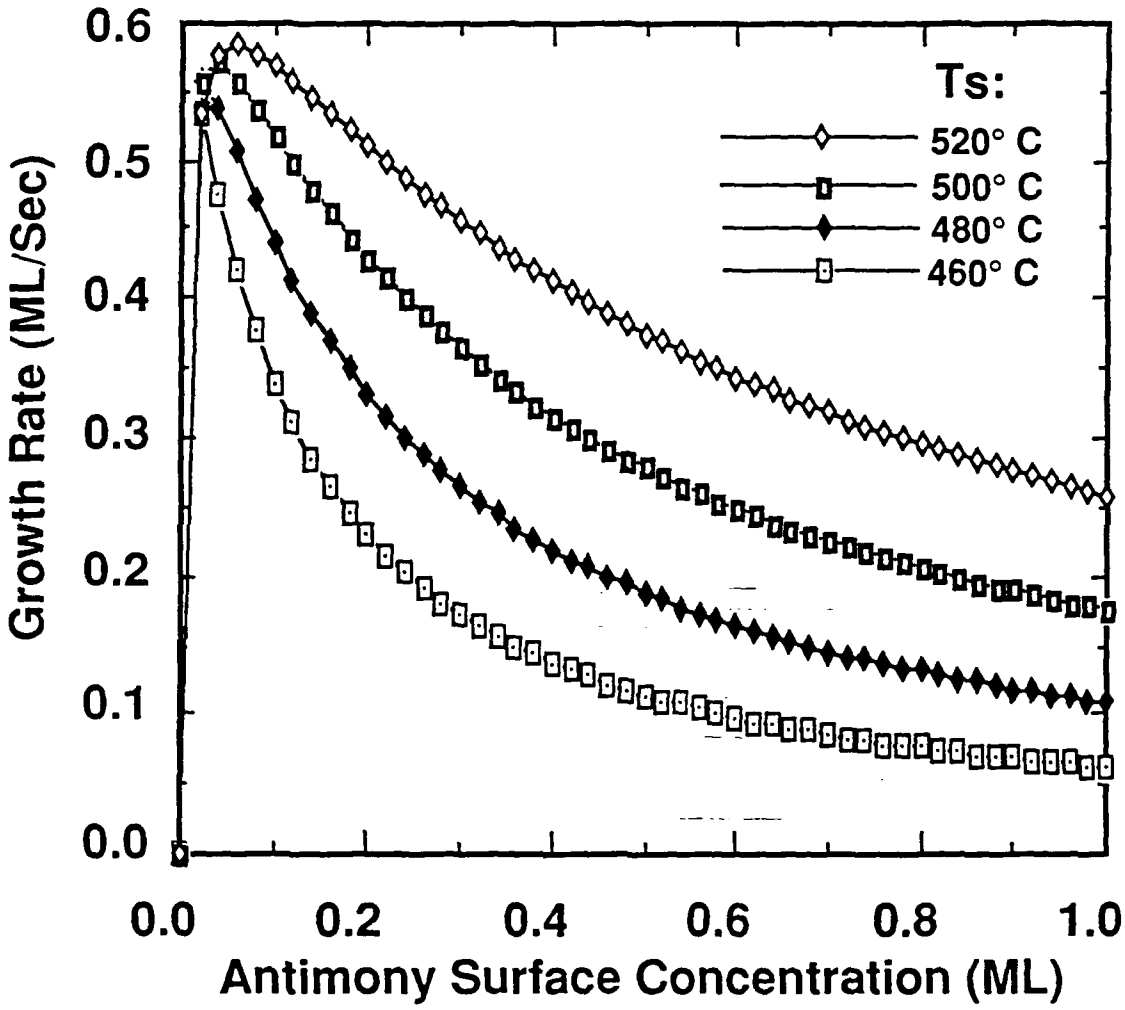
Growth Rate (ML/Sec)
0.6
0.5
0.4
0.3
0.2
0.1
0.0
Ts:
520° C
500° C
480° C
460° C
0.0
0.2
0.4
0.6
0.8
1.0
Antimony Surface Concentration (ML)

Figure 2

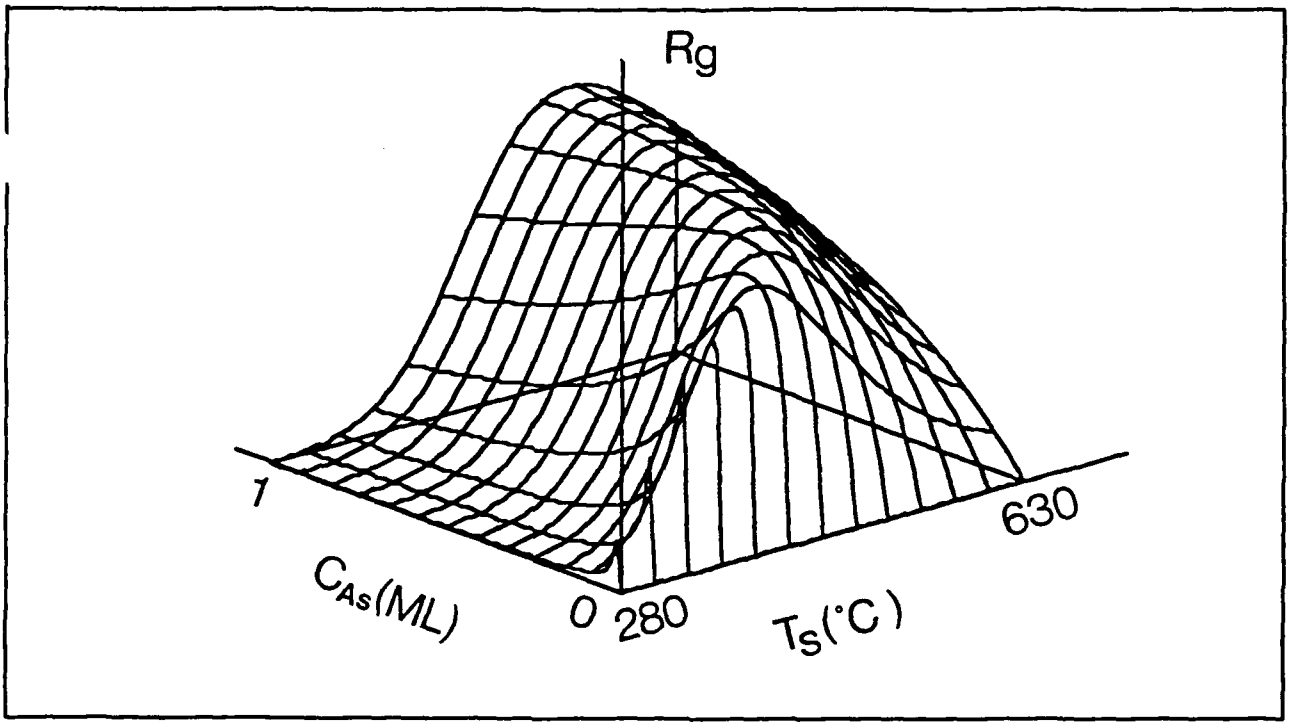

Figure 3

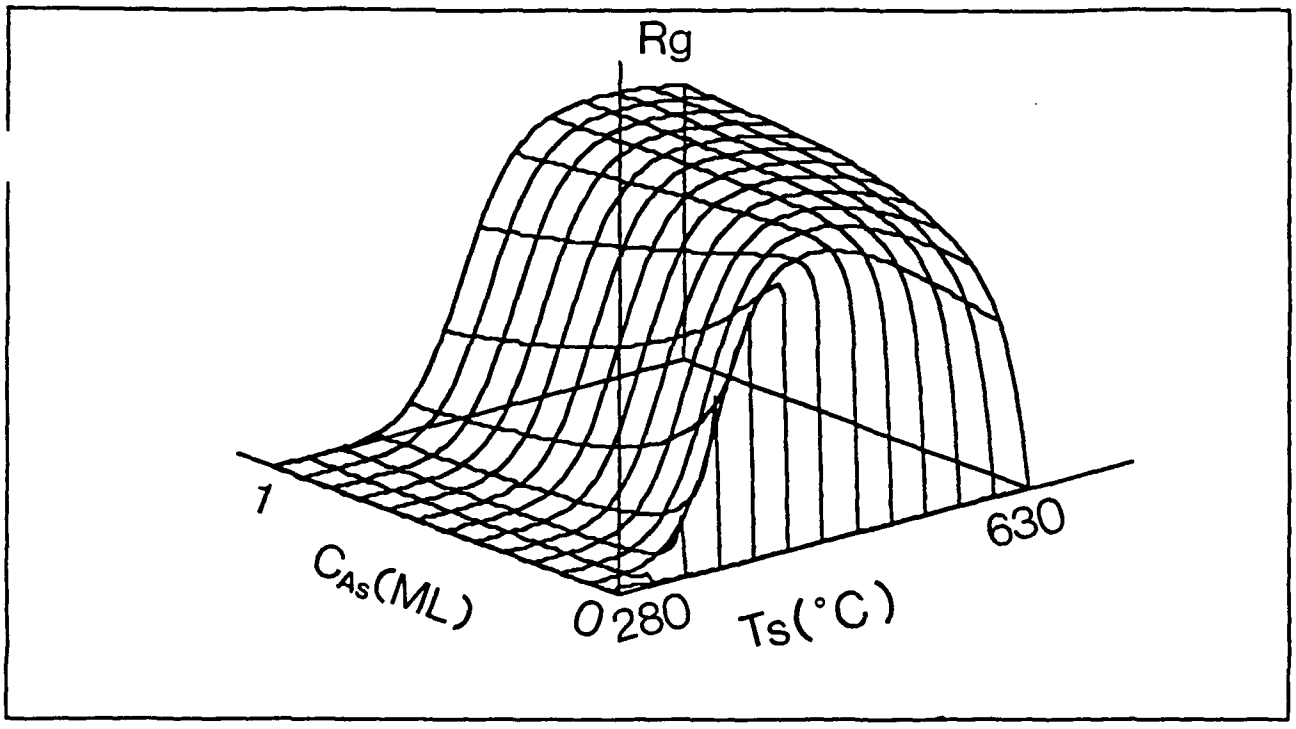

Figure 4

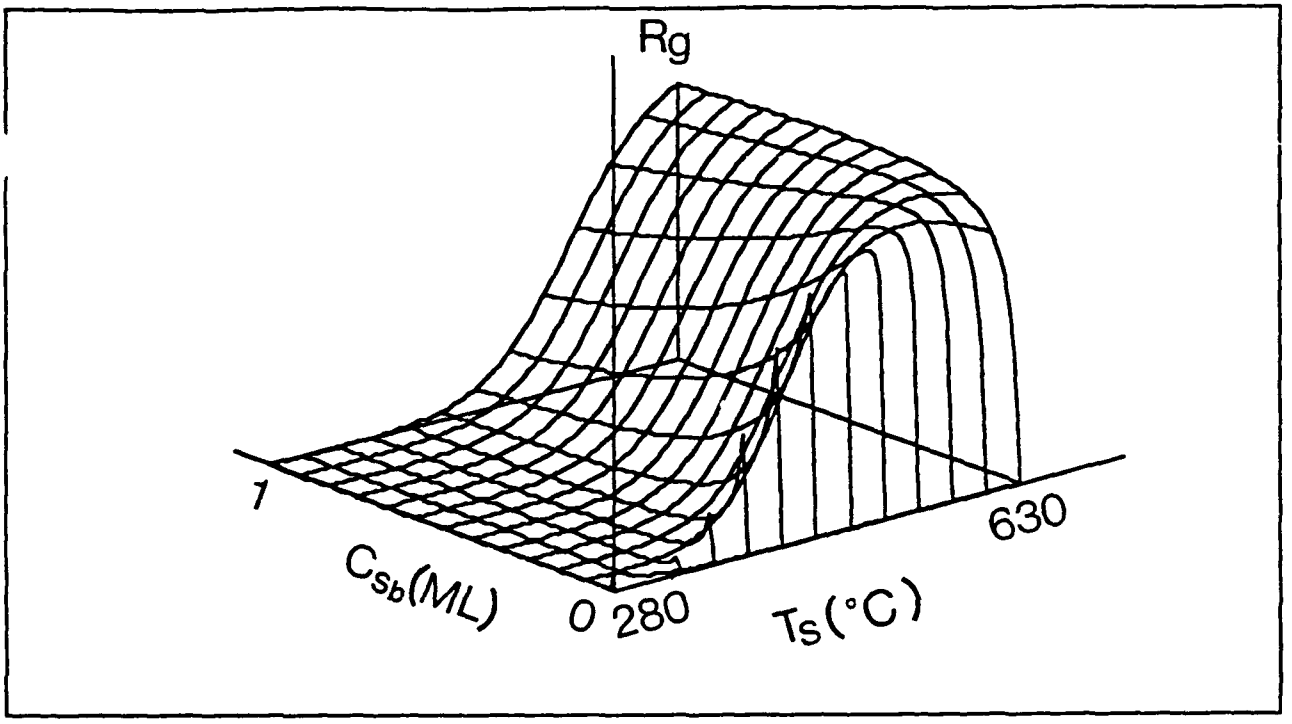

Figure 5

To be published in Appl. Phys. Lett.
(1990)

Determination of V/III ratios on phosphide surfaces during gas-source molecular-beam epitaxy

T.P. Chin, B.W. Liang, H.Q. Hou, M.C. Ho, C.E. Chang, and C.W. Tu

Department of Electrical and Computer Engineering 0407, University of California, San Diego, La Jolla, California 92093-0407

Phosphorus-controlled growth rate of homoepitaxial (100) InP, GaP, and AlP on GaP substrates by gas-source molecular-beam epitaxy (GSMBE) was investigated. Elemental group-III sources and thermally cracked phosphine were used. The growth rate was monitored by the specular-beam intensity oscillations of reflection high-energy-electron diffraction (RHEED). This technique gives exact values of V/III ratio on the surface by measuring the amount of phosphorus which is actually incorporated into the film. Here the V/III ratio is defined as P-controlled growth rate divided by group-III-controlled growth rate instead of the beam flux V/III ratio. Also the phosphorus surface desorption activation energies were measured to be 0.82 eV and in the range between 0.89-0.97 eV for InP and GaP, respectively.

Considerable potential exists for phosphorus-containing semiconductor materials in electronic and optoelectronic device applications. InP is a promising material for microwave sources and amplifiers operating at high power and high frequencies with lower noise. Long-wavelength (1.3 μm or 1.55 μm) optical-fiber communication systems also employ InP in devices. GaP and AlP have been proposed for high-temperature electronic devices due to the large band gap and small lattice mismatch between each other.[1,2] Heterojunction bipolar transistors (HBT) of GaP/$Al_xGa_{1-x}P$ working at temperatures as high as 550°C has been reported.[3] GaP has been widely used to make yellow, red and green light emitting diodes.[4]

Many of the applications described above will require multi-layer structure and abrupt changes in composition or doping. Gas-source molecular-beam epitaxy is a viable technique for growing phosphides because it may provide more precise control of phosphorus flux than conventional molecular-beam epitaxy (MBE) and better layer thickness control than liquid-phase epitaxy or vapor-phase epitaxy.[5] Critical issues of high-quality epilayer growth are the growth temperature and V/III ratio. In conventional MBE, the V/III ratio is obtained by measuring beam equivalent pressure. In GSMBE the high hydrogen background pressure (typically $1x10^{-5}$ Torr) makes accurate V/III ratio measurement by ion gauge difficult. Another problem is that the V/III ratio at the substrate surface depends on the growth temperature, thus will be different from the beam flux ratio. Panish and Sumski demonstrated a calculation of the group-V beam flux at the substrate surface by converting the equilibrium group-V partial pressure in a solid+liquidus system for GaAs and InP in GSMBE.[6] Group-V-controlled growth rate measurement goes even further by measuring the amount of group-V incorporated into the epilayer regardless the chamber geometry, ionization factor of the ion gauge and high hydrogen background pressure.[7,8] Similar experiment of arsenic-controlled growth rate measurement in conventional MBE has been used to measure the arsenic incorporation rate and sticking

coefficients of both As_2 and As_4 on GaAs (100).[9] Here we report for the first time phosphorus-controlled growth rate measurement of InP, GaP and AlP in GSMBE.

The GSMBE system consists of a modified Varian Modular GEN-II MBE reactor equipped with a 2200 l/s (H_2) cryopump and an ion pump (which is turned off during growth). Two separate gas cabinets house two gas-source supply systems (100% arsine and 100% phosphine) as well as scrubbers. Both gases are introduced into the growth chamber through the same Varian hydride injector. The normal cracking temperature is 1000°C. The phosphine flow rate in this study is typically 1-4 sccm. The background pressure ranges between 0.8×10^{-5} and 2×10^{-5}Torr during growth. The growth rates are monitored by the specular beam intensity oscillation of RHEED. A dual-channel differential amplifier[10] produces clean RHEED signals after subtracting the background noises. The oscillation is then recorded in an IBM PC AT compatible computer to measure the growth rate.

InP (100) substrates were degreased in a 1% Alconox solution and then rinsed with DI water. They were etched afterwards in a solution of H_2O_2:NH_4OH:H_2O (2:5:10), rinsed, and blown dry. For GaP (100), there is an additional step of 50% HCl dip before the final rinse. Each sample was bonded onto a 3-inch Si wafer with In. The Si wafer was then mounted onto a Mo transfer ring with Ta wires. Growth temperatures were calibrated with a pyrometer and the melting point of InSb.

Fig. 1(a) illustrates a typical RHEED oscillation and shutter operating sequence during the growth of GaP at 610°C. It started with a phosphorus-stabilized surface. Then Ga-induced oscillation was observed after the Ga shutter was opened. The RHEED intensity decreased after the phosphine shutter was closed due to the Ga accumulation on the substrate which formed a rough surface. The final step involved closing the Ga shutter and opening the phosphine shutter again. Here the oscillation resumed with incoming phosphorus species and previous Ga accumulated on the surface. This represents phosphorus-controlled growth because there was an excess amount of Ga atoms on the surface and the available amount of phosphorus limited the growth rate. While routinely

taking data, we just deposited several layers of Ga on the surface without phosphine, then the closed Ga shutter and opened the phosphine shutter at the same time. The resultant oscillation is shown in Fig. 1(b). The same experiments were performed in growing InP at 470°C and AlP at 615°C. Figure 2 shows the growth rates of (a) GaP, (b) AlP, and (c) InP as a function of the reciprocal group-III cell temperatures. The phosphorus-controlled growth rates, as measured by the procedures just mentioned, are shown with thick lines. They are independent of group-III fluxes.

For the case of InP, a different approach was also used to obtain phosphorus-controlled growth. With phosphine flow rate fixed the In-controlled growth rate was measured under various In fluxes. As the open circles show in Fig.2(c), the natural logarithm of the growth rate increases linearly with the reciprocal In cell temperature. This linear dependence stops at certain points then the growth rate become constant as In flux increases more. These points at which the growth rate saturates indicates unity V/III ratios, that is, In-controlled growth rate equals P-controlled growth rate. Growth rate in the plateau region is controlled by the phosphine flow rate, independent of the In flux. Fig.3(a) and (b) show RHEED oscillations of InP using different In fluxes. Both oscillations were taken under indium-rich conditions. At time t_1 the In shutter was opened. Since the V/III ratio was less than unity in this region, the excess In atoms were accumulated on the surface so that the growth continued even when the In shutter was closed at t_2. The V/III ratio in Fig.3(b) was even smaller than that in Fig.3(a). This results in more oscillations after t_2 in Fig.3(b) than that in Fig.3(a). One important feature of these oscillations is that the growth rate between t_1 and t_2 is the same as the growth rate after t_2. This identifies phosphorus-limited growth and the growth rate in this region depends only on the phosphine flow rate. Fig.4 combines the data from InP, GaP, and AlP. It shows linear behavior of phosphorus-limited growth rate versus phosphine flow rate in GSMBE. This demonstrates the precise flux control capability of GSMBE. The slope will strongly depend on growth temperature. Here the same slope

shared by the three different materials suggests that the P_2 incorporation coefficients in InP, GaP and AlP are equal under growth temperatures used in this study.

From the results in Fig. 2 and Fig. 4, we can obtain an accurate measure of the V/III ratio while growing all phosphides. For a given group-III flux and V/III ratio, we can set the corresponding phosphine flow rate accurately. An InP layer with 77K mobility 62,600 cm^2/V-sec and background carrier concentration N_d-N_a of $5.1x10^{14}$ cm^{-3} was achieved under V/III≈1 condition. Electrical and optical properties of epilayers grown under different V/III ratios are currently under investigations. Preliminary study of growth of arsenides by arsine in GSMBE yields similar results. Accurate V/III ratio control is very important for composition control in growing compounds containing mixed group-V elements, e.g., $GaAs_xP_{1-x}$ and $In_yGa_{1-y}As_xP_{1-x}$. The value of x in these compounds is not easily determined by the flow rate or the beam flux measured by an ion gauge. Combining the results of both phosphine and arsine will provide a convenient and precise way to control the x value in mixed-group-V compounds.[11]

The substrate temperature (Ts) dependence of phosphorus-controlled growth was also investigated on GaP and InP. The results are shown in Fig.5. On InP, the growth rate starts to decrease for Ts≥440°C. The P_2 surface desorption activation energy is estimated to be 0.82 eV. For GaP the phosphorus-controlled growth rate is fairly constant at substrate temperature from 550°C to 650°C and then decreases for Ts>650°C due to phosphorus desorption. The activation energy is measured to be in the range of 0.89-0.97 eV on the Arrhenius plot. These values are much larger compared to the As_2 incorporation activation energy obtained by Chow and Fernandez,[9] which were measured to be 0.2 eV on GaAs with similar experiments in conventional MBE.

In conclusion, the phosphorus-controlled growth of InP, GaP and AlP by GSMBE was determined experimentally. Growth rates were measured under different group-III fluxes, phosphine flow rates, and substrate temperatures. This technique, which measures the amount of phosphorus actually being incorporated in the epilayer growth can achieves

precise control of V/III ratio. Phosphorus surface desorption activation energies are also measured for GaP and InP.

This work is partially supported by Wright Research and Development Center and the Office of Naval Research and the Powell foundation.We wish to thank Professor H.H. Wieder for critical reading of the manuscript.

REFERENCES:

1. T.E. Zipperian and L.R. Dawson, Appl. Phys. Lett. 39, 895 (1981)

2. D.L. Keune, M.G. Crawford, A. H. Herzog and B. J. Fitzpatrick, J. Appl. Phys. 43, 3417 (1972)

3. T.E. Zipperian and L.R. Dawson, J. Appl. Phys. 54, 6019 (1983)

4. E.W. Williams and R. Hall, *Luminescence and the Light Emitting Diode*, (Pergamon, Oxford, 1978)

5. M.B. Panish and H. Temkin, Annu. Rev. Mater. Sci.19, 209 (1989)

6. B.F. Lewis and R. Fernandez, J. Vac. Sci. Technol. B 4 , 560 (1986)

7. R. Fernandez, J. Vac. Sci. Technol. B 6, 745 (1988)

8. R. Chow and R. Fernandez, Mat. Res. Soc. Symp. Proc. 145, 13 (1989)

9. M.B. Panish and H. Temkin, Appl. Phys. Lett. 44, 785 (1984)

10. C.E. Chang, T.P. Chin, and C.W. Tu, submitted to Rev. of Sci. Instrum. (1990)

FIGURE CAPTIONS:

Figure 1 : (a) RHEED oscillations of Ga and phosphorus-controlled growth on GaP(100). The intensity decreases when the Ga is deposited.
(b) Typical phosphorus-induced RHEED oscillation observed. The intensity recovers after Ga is consumed. The vertical scale and the sample azimuthal angle are different from those in (a) in order to observe better oscillations.

Figure 2 : Growth rate versus reciprocal group-III cell temperatures for (a) GaP, (b) AlP, and (c) InP.

Figure 3 : RHEED oscillations on InP (100) for $V/III_b < V/III_a < 1$. Notice the growth continues after In shutter is closed at t_2 due to accumulated In on the surface.

Figure 4 : Phosphorus-controlled growth rate versus phosphine flow rate.

Figure 5 : Arrhenius plot of phosphorus-controlled growth rate versus substrate temperature.

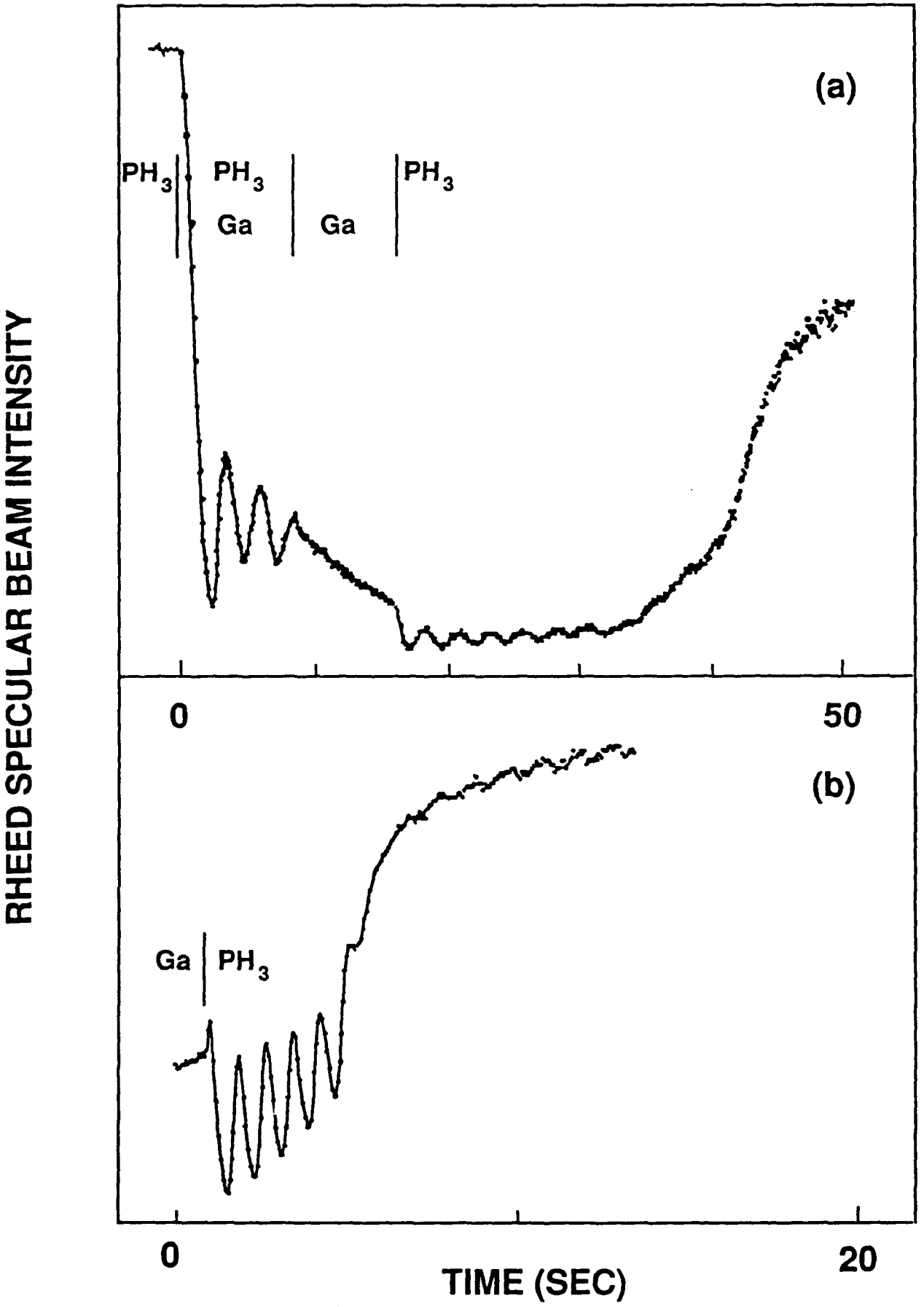
RHEED SPECULAR BEAM INTENSITY
(a)
PH3
PH3
Ga
Ga
PH3
0
50
(b)
Ga
PH3
0
20
TIME (SEC)

Figure 1

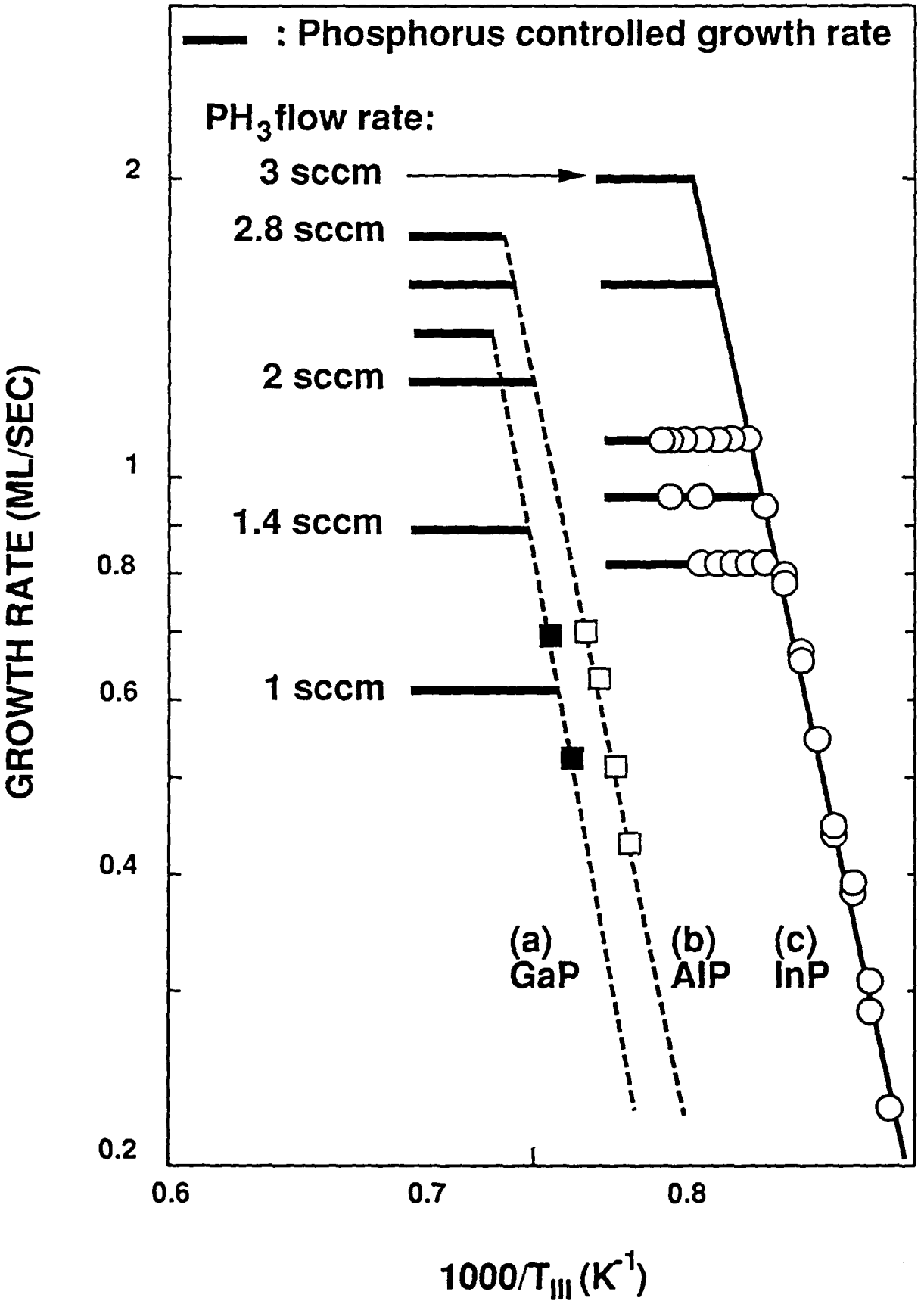
: Phosphorus controlled growth rate
PH3 flow rate:
3 sccm
2.8 sccm
2 sccm
1.4 sccm
1 sccm
(a) GaP
(b) AlP
(c) InP
GROWTH RATE (ML/SEC)
2
1
0.8
0.6
0.4
0.2
0.6
0.7
0.8
1000/T_III (K^-1)

Figure 2

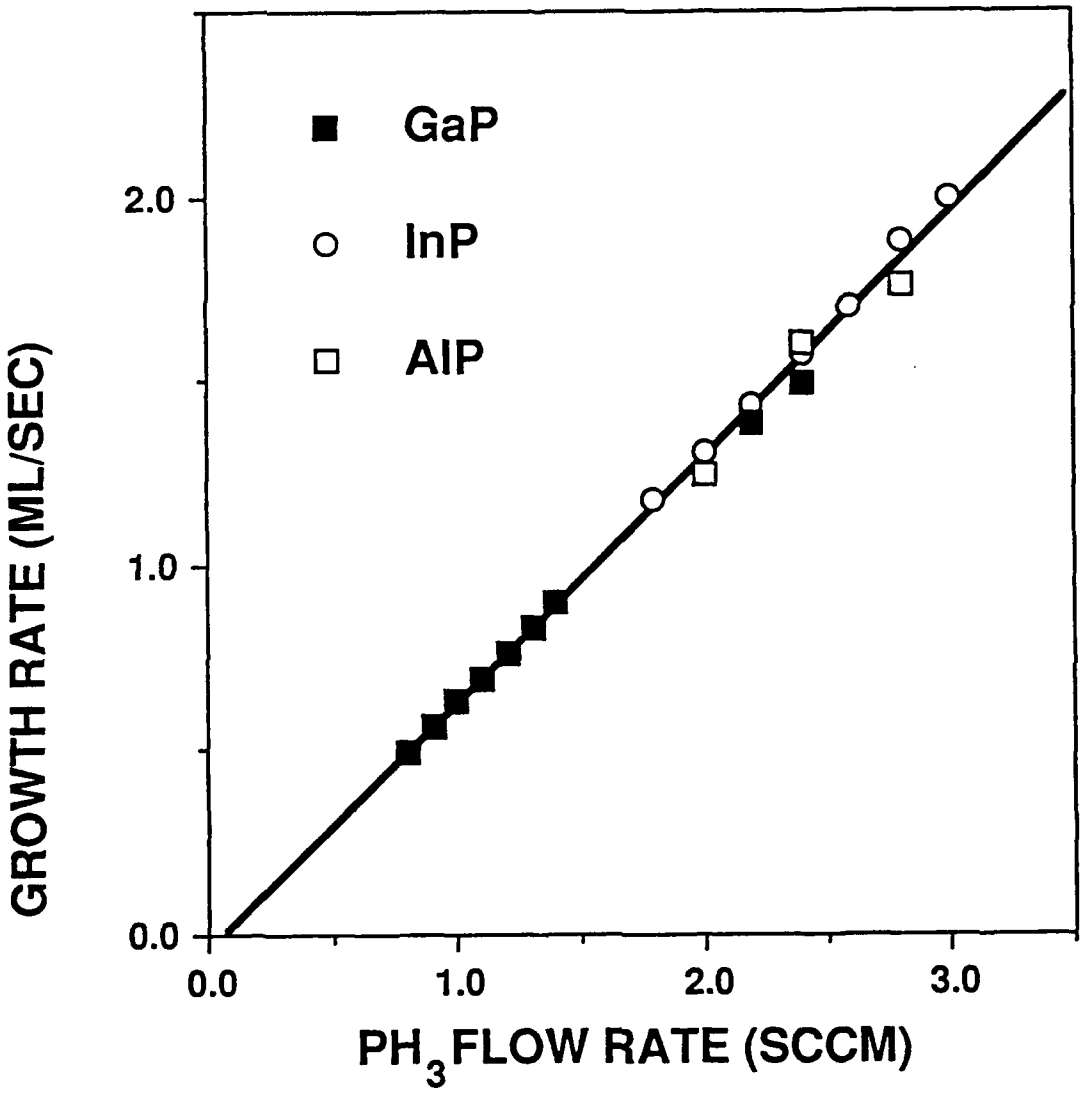
GaP
InP
AlP
2.0
1.0
0.0
0.0
1.0
2.0
3.0
GROWTH RATE (ML/SEC)
PH3 FLOW RATE (SCCM)

Figure 3

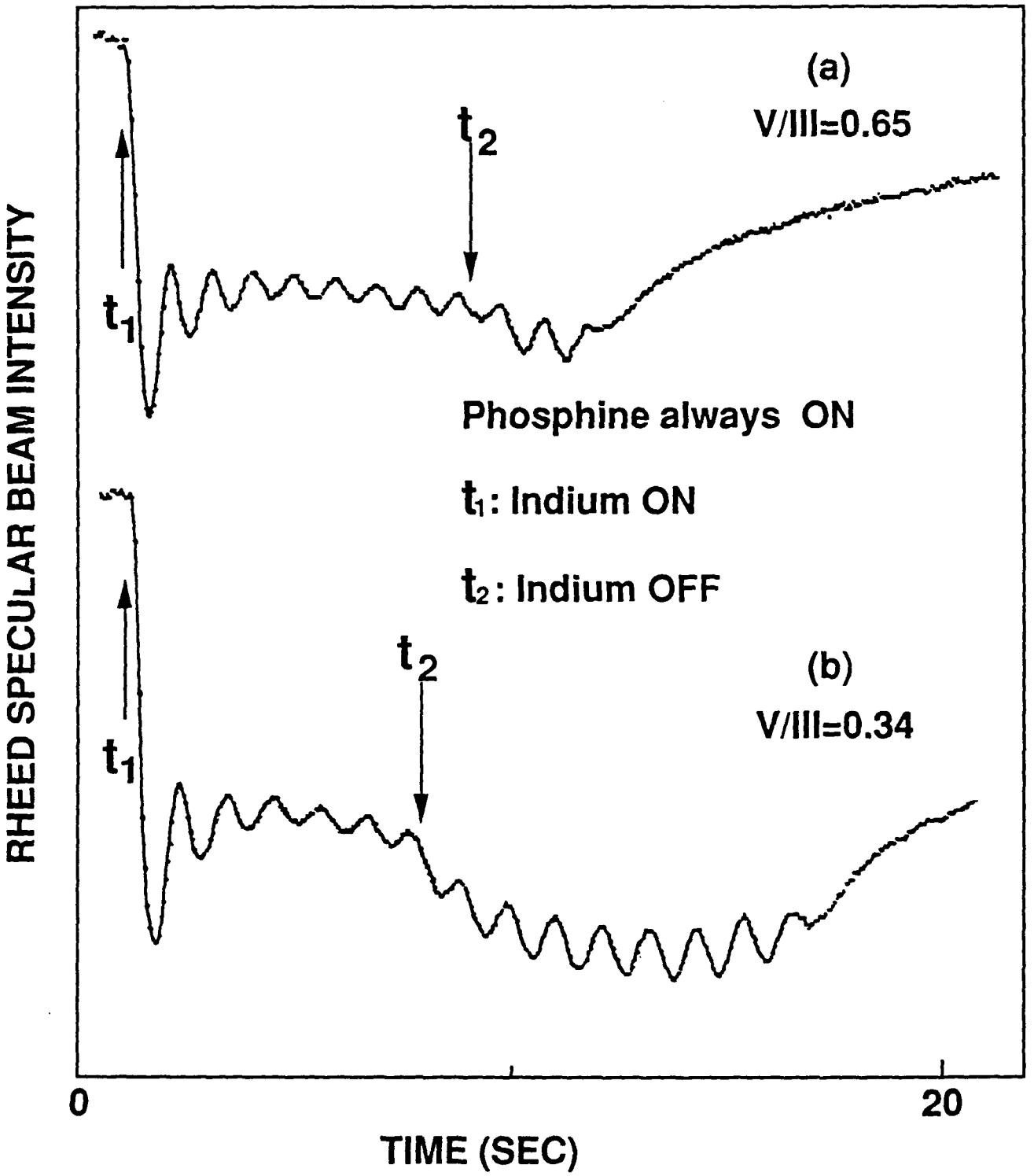
RHEED SPECULAR BEAM INTENSITY
(a)
V/III=0.65
t_2
t_1
Phosphine always ON
t_1: Indium ON
t_2: Indium OFF
t_2
(b)
V/III=0.34
t_1
0
20
TIME (SEC)

Figure 4

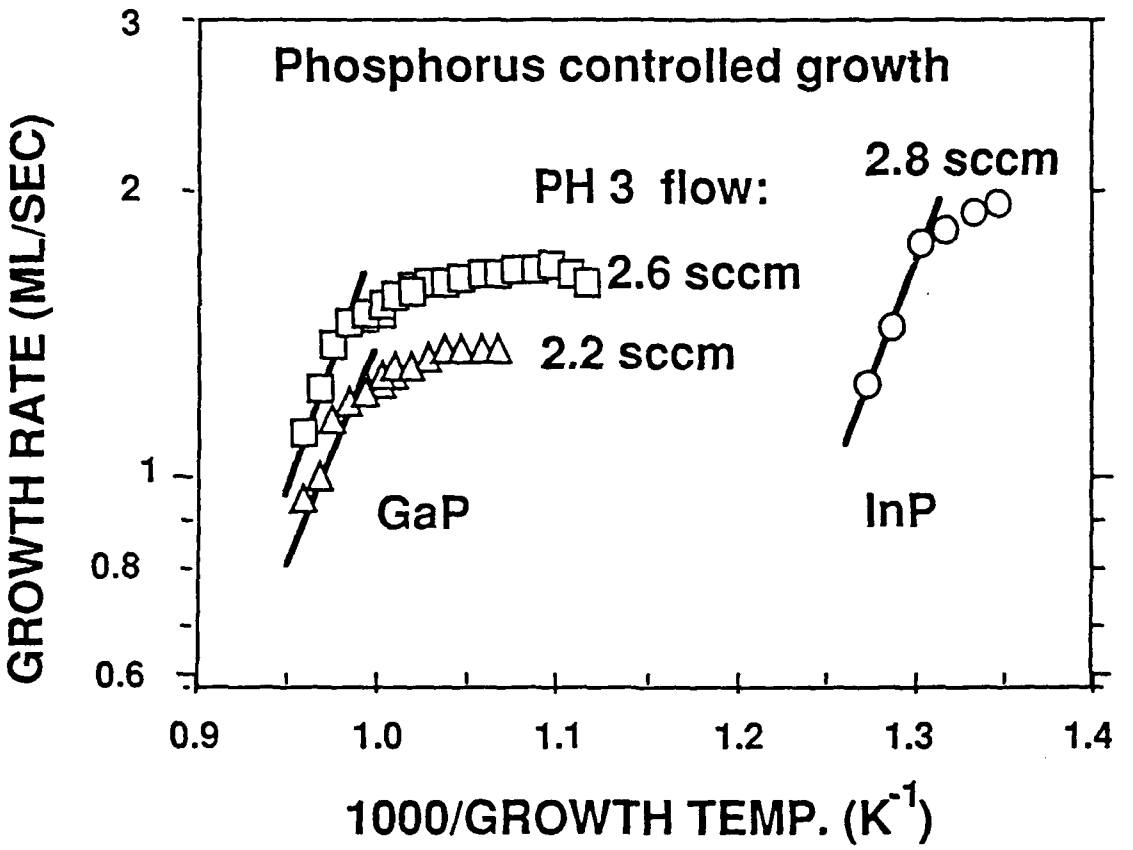
Phosphorus controlled growth
PH 3 flow:
2.8 sccm
2.6 sccm
2.2 sccm
GaP
InP
GROWTH RATE (ML/SEC)
3
2
1
0.8
0.6
0.9
1.0
1.1
1.2
1.3
1.4
1000/GROWTH TEMP. (K-1)

Figure 5

Submitted to Appl. Phys. Lett.
(1990)

High-resolution X-ray Diffraction of InAlAs/InP Superlattices Grown by Gas-source Molecular-beam Epitaxy

J.C.P. Chang, T.P. Chin, K.L. Kavanagh and C.W. Tu

Department of Electrical and Computer Engineering, 0407, University of California, San Diego, La Jolla, CA 92093-0407

Structural properties of InAlAs/InP superlattices grown by gas-source molecular-beam epitaxy (GSMBE) on (001) InP were investigated extensively with high resolution x-ray diffraction (HRXRD). Very high-quality material was obtained as indicated by narrow peak widths, numerous satellite peaks and distinct Pendellosung fringes. Intermixing of group-V elements at each interface was quantified by dynamical simulations of (004), (002), and (115) reflections. The accuracy of the fits to both peak positions and peak intensities for all three reflections provides strong evidence for the proposed four-layer periodic structure.

In this letter we present high resolution x-ray diffraction (HRXRD) data from InAlAs/InP superlattices grown by gas-source molecular-beam epitaxy (GSMBE) on (001) InP. Narrow peak widths and clear Pendellosung oscillations are observed, indicative of very high quality material both in lateral uniformity and periodicity. We also quantify from theoretical simulations of the data based on dynamical diffraction theory the intermixing which occurs at each interface. Such intermixing is to be expected from this system since the growth requires that the group V elements, As and P, be switched at each heterointerface. Compositional intermixing and localized strain have been detected by HRXRD and other techniques at similar heterointerfaces including InGaAs(P)/InP[1-2] superlattices, InGaP/GaAs[3-4] *multiple quantum wells and* AlInP/GaAs[5] single quantum wells. In this work we quantify the composition and thickness of the interfacial layers occurring at InAlAs/InP superlattices. Simulations of (004), (002), and (115) x-ray rocking curves with excellent fits to the data are obtained if one monolayer thick strained intermixed layers are included in the superlattice structure.

The InAlAs/InP superlattice samples were grown by GSMBE using elemental group-III effusion cells and thermally cracked arsine and phosphine[6]. The InP substrate was first degreased in a 1% Alconox solution, then etched with H_2O_2:NH_4OH:H_2O (2:5:10) and finally rinsed with DI water before being loaded into the MBE system. The shutter/valve sequence for growing superlattices and the nominal structure are shown in Fig. 1 (a). The growth temperature of the structure was 520°C. The 4-second hydride (arsine or phosphine) flow before growing each new layer was implemented to stabilize the gas flow while switching the hydrides.

X-ray rocking curves were recorded using a diffractometer with a four-reflection monochromator consisting of two channel-cut germanium crystals (220 reflections), as first proposed by DuMond[7] and later described by Bartels[8]. This arrangement provides a very

clean, symmetric beam profile with a full width at the half maximum (FWHM) of 12 arcsec. Cu $K\alpha_1$ radiation (λ=1.54056Å) was used for all reflections. Data were taken in 6 arcsec intervals with a 20 second counting time per point.

Simulations were performed with a PC386 computer using dynamical x-ray diffraction theory based on the solution of the Takagi-Taupin equations[9]. In the simulation, we consider each sample to be subdivided into layers of constant lattice parameter (*i.e.*, constant strain) and structure factor. The effect of the four-reflection monochromator in a (+,-,-,+) orientation was included in the calculation that follows the procedures described by Tanner[10] and Slusky and Macrander[11], which ignores the effects of vertical divergence of the beam. Only reflecting power from the σ polarization was simulated since the monochromator effectively blocks the π-polarized radiation[11]. The FWHM of our simulated rocking curve of the four-reflection monochromator was 12 arcsec, exactly the same as calculated by Bartels[7]. This curve was then correlated with the reflectivity curve of the sample crystal to give the final rocking curve. Peak broadening due to sample curvature was simulated by convoluting a rectangle of width 10 arcsec with the intensities derived from a flat sample.

Fig. 2 shows the (004) scan of a 20-period 80Å $In_xAl_{1-x}As$/80Å InP superlattice with a nominal composition x=0.52 grown on (001) InP. Sharp and well defined satellite peaks could be detected up to order n=-5. The FWHM's of the experimental and simulated (without curvature) zeroth-order satellite peak are 50 arcsec and 48 arcsec, respectively. Such comparable FWHM's indicate that the superlattice crystal quality is nearly perfect. Pendellosung oscillations, clearly seen in the wings of the substrate peak, zeroth-order peak, +1 and -1 peaks suggest high crystal quality and perfection in the epilayer surface and interface. The superlattice period[12], obtained from the averaged angular spacing between satellite peaks (1202 arcsec), was calculated to be 155Å. The fact that the highest

intensity peak within the envelope of superlattice reflections appears at a larger Bragg angle than the substrate implies the material is negatively strained, instead of perfectly lattice-matched. The averaged perpendicular x-ray strain[12] $<\varepsilon_\perp>$ ($=<\Delta a_\perp/a_{InP}>$) of the superlattice, calculated from the angular separation between the main (n=0) superlattice and the substrate peak, was found to be -0.43%. If we assume that InP and $In_xAl_{1-x}As$ layers have equal thicknesses and that the InP layer is strain free (it is the same material as the substrate), $<\varepsilon_\perp>$ equals half the strain of the $In_xAl_{1-x}As$ layers (with no plastic relaxation). With a correction for tetragonal distortion[13] (Poisson ratio $\alpha = 0.89$) and application of Vegard's law, the In composition was calculated to be 0.49. From the period (60 arcsec) of the Pendellosung oscillations[12], the number of periods in the superlattices was verified to be equal to 20.

The simulated rocking curve shown in Fig. 2 (b) was obtained if we assume a perfect 20-period structure with abrupt interfaces, *i.e.* a bi-layer model with layer thicknesses 78Å for both InP and $In_xAl_{1-x}As$ layers and x= 0.49. This model resulted in a poor fit to the relative peak intensities of the superlattice peaks to the substrate peak, although it fit the peak positions very well. Since no physically viable combination of layer thicknesses and In compositions could make the $|n|>1$ satellite peaks increase in intensity by one order of magnitude, we, therefore, decided that the bi-layer model must be modified by the addition of a strained layer at each interface. This four-layer model, shown in Fig. 1 (b), considered the top several monolayers of each InP layer to have some mixture of As and formed $InP_{1-x}As_x$ at the InAlAs-on-InP interface, while the top several monolayers of $In_zAl_{1-z}As$ were replaced by a quaternary compound $In_zAl_{1-z}As_{1-y}P_y$ at the InP-on-InAlAs interface. The simulation program developed for this study allowed input compositions x, y, z and thickness for each layer to be varied. The period and averaged strain were kept constant, since the $InP_{1-x}As_x$ layer gave a positive strain and the quarternary layer contributed an additional negative strain. Fig. 2 (c) shows a simulation with the best fit obtained with a

four-layer model consisting of 73Å of InP, 3Å of $InP_{0.40}As_{0.60}$, 76Å of $In_{0.477}Al_{0.523}As$, and 3Å of $In_{0.477}Al_{0.523}As_{0.95}P_{0.05}$. This fit is excellent both in the shape of the superlattice envelope function and the intensities of the superlattice reflection relative to the substrate peak. Better fits to the experimental rocking curves could not be obtained either by choosing different lattice-parameter thickness profiles or by using 2 to 3 monolayers of interdiffused material. A three-layer model with only one intermixed layer at either the InAlAs-on-InP or InP-on-InAlAs interface also was not useful. Over 500 simulations of systematically chosen layer structures revealed that the intensity of the satellite peaks were very sensitive to the composition of the interfacial region and layer thickness. We found that the $InP_{1-x}As_x$ layer with positive strain affected the intensity of the $n<0$ satellite peaks, while the InAlAsP layer with negative strain was crucial for the intensities of the $n>0$ satellite peaks.

To support the validity of this four-layer model[14,15], (002) rocking curves were also recorded and calculated using the best fit structure obtained from the (004) simulation. Although the (002) reflection is less suitable for calculation of strain, the satellite peaks are much stronger compared to those of the (004) reflections. Hence, the (002) reflection is more sensitive to superlattice properties. As shown in Fig. 3 (a), sharp and well defined satellite peaks could be seen up to $n=+7$ in the (002) experimental data. Excellent agreement between the simulated curve, shown in Fig. 3 (b), and the experimental (002) curve clearly shows the self-consistency of this model.

Symmetric reflections are sensitive to perpendicular strain only, while asymmetric reflections measure both perpendicular and parallel strains[15]. To investigate the coherency of the strained layers, the (115) reflection was measured and the result is shown in Fig. 4 (a). Fig. 4 (b) was calculated using the best fit parameters from the (004) simulation with a parallel x-ray strain[16] (with respect to the substrate lattice constant) $\varepsilon_{//}$ equal to zero. The

excellent fit again adds further support to the self-consistency of the 4-layer model and confirms that plastic relaxation had not occurred.

The best structure determined by x-ray rocking curve simulations indicates that one monolayer of $InP_{0.4}As_{0.6}$ formed before InAlAs is grown and one monolayer of $InAlAs_{0.95}P_{0.05}$ formed on top of the InAlAs layer. We conclude that during growth 60% of the phosphorus on the top monolayer of InP was replaced by arsenic during the 4 second surface passivation by arsine. However, only 5% of arsenic in the top monolayer of InAlAs was exchanged by phosphorus within the same period of time. This is a reasonable result due to the low congruent evaporation temperature of InP (365°C). At the growth temperature of 520°C, the evaporation of phosphorus from InP and substitution of phosphorus vacancies by arsenic under arsenic overpressure is expected. Furthermore, due to the higher melting temperature of AlAs (2013K), InAlAs is expected to be stable at the growth temperature.

We have also considered the possibility of exchange or interdiffusion between In and Al occurring in addition to intermixing of As and P. This could form an unstrained InAlAsP (instead of InPAs) interfacial layer which would have the advantage of being thermodynamically stable. However, this model was ruled out by further simulations. Extra strain or large variations in structure factors from the interfacial region is necessary to produce the observed modulation in the satellite peak intensities. If the interface layers are unstrained the structure factor difference becomes the only factor. However, the magnitude of the structure factors of any of these layers is dominated by the In component, and hence they vary very little. Furthermore, simulations have shown that interfacial layers with strains of opposite sign at the two interfaces are necessary to make the intensities of odd satellites stronger than those of even ones[18], as is observed in our experimental curves. Thus, highly strained interfacial layers of opposite sign (in our case, InPAs layer with

strain 0.37% and InAlAsP layer with strain -0.75%) must be formed to have the observed marked effect on the modulation of satellite peak intensities.

In summary, we have used HRXRD to characterize the interface intermixing of As and P in InAlAs/InP superlattices. Excellent fits to (004), (002) and (115) rocking curves were obtained by simulations based on dynamical theory with the inclusion at each interface of a one-monolayer-thick strained intermixed layer. These simulations indicate that only As-P exchange occurs, and the composition of the interfacial layers are $InP_{0.40}As_{0.60}$ and $In_{0.477}Al_{0.523}As_{0.95}P_{0.05}$ at the InP and InAlAs surfaces, respectively.

Acknowledgements

We gratefully acknowledge partial support from IBM, Northern Telecom, the Powell Foundation, and the Office of Naval Research. We wish to thank I. Bassignana, B.K. Bowen, S.N.G. Chu, H.Q. Hou, and B.W. Liang for many useful discussions.

References

1. J.M. Vandenberg, S.N.G. Chu, R.A. Hamm, M.B. Panish, and H. Tempkin, Appl. Phys. Lett. **49**, 1303 (1986).
2. J.M. Vandenberg, R.A. Hamm, M.B. Panish, and H. Temkin, J. Appl. Phys. **62**, 1278 (1987).
3. H.Y. Lee, M.J. Hafich, and G.Y. Robinson, J. of Cryst. Growth **105**, 244 (1990).
4. H.Y. Lee, M.J. Hafich, G.Y. Robinson, K. Mahalingam, and N. Otsuka, paper presented at Sixth International Conference on Molecular Beam Epitaxy, La Jolla, California, August 27-31, 1990.
5. S. Nagao, M. Takashima, Y. Inoue, M. Katoh and H. Gotoh, paper presented at Sixth International Conference on Molecular Beam Epitaxy, La Jolla, California, August 27-31, 1990.
6. T.P. Chin, B.W. Liang, H. Q. Hou, M.C. Ho, C.E. Chang and C.W. Tu, submitted to Appl. Phys. Lett. (1990).
7. J.W. M. DuMond, Phys. Rev. **52**, 872 (1937).
8. W.J. Bartels, J. Vac. Sci. Technol. B**1**, 338, (1983).
9. S. Bensoussan, C. Malgrange, M. Sauvage-Simkin, J. Appl. Cryst. **20**, 222 (1987).
10. B.K. Tanner, Adv. X-ray Analysis **33**, 1 (1990).
11. S.E.G. Slusky and A.T. Macrander, J. Appl. Cryst. **20**, 552 (1987).
12. B.M. Paine, Mat. Res. Soc. Symp. Proc. **69**, 39 (1986).
13. J. Hornstra and W.J. Bartels, J. Cryst. Growth **44**, 513 (1978).
14. M. H. Lyons and M.A. Halliwell, Inst. Phys. Conf. Ser. No. **76**, 445 (1985).
15. M. A. G. Halliwell and M.H. Lyons, paper presented at the Electrochemical Society Meeting, Montreal, Quebec, May 1990.
16. V.S. Speriosu, M.-A. Nicolet, S.T. Picraux and R.M. Biefield, Appl. Phys. Lett. **45**, 223 (1984).
17. C.R. Wie, H. M. Kim and K. M. Lau, SPIE **877**, 41 (1988).

18. E.G. Scott, M. H. Lyons, M. A. Z. Rejman-Greene and G.J. Davies, J. Cryst. Growth **105**, 249 (1990).

Figure Captions

Figure 1 : (a) Shutter and valve sequences for the growth of InAlAs/InP superlattices. The solid lines indicate when beams are on. There is a 4 s interruption while arsine and phosphine flow are switched. (b) The Four-layer model including strained interfacial layers formed by As-P exchange.

Figure 2 : Experimental (a) and simulated (004) x-ray rocking curves of a 20-period superlattice consisting of (b) 78 Å $In_{0.48}Al_{0.52}As$ / 78 Å InP (abrupt interface) or (c) 76Å $In_{0.477}Al_{0.523}As$ / 3Å $In_{0.477}Al_{0.523}As_{0.95}P_{0.05}$ / 73 Å InP / 3Å $InP_{0.40}As_{0.60}$ (4-layer model).

Figure 3 : Experimental (a) and calculated (b) rocking curves for the (002) reflection from a 20-period superlattice assuming a four-layer model as in Fig. 2 (c).

Figure 4 : Experimental (a) and calculated (b) rocking curves for the (115) reflection from a 20-period superlattice assuming a four-layer model as in Fig. 2 (c).

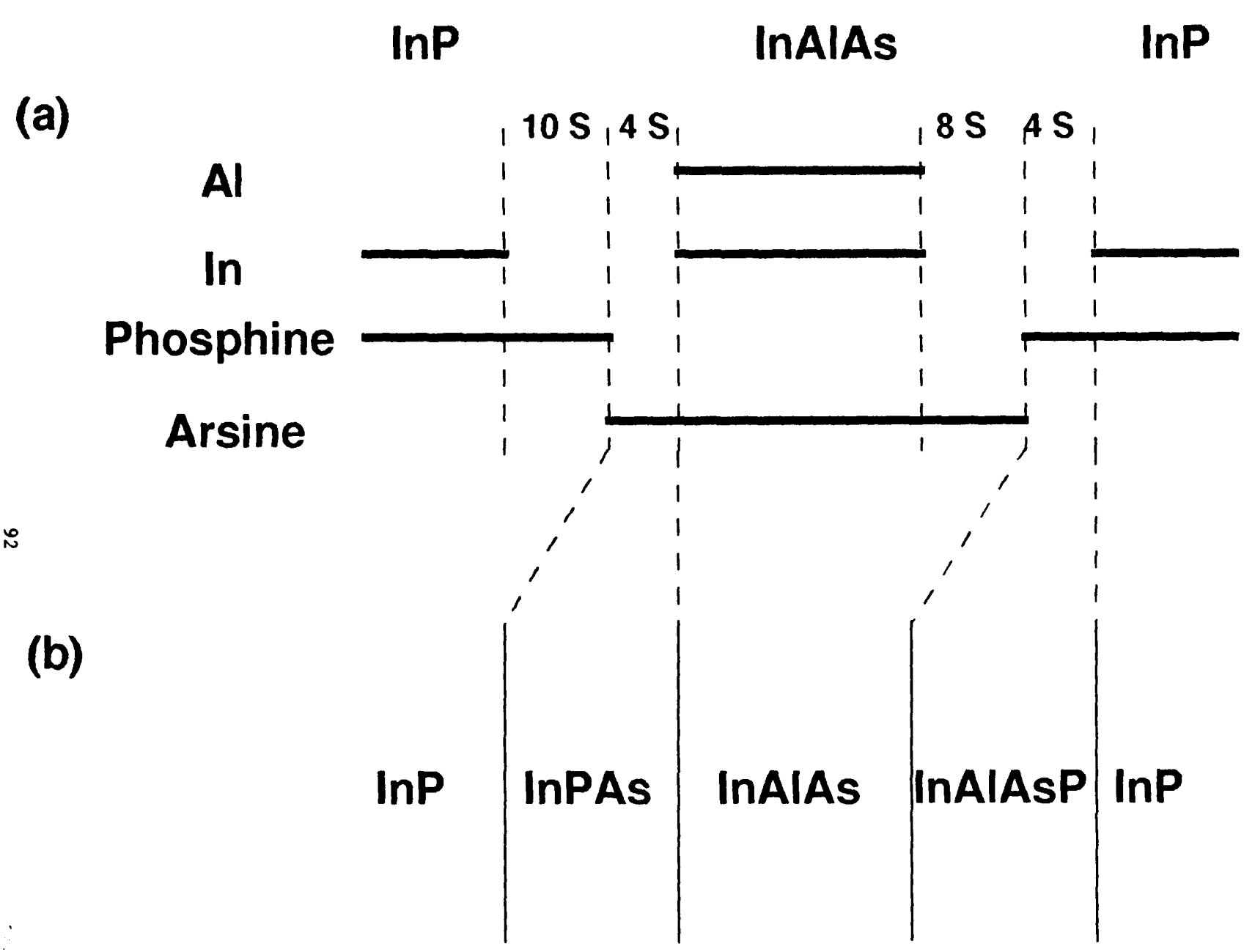
InP
InAlAs
InP
(a)
10 S
4 S
8 S
4 S
Al
In
Phosphine
Arsine
(b)
InP
InPAs
InAlAs
InAlAsP
InP

Figure 1

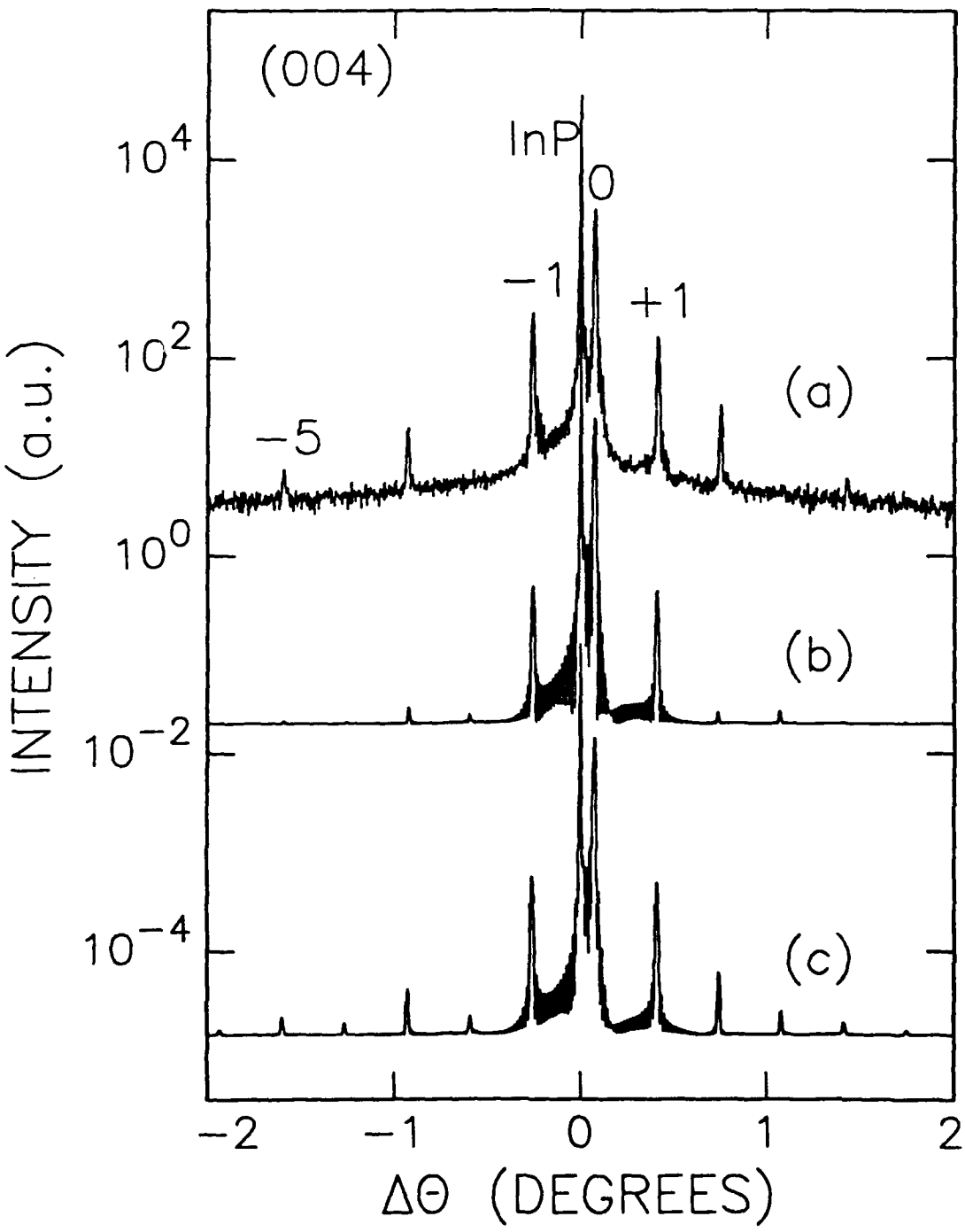
(004)
InP
0
−1
+1
−5
(a)
(b)
(c)
10^4
10^2
10^0
10^{-2}
10^{-4}
INTENSITY (a.u.)
−2
−1
0
1
2
ΔΘ (DEGREES)

Figure 2

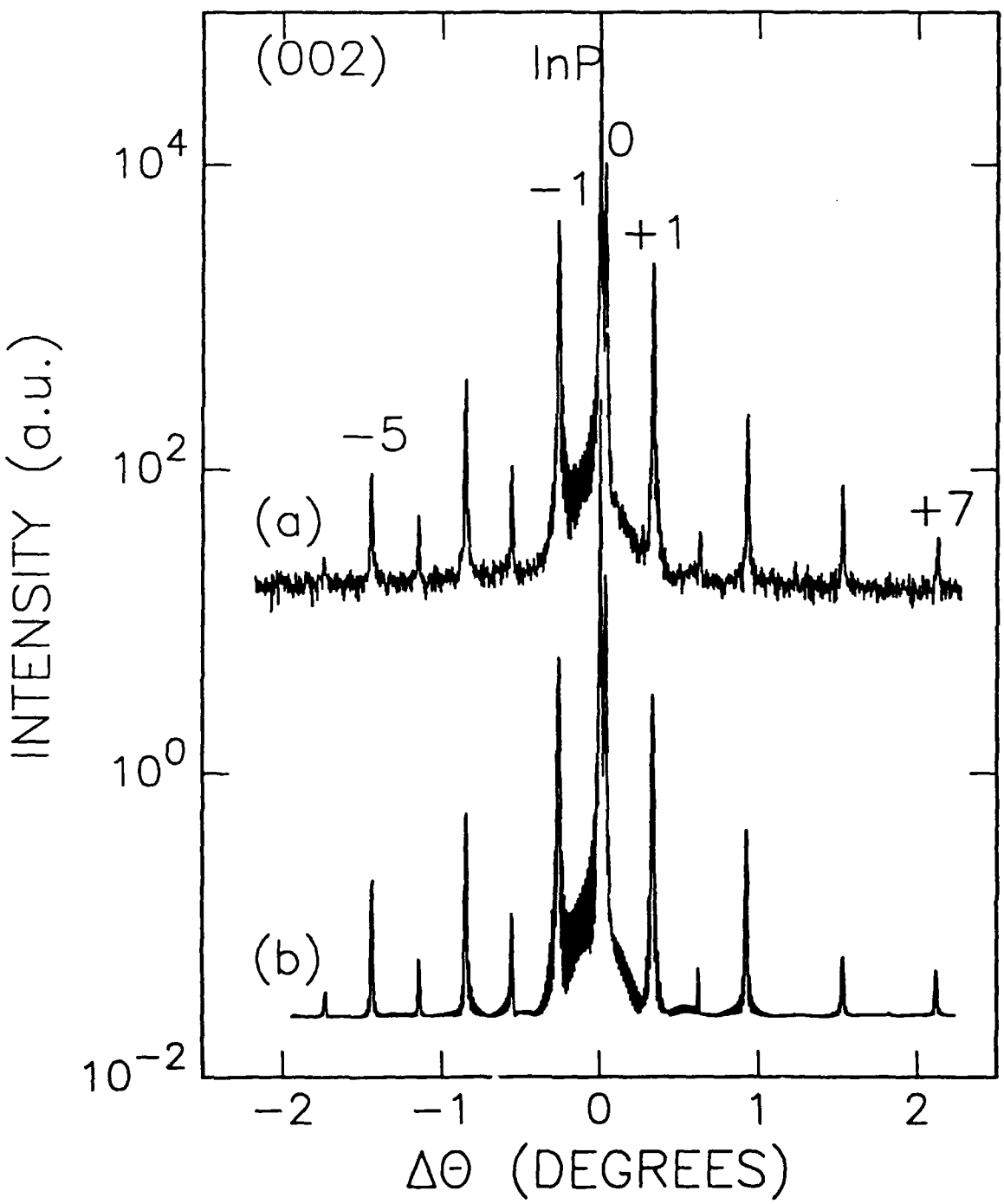
(002)
InP
0
−1
+1
−5
+7
(a)
(b)
10^4
10^2
10^0
10^{-2}
INTENSITY (a.u.)
−2
−1
0
1
2
ΔΘ (DEGREES)

Figure 3

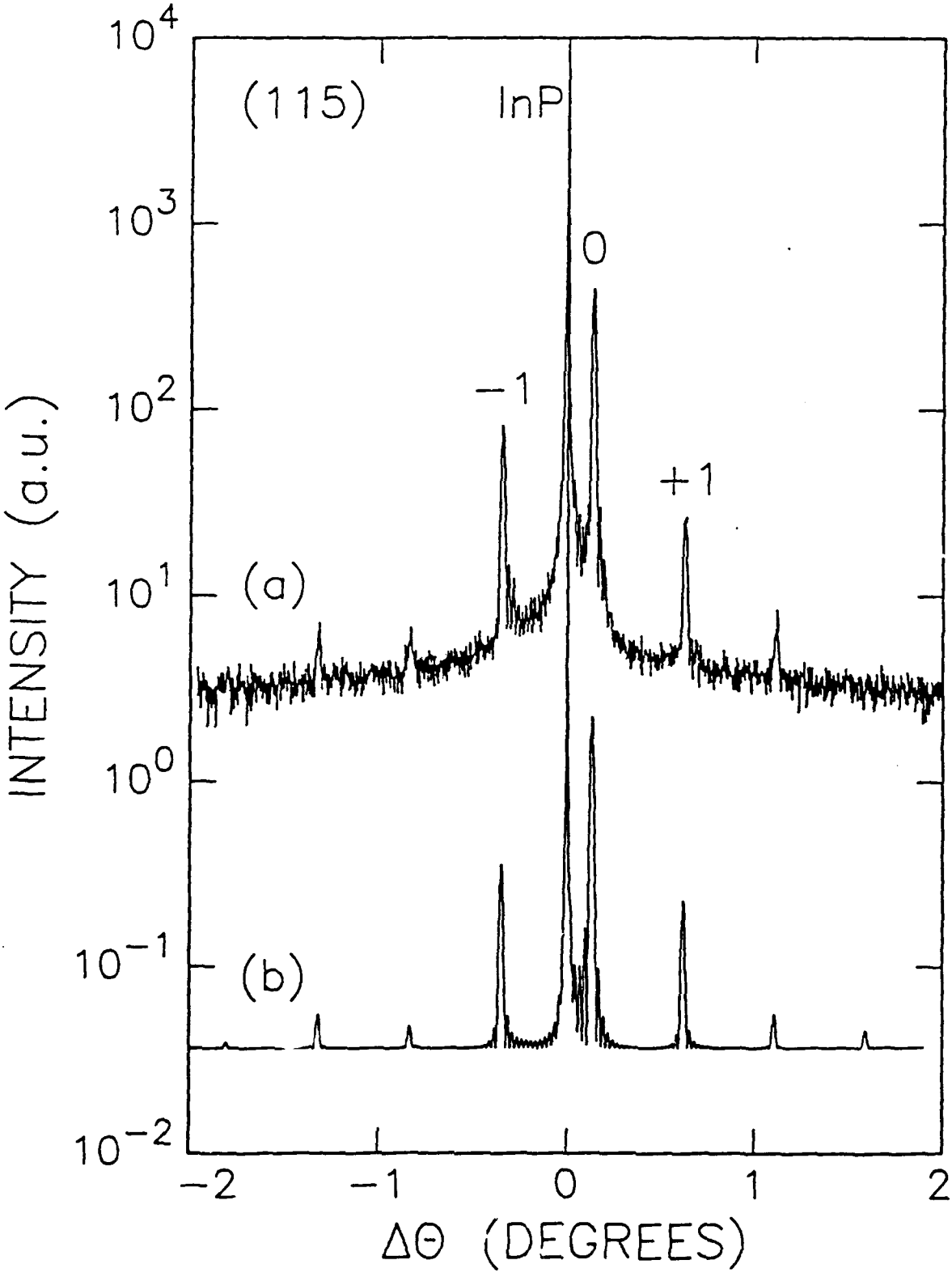
(115)
InP
0
−1
+1
(a)
(b)
INTENSITY (a.u.)
10^4
10^3
10^2
10^1
10^0
10^{-1}
10^{-2}
−2
−1
0
1
2
ΔΘ (DEGREES)

Figure 4

Submitted to Rev. Sci. Instrum.
(1990)

A Differential reflection high energy electron diffraction measurement system

C. E. Chang, T.P. Chin, and C.W. Tu

University of California, San Diego,
Department of Electrical and Computer Engineering,
La Jolla, California 92093-0407

An economical, real-time differential reflection high energy electron diffraction (RHEED) measurement system which is effective in a high-noise environment is described. Two fiber optic cables sample the RHEED intensities from the phosphorescent screen in a molecular beam epitaxy (MBE) growth chamber. The first cable observes the RHEED oscillations with the inherent background noise while the second cable monitors the background noise. The differential RHEED unit subtracts the RHEED signal combined with the background noise from the background noise, leaving only the RHEED signal. The resultant "clean" RHEED oscillation is displayed on an IBM compatible computer.

INTRODUCTION

Reflection high energy electron diffraction (RHEED) has evolved to become the primary method used to observe the epitaxial growth of crystals in molecular beam epitaxy (MBE) machines. Monitoring the intensity of the RHEED oscillations allows optimization of the epitaxial growth conditions for binary and ternary compound semiconductors in the MBE growth chamber.[1] The growth rate of a single monolayer can be determined from the period of the RHEED oscillation.

Conventional low-cost RHEED techniques utilize a photodiode or a photomultiplier tube to monitor the RHEED pattern intensity on the phosphorescent screen. The signal from the diode is amplified to drive an X-Y recorder. Due to the low intensity of the diffracted spot on the phosphorescent screen, background noise can approach and even exceed the RHEED signal.

The differential RHEED technique attempts to alleviate the inconveniences associated with conventional photodiode or photomultiplier RHEED techniques. This can be realized by sampling the RHEED pattern at two different points. The first point observes the RHEED pattern along with the background noise. The second point samples the background noise near the first point. The background noise may consist of surrounding lighting, MBE equipment vibrations, and diffuse background scattered electrons. Although in principle the diffuse scattering intensity also oscillates with time, its signal level is low (near the noise level); thus, the homogeneity of the background noise can be assumed. The subtraction of the RHEED information (measured RHEED intensity

along with the associated background noise) from the background noise will yield the intrinsic RHEED intensity. This process should effectively remove the background noise in real time (without the inconvenient lag time between data acquisition and signal processing to display the RHEED oscillations). Figure 1 illustrates the basic setup of the differential RHEED system. A fiber optic cable sends the RHEED pattern and noise from the phosphorescent screen to a phototransistor in the phototransistor box. A second ancillary fiber optic cable conveys the noise to another matching phototransistor. Operational amplifiers inside the differential RHEED unit subtracts the first signal from the second, leaving only the intrinsic RHEED intensity. An IBM compatible computer outfitted with an analog-to-digital (A/D) converter and an oscilloscope/fast fourier transform (FFT) package will display, process, analyze, and store the RHEED oscillation. The period of oscillations (time to grow one monolayer) can be obtained with a FFT.

I. DIFFERENTIAL RHEED APPARATUS

The differential RHEED system can be subdivide into two sections. The first section deals with the differential RHEED unit while the second section deals primarily with the low-cost computer data acquisition/analysis system.

A. Differential RHEED unit

Simple mechanical arms position the fiber optic cables to the points-of-interest on the phosphorescent viewport of the MBE

machine. The small diameter of the fiber cable allows accurate positioning of the fiber optic cable over the intensity maxima or minima of the RHEED spots. Two feet of shielded plastic fiber optic cable about 1mm in diameter transports the low intensity RHEED information and noise to the phototransistor box. The end of the fiber optic cables are "polished" with a flame to yield a more optically transparent end.[2] The short run of fiber optic cables minimizes signal loss without sacrificing the ease of placement advantages of the fiber optic cable.

Two VarTec VT1113 phototransistors in a TO-18 package, converts the optical RHEED information or noise into an electrical signal in the phototransistor box. The common emitter configuration of the phototransistor provides enough voltage and current to drive the signal through the long length of shielded cable to the RHEED amplifier. The fiber optic cable to phototransistor interface consists of a common 3/8" to 1/4" Swagelok pipe fitting with a rubber cork (figure 2). A small drop of superglue attaches the phototransistor to the 3/8" end of the Swagelok while the silicone sealant dries. The inside diameter of the Swagelok precisely fits the cylindrical TO-18 package of the phototransistor. On the other Swagelok end, a 1/4" diameter rubber cork with a small hole drilled in the center firmly positions the fiber optic cable over the active area in the phototransistor package. When the nut on the Swagelok is tightened, it compresses the rubber cork which in turn, tightens its grip on the fiber optic cable. The electrical RHEED signals leave the phototransistor box via BNC connectors, and the 15VDC required by

the phototransistors enters the phototransistor box through a 1/4" phono plug.

The differential DC coupled RHEED amplifier unit amplifies the signals from two phototransistors, subtracts the first signal from the second, and corrects for the DC offset. Figure 3 illustrates the schematic diagram of the RHEED amplifier unit. In the first stage, operational amplifiers (U1A and U1B) in the non-inverting mode provide variable gain from 1 to 5 for the incoming signal from each of the two phototransistors. The variable gain allows matching of the noise levels of the two signals. With equal noise amplitudes in each channel a third operational amplifier (U2A) in the differential mode subtracts the first signal (that contains the RHEED information) from the second signal (that just contains the noise). Assuming equal phase in the noise, this will result in the actual RHEED intensity. Due to the inherent unequal DC offset in the phototransistors from the same make and batch, a fourth operational amplifier (U2B) adds or subtracts a D.C. constant to the RHEED oscillation signal. Capacitors could have been used to block the D.C. offset; however, the long period of the RHEED oscillations (about 1 second) would require large capacitor values. Furthermore, the capacitance value tolerance between two capacitors could alter the phase of the noise between channels; thus, reducing the overall effectiveness of the differential amplifier. Switches on the differential RHEED unit allow the unit to operate in the differential mode or to operate as two separate single channel amplifiers. High input resistance JFET TL082 operational amplifiers were used throughout the circuit. Capacitors (.1uF and 1 uF) bypass the line noise from the power supply to ground in order

to reduce the noise, thus, they should be located as close to the operational amplifier as physically possible. To minimize the effect of line noise, a simple IC regulated +/- 15V power supply with large computer grade electrolytic filter capacitors is used.

B. Computer Data Acquisition

The data acquisition computer consisted of an Intel 80286 based IBM AT compatible with a 80287 math coprocessor, VGA graphics, 1Mb RAM, and a 40Mb hard drive. A Metrabyte[3] DAS-8 12 bit A/D converter combined with the UnkleScope[4] software package converted the the IBM AT compatible computer into a relatively low-cost computerized data acquisition system. The 12 channel A/D board provided enough resolution at a fast enough sampling rate (20,000 samples/sec) to accurately digitize the RHEED intensity in real time. The Unklescope oscilloscope package effectively displays the RHEED pattern on the computer monitor. The ability to store he RHEED pattern measurement on the hard drive allows an FFT or a printer plot to be performed at a later time.

II. PERFORMANCE

The differential RHEED system is installed on a highly modified Varian Modular Gen II MBE growth chamber. Figure 4 and 5 illustrates the RHEED measurements conducted on a GaAs (100) wafer under various circumstances. Figure 4 shows the results of a single-channel RHEED measurement made with the differential RHEED system. High-frequency noise of a significant amplitude

plagues the dampened sinusoidal RHEED oscillations. Conventional RHEED measurements plotted with X-Y plotters lack the high frequency noise from the MBE machine since the mechanical limitations of the plotter acts as a low-pass filter. The large amplitude of the background noise obscures the RHEED oscillations, thus making it difficult to determine the period of oscillations with accuracy. Although the RHEED information can be filtered in the digital domain or converted to the frequency domain with an FFT, the IBM computer can not process the data while acquiring data with enough resolution at the same time. Figure 5 illustrates the RHEED measurement made with the differential RHEED amplifier in the differential mode. The ancillary fiber optic cable was placed on a low intensity spot about 2 inches away from the primary fiber optic cable. This clearly shows that the differential RHEED amplifier in the differential mode can effectively remove a significant quantity of the background noise, resulting in a clearly defined RHEED oscillation.

The noise typically encountered in the RHEED information with and without the differential mode is shown in figure 6. In the single mode, a 60Hz AC line-frequency signal primary from the electron gun filament dominates the background noise. Mechanical vibrations from the compressor of the Varian UHV8 cyropump caused the large 15Hz and those from the expander of the cryopump caused the 4Hz (apparent in the figure as a rise in the overall noise with time) background noise. In the differential mode, the lower frequency single-source noise (4Hz and 15Hz) is almost completely cancelled by the differential amplifier. Although the 60Hz noise remains, it is greatly reduced in amplitude so it does not make a significant

contribution to the RHEED oscillation. The residual 60Hz noise may be caused by the noise phase difference from both the electron gun and the surrounding fluorescent lights.

III. SUMMARY

A simple, relatively low-cost differential RHEED measurement system that effectively removes the background noise from the RHEED intensity oscillations in real time has been described. The differential option effectively removes the high-frequency noise from within the MBE machine.

ACKNOWLEDGMENTS

This work is partially supported by the Charles Lee Powell Foundation, the Air Force Wright Research and Development Center under contract No. F33615-88-C-1862 and the Office of Naval Research under the grant No. N00014-89-J-1147. We wish to thank B.W. Liang for his valuable discussions.

REFERENCE

[1] M.A. Herman and H. Sitter, *Molecular Beam Epitaxy*, Springer-Verlay, Berlin, 1989, pp.19-23.

[2] C.J. Sa and H.H. Wieder, Review of Scientific Instruments 61, 918 (1990).

[3] MetraByte Corp., 440 Myles Standish Blvd., Taunton MA 02780.

[4] Unkel Software Inc., 62 Bridge St., Lexington MA 02780.

FIGURE CAPTIONS

Figure 1: Setup of the Differential RHEED system. Two fiber optic cables sample the RHEED pattern from the viewport. The differential amplifier subtracts the noise from the actual RHEED pattern. A computer data acquisition system displays the RHEED signal in real time.

Figure 2: A fiber optic cable to a phototransistor interface accomplished with a Swagelok pipe fitting. The rubber cork centers the cable over the active area of the phototransistor. The Swagelok nut compresses the cork to grip the fiber optic cable.

Figure 3: Schematic diagram of the Differential RHEED amplifier.

Figure 4: RHEED oscillation of GaAs made with the Differential RHEED amplifier in the single channel mode.

Figure 5: RHEED oscillation of GaAs made with the Differential RHEED amplifier in the differential mode.

Figure 6: Typical background MBE noise in both the single channel mode and in the differential mode.

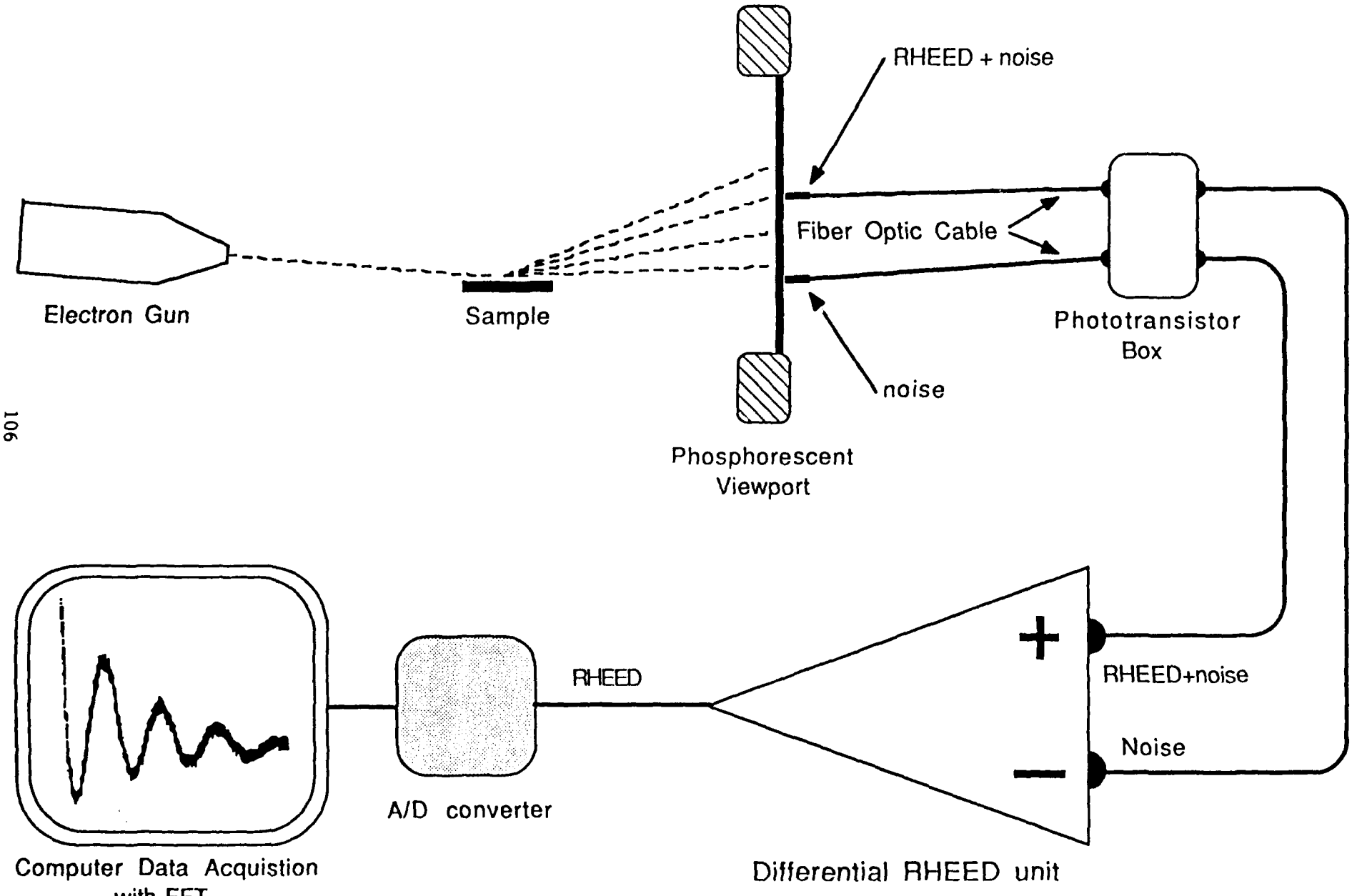
RHEED + noise
Fiber Optic Cable
Electron Gun
Sample
Phototransistor Box
noise
Phosphorescent Viewport
RHEED
RHEED+noise
Noise
A/D converter
Computer Data Acquistion with FFT
Differential RHEED unit

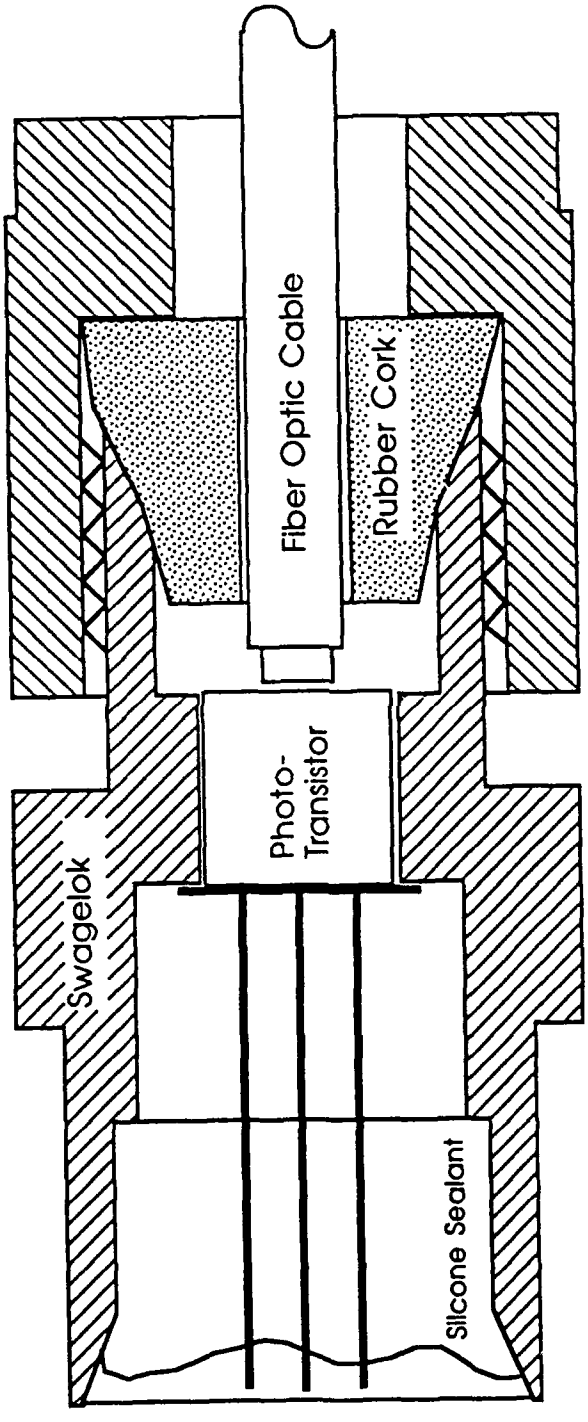
Fiber Optic Cable
Rubber Cork
Photo-
Transistor
Swagelok
Silcone Sealant

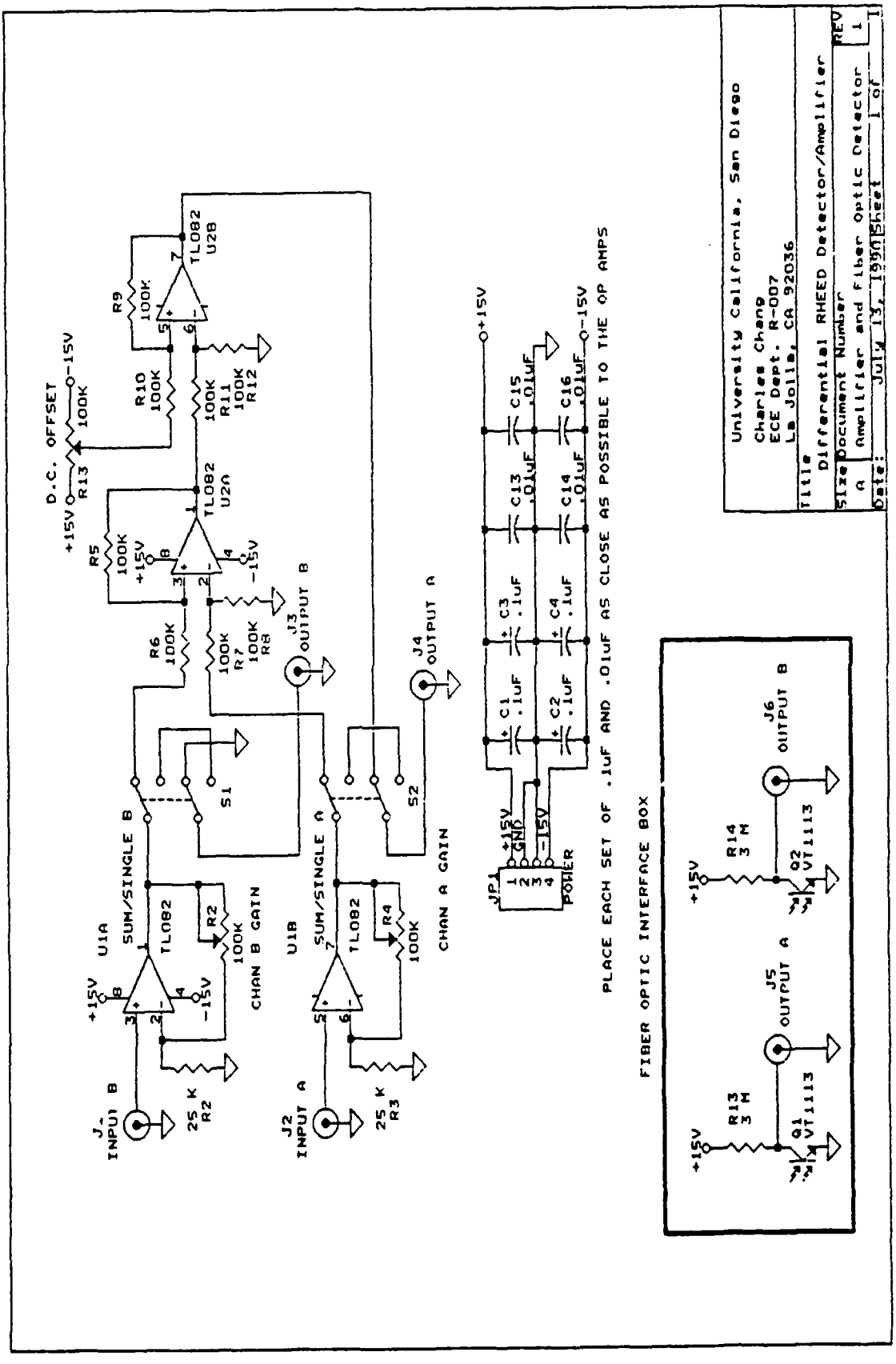
University California, San Diego
Charles Chang
ECE Dept. R-007
La Jolla, CA 92036
Title
Differential RHEED Detector/Amplifier
Size
Document Number
REV
A
Amplifier and Fiber Optic Detector
1
Date: July 13, 1990 Sheet 1 of 1
D.C. OFFSET
+15V
-15V
R13 100K
R9 100K
R10 100K
R11 100K
R12 100K
R5 100K
R6 100K
R7 100K
R8 100K
TL082 U2A
TL082 U2B
U1A SUM/SINGLE B
U1B SUM/SINGLE A
TL082
R2 100K
R4 100K
CHAN B GAIN
CHAN A GAIN
S1
S2
J1 INPUT B
J2 INPUT A
J3 OUTPUT B
J4 OUTPUT A
25 K R2
25 K R3
C1 .1uF
C2 .1uF
C3 .1uF
C4 .1uF
C13 .01uF
C14 .01uF
C15 .01uF
C16 .01uF
JP1
GND
POWER
PLACE EACH SET OF .1uF AND .01uF AS CLOSE AS POSSIBLE TO THE OP AMPS
FIBER OPTIC INTERFACE BOX
R13 3 M
R14 3 M
Q1 VT1113
Q2 VT1113
J5 OUTPUT A
J6 OUTPUT B

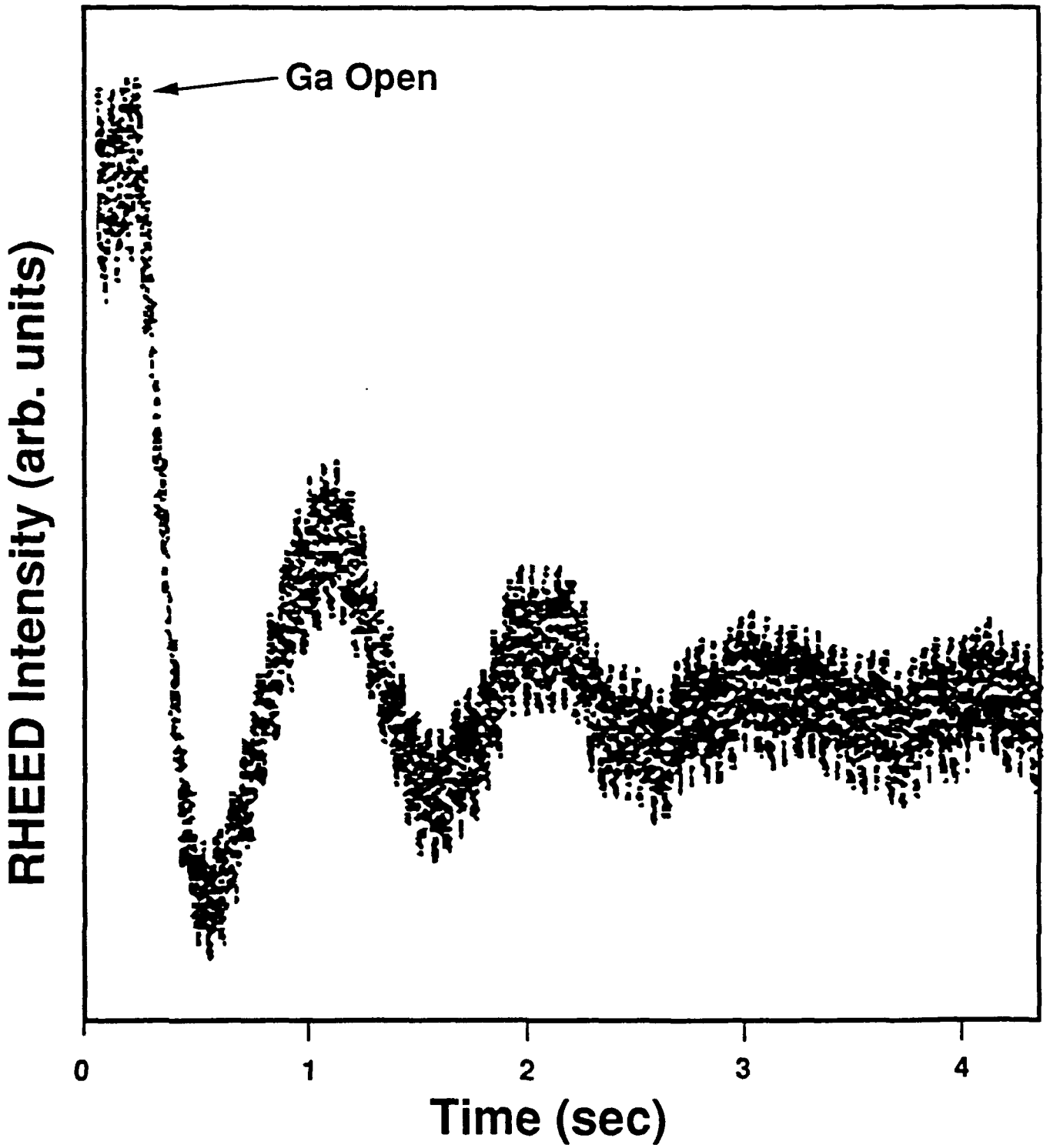
Ga Open
RHEED Intensity (arb. units)
0
1
2
3
4
Time (sec)

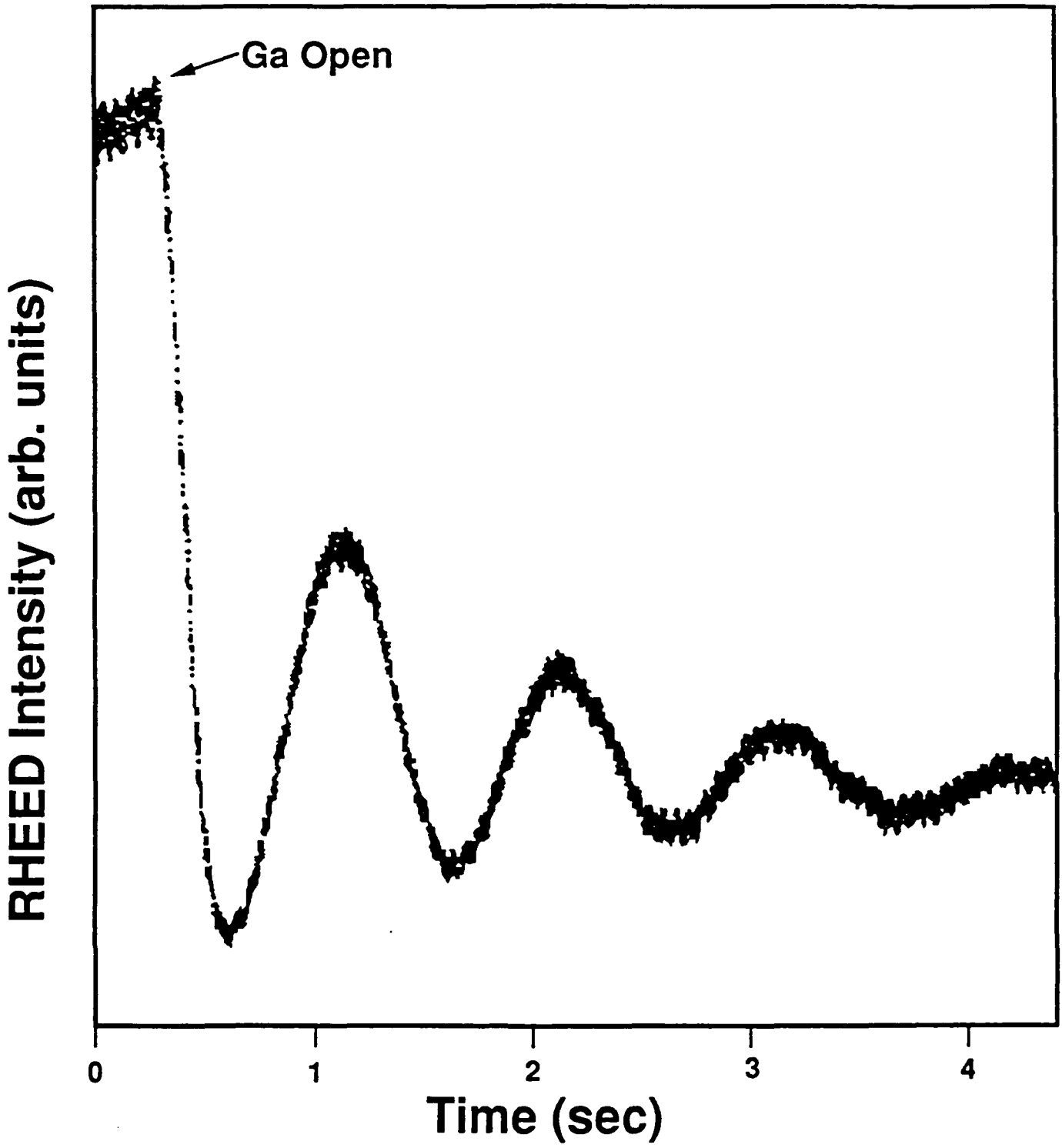
Ga Open
RHEED Intensity (arb. units)
0
1
2
3
4
Time (sec)

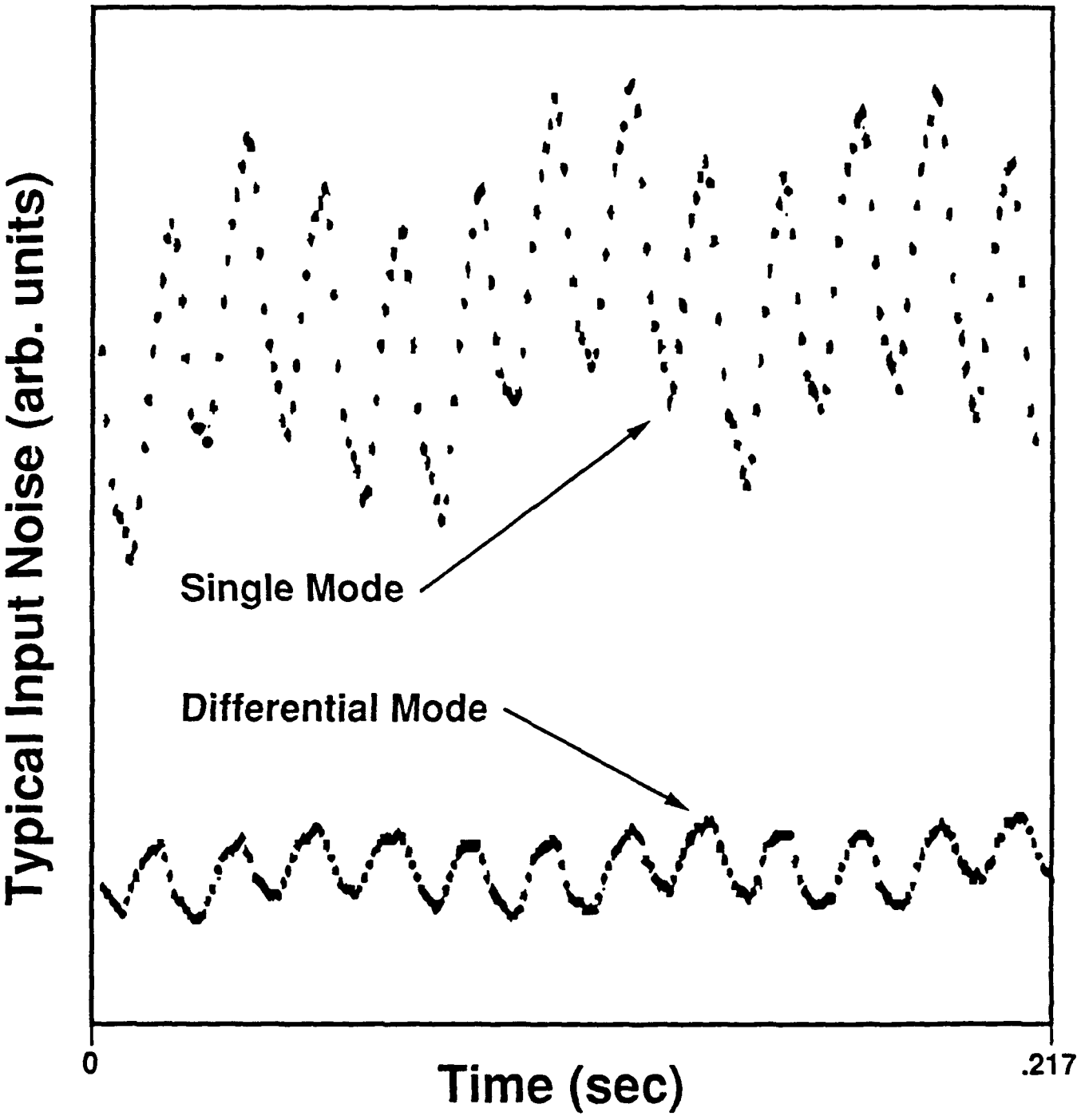
Typical Input Noise (arb. units)
Single Mode
Differential Mode
0
.217
Time (sec)